WINGLET DESIGN AND ANALYSIS FOR LOW ALTITUDE SOLAR POWERED UAV

A THESIS SUBMITTED TO
THE GRADUATE SCHOOL OF NATURAL AND APPLIED SCIENCES
OF
MIDDLE EAST TECHNICAL UNIVERSITY

BY

ALİ İHSAN GÖLCÜK

IN PARTIAL FULFILLMENT OF THE REQUIREMENTS
FOR
THE DEGREE OF MASTER OF SCIENCE
IN
AEROSPACE ENGINEERING

FEBRUARY 2016

Approval of the thesis:

WINGLET DESIGN AND ANALYSIS FOR LOW ALTITUDE SOLAR POWERED UAV

Submitted by **ALİ İHSAN GÖLCÜK** in partial fulfilment of the requirements for the degree of **Master of Science in Aerospace Engineering Department, Middle East Technical University** by,

Prof. Dr. Gülbin Dural Ünver
Dean, Graduate School of **Natural and Applied Sciences** _____

Prof. Dr. Ozan Tekinalp
Head of Department, **Aerospace Engineering** _____

Assoc. Prof. Dr. Dilek Funda Kurtuluş
Supervisor, **Aerospace Engineering Dept., METU** _____

Examining Committee Members

Prof. Dr. Ozan Tekinalp _____
Aerospace Engineering Dept., METU

Assoc. Prof. Dilek Funda Kurtuluş _____
Aerospace Engineering Dept., METU

Asst. Prof. Dr. Ali Türker Kutay _____
Aerospace Engineering Dept., METU

Prof. Dr. Ünver Kaynak _____
Mechanical Engineering Dept., TOBB

Asst. Prof. Dr. Gökhan Durmuş _____
Aerospace Science Dept., Anadolu University

Date: 04/02/2016

I hereby declare that all information in this document has been obtained and presented in accordance with academic rules and ethical conduct. I also declare that, as required by these rules and conduct, I have fully cited and referenced all material and results that are not original to this work.

Name, Last Name : ALİ İHSAN GÖLCÜK
Signature :

ABSTRACT

WINGLET DESIGN AND ANALYSIS FOR LOW ALTITUDE SOLAR POWERED UAV

Gölcük, Ali İhsan

M. S., Department of Aerospace Engineering

Supervisor: Assoc. Prof. Dr. Dilek Funda Kurtuluş

February 2016, 99 pages

To improve the aerodynamic performance of aircraft, comprehensive studies have been carried out in different areas such as wing optimization, tail types and fuselage shape, etc… One of the most important factors affecting the aerodynamic performance of the aircraft is lift induced drag caused by wingtip vortices. Winglet is a device referred as a small, vertical and angled extension attached at aircraft wingtip. It is used to minimize strength of vortices and reduce the lift induced drag.

Various types of winglets have been designed and investigated to enhance aerodynamic performances of aircraft. This thesis describes winglet design and analysis performed on rectangular wing of MH 114 airfoil for TÜBİTAK Unmanned Air Vehicle (UAV). The aim of this study is designing elliptical winglet and performing Computational Fluid Dynamics (CFD) analysis for different winglet parameters. The main objective of this study is to compare aerodynamic characteristics of base wing and wing with winglet and investigate the performance of winglets shape in terms of different parameters such as cant angle, sweep angle, taper ratio, toe angle and twist angle.

Winglet drawing is done in CATIA. In design algorithm, firstly, cant angle, sweep angle and taper ratio parameters are used in a triple combination with each other (27 models). Secondly, toe (6 models) and twist (6 models) parameters are applied to winglet separately which has the best L/D values in the first 27 models. Totally 39 different winglet models are investigated.

The computational simulation was performed at low subsonic flow speed in ANSYS using finite volume approach. k-ω SST is used as a turbulence model. To compute the flow around the model, 3-D unstructured tetrahedral mesh is used. The aerodynamic characteristics of lift coefficient (C_L), drag coefficient (C_D) and lift to drag ratio (L/D) were compared for 39 different winglet models at cruise conditions and zero angle of attack (AOA). To investigate stall characteristic of clean wing and winglet (has best L/D ratio), they were compared at different AOA (-5° to 20°). Moreover, viscous and pressure effects of drag and lift force of clean and the best case configurations are compared and examined. A further point, at different velocities, clean wing and wing with winglet were analyzed in order to observe L/D change.

Analysis showed that, elliptical winglet increased L/D value on the order of 8.32% compared to base wing. Hence, a significant improvement in aerodynamic performance is obtained for TİHAS.

Keywords: Elliptical winglet, Induced drag, CFD

ÖZ

DÜŞÜK İRTİFA VE GÜNEŞ ENERJİLİ İHA İÇİN UÇ KANATÇIK TASARIMI

Gölcük, Ali İhsan

Yüksek Lisans, Havacılık ve Uzay Mühendisliği Bölümü

Tez Yöneticisi: Doç. Dr. Dilek Funda Kurtuluş

Şubat 2016, 99 sayfa

Hava araçlarının aerodinamik performanslarını artırmak için kanat optimizasyonu, kuyruk tipi ve gövde şekli gibi farklı alanlarda bir çok çalışma yapılmıştır. Aerodinamik performansı etkileyen en önemli faktörlerden biri de kanat ucunda oluşan indüklenmiş girdaplardır. Kanatçık, hava araçlarında kanat uçlarına takılan, küçük, açısal olarak dikey doğrultuda bükülmüş yapılardır. Kanat uçlarında oluşan girdapların zayıflatılması ve indüklenmiş sürüklenmenin oluşturduğu etkinin azaltılması için kullanılmaktadır.

Aerodinamik performansı artırmak amacı ile bir çok kanatçık tasarlanmıştır. Bu çalışma Tübitak İnsansız Hava Aracı Sistemi (İHA)'nin dikdörtgen kanadı için bir uç kanatçık tasarım ve analizinden bahsetmektedir. Çalışmanın hedefi, farklı parametreler kullanarak bir eliptik kanatçık dizaynı oluşturmak ve bu dizaynların akışkanlar analizini yapmaktır. Ana hedef ise kanatçıksız kanat ile kanatçıklı kanadın aerodinamik performanslarını karşılaştırmak ve kanatçığın şeklini oluşturan parametreler, cant açısı, süpürme açısı, daralma oranı, toe açısı ve bükülme açısının kanatçık performansına etkisini araştırmaktır.

Kanatçık tasarımları CATIA kullanılarak yapılmıştır. İlk olarak cant açısı, daralma oranı ve sürükleme açısı birbirleri ile 3 farklı kombinasyonda kullanılarak 27 farklı dizayn oluşturulmuştur. Bu dizanlar içerisinden en iyi L/D değerine sahip tasarım için toe ve bükülme açıları denenmiştir. Bu analizler içinden de en iyi L/D değerine sahip tasarım alınmış ve kanatçıksız kanat ile aerodinamik performansları açısından karşılaştırılmıştır. Toplamda 39 farklı model tasarlanmış ve analizlari yapılmıştır. Hesaplamalı akışkanlar analizleri ANSYS de yapılmıştır. Türbülans modeli olarak k-ω SST kullanılmıştır. 39 model için aerodinamik karakteristler, kaldırma katsayısı (C_L), sürükleme katsayısı (C_D), ve L/D karşılaştırılmıştır. Sürükleme ve kaldırma kuvvetini oluşturan viskoz ve basınç sürükleme ve kaldırma kuvvetlerinin kanatçıksız kanat ve kanatçıklı kanat üzerindeki etkileri karşılaştırılmıştır. Kanatçıkların hava aracının perdövites hızına etkisini incelemek için farklı açılar için de analizleri yapılmıştır. Bunun yanında farklı hızlarda da kanat ve kanatçık analizleri de yapılmıştır.

Analizler sonucunda, kanatçıklı kanadın kanatçıksız kanada göre L/D değerinin %8.32 artttığı gözlemlenmiştir. Sonuç olarak TİHAS için önemli bir performans artışı elde edilmiştir.

Anahtar Kelimeler: Eliptik Kanatçık, İdüklenmiş sürüklenme

To my mother, father and grandfather…

ACKNOWLEDGEMENTS

I would like to thank all of my friends, family and Tübitak Uzay workers for their support during my time writing this work. I certainly could not have done this without all of the levels of help from everyone I know.

Specifically, I would like to thank my mother and father for their support and encouragement for me before and during grad school. I would not be who I am today without them.

Overall, I would like to thank my advisor Assoc. Prof. Dr. Dilek Funda KURTULUŞ, for accepting me as a graduate student, certainly the greatest opportunity I have had. Also, I would like to express my sincere gratitude to my supervisor for her guidance, advices, motivation, continuous supports and encouragements throughout this study.

Lastly, I would like to thank my friends Okan İSPİR, A. Emre ÖRÜN and Samet AKÇAY for all of their support and help.

TABLE OF CONTENTS

LIST OF TABLES

TABLES

LIST OF FIGURES

FIGURES

LIST OF SYMBOLS

Symbol	Description	Unit
C_L	Wing Lift Coefficient	-
C_D	Wing Drag Coefficient	
L/D	Lift to Drag Ratio	
c_f	Skin-Friction coefficient	
AR	Aspect Ratio	-
b	Wing Span	m
L/D	Lift to Drag Ratio	-
S_{ref}	Wing Reference Area	m^2
V_∞	Velocity	m/s
W	Weight	kg
λ	Taper Ratio	-
Λ	Sweep Angle	degree
μ	Dynamic Viscosity	kg/m.s
δ	Laminar Boundary Layer Thickness	mm
τ	Wall Shear Stress	
ρ	Density	kg/m^3
Re	Reynold Number	

LIST OF ABBREVIATIONS

Abbreviation	Description
AOA	Angle of Attack
TİHAS	TÜBİTAK Unmanned Aircraft System
PCB	Printed Circuit Board
IMU	Inertial Measurement Unit
RF	Radio Frequency
CFD	Computational Fluid Dynamics
VLM	Vortex Lattice Method
UAV	Unmanned Air Vehicle
MALE	Medium Altitude Long Endurance

CHAPTER 1

INTRODUCTION

Since the aviation industry begins, the development has been continuous about aircrafts. Economics (fuel prices) and environmental concerns are some of the most important factors force the aviation industry to develop. In this fashion, companies and universities have done a lot of works at each field such as aerodynamics, structure, propulsion, and control mechanism in order to enhance aircraft performance. One of the studies to increase aerodynamic performance of aircrafts is wingtip use because fuel consumption is related to drag reduction.

Aircraft flying through the air is exposed to two types of drag forces, parasite drag and pressure drag (subsonic flow), *Figure 1.1*. Parasite drag is related to wetted area of aircraft and result of viscous effects. However, pressure drag is a result of air moving along the surface of the wing and flow separation over the boundary layer of body.

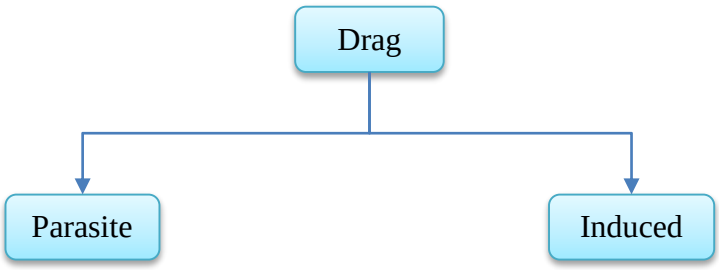

Figure 1.1 Classification of drag force (subsonic flow)

Induced drag is a part of the pressure drag that results of pressure difference at the tip of the wing between upper and lower surface. Instability of this pressure difference produces lift force upwards of the wing. Also, as a consequence of pressure imbalance, circular flow pattern is formed *Figure 1.2*.

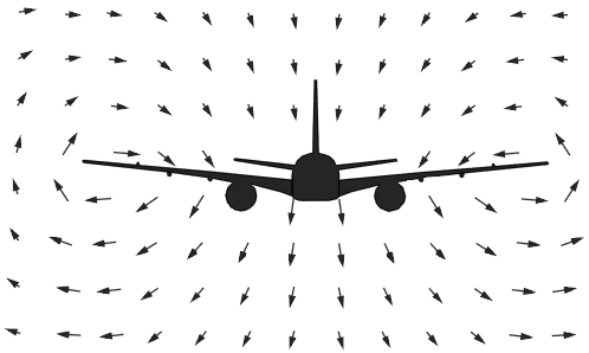

Figure 1.2 Flow pattern due to pressure difference [1]

Pressure difference of wing's upper and bottom surface causes the flow tends to curl at the wingtips being forced from under the high pressure region to low pressure region. As can be seen from the *Figure 1.3*, on the top surface of the wing, spanwise component of flow from wingtip to wing root cause the streamlines bend toward wing root and on the bottom surface of the wing, spanwise component of flow from wing root to wingtip cause the streamlines bend toward the wingtip [2].

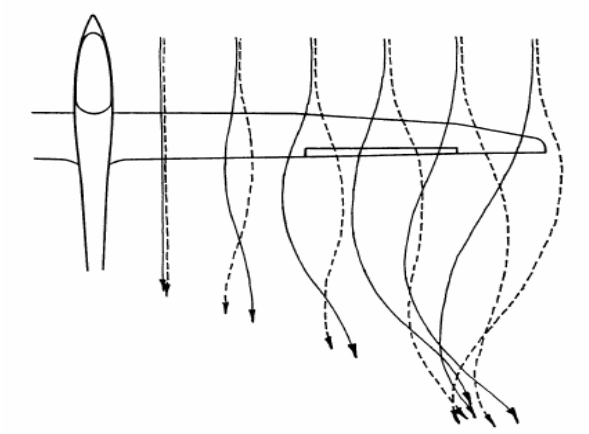

Figure 1.3 Spanwise flow [3]

The flow around the wingtip is referred as wingtip vortices and as a consequence of spanwise flow, vortex wake starts as a vortex sheet shed from the trailing edge of the wing by forming flown pattern [1] (*Figure 1.4*).

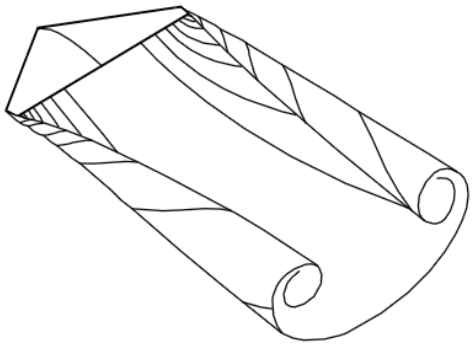

Figure 1.4 Vortex sheet [1]

This vortex adjust the flow field and induces the velocity component in the downward direction at the wing. This event is called downwash. Relative velocity canted towards at each airfoil section of the wing is a result of induced flow patter. Lift vector is tilted backwards because of this downwash effect and component in the direction of the drag called induced drag (*Figure 1.5*).

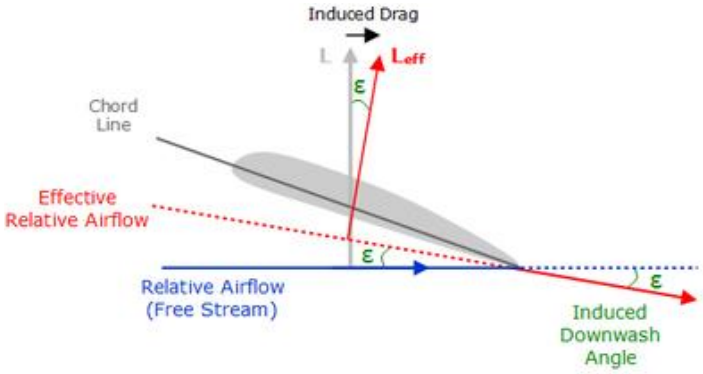

Figure 1.5 Induced drag [4]

1.1. Wingtip

Wingtip is a device invented to improve the aerodynamic efficiency of aircraft by reducing induced drag and tip vortex. Besides the aerodynamic improvement, wingtips improve aircraft handling characteristics and are also used for appearance of aircraft. There are many types of wingtips designed in different shapes and sizes according to their purpose and some of them is shown in *Figure 1.6*.

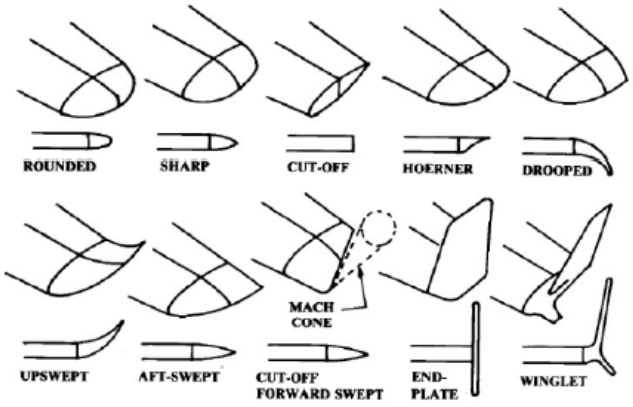

Figure 1.6 Wingtips [5]

These devices increase effective aspect ratio of wing without so much material increasing. However, since the length of wing is increased, parasite drag also increases due to the surface area increase. Also, there may be need an extra structurally reinforcing at the wingtip because wingtips create sides force and increase bending moment.

Today, various wingtips can be seen on almost all the commercial aircrafts such as Boeing and Airbus aircraft series to increase range and endurance by reducing induced drag effect. Moreover, wingtips also have been used on different kinds of UAVs to increase, handling characteristic, range and endurance lately. Especially for long endurance UAV, reduction of tip vortex and induced drag leads to an increase the endurance and range as well.

1.1.1. Winglets

Winglets are small, vertical and winglike structures that most widely used kind of wingtips mounted at the tips of a wing. The history of winglets begin in early 1970s with Richard T. Whitcomb [6] creator of winglet. As mentioned previous section, the motivation behind usage of winglet is to provide benefits in terms of aerodynamic efficiencies by reducing wingtip vortex and induced drag. In this fashion, as can be seen from the *Figure 1.7*, Whitcomb has made a different wingtip design. Primary surfaces, upper winglet, was located above the wingtip while smaller and secondary surface was placed forward below the wingtip with different sizes. Wind tunnel investigations (*Figure 1.8*) of this winglet shows that, at design Mach number 0.78, winglet reduced the induced drag effect by about 20% and increased L/D ratio as 9%.

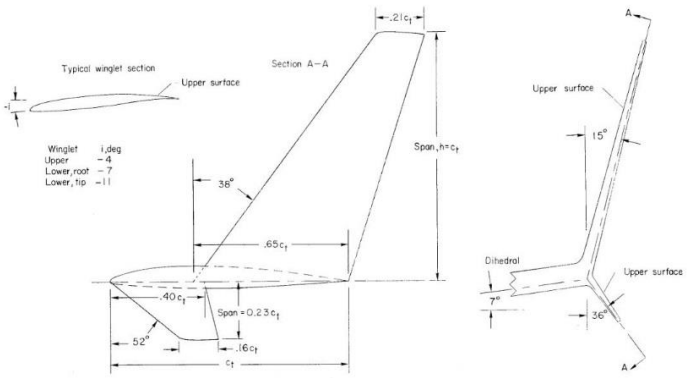

Figure 1.7 Whitcomb's winglet design configuration [6]

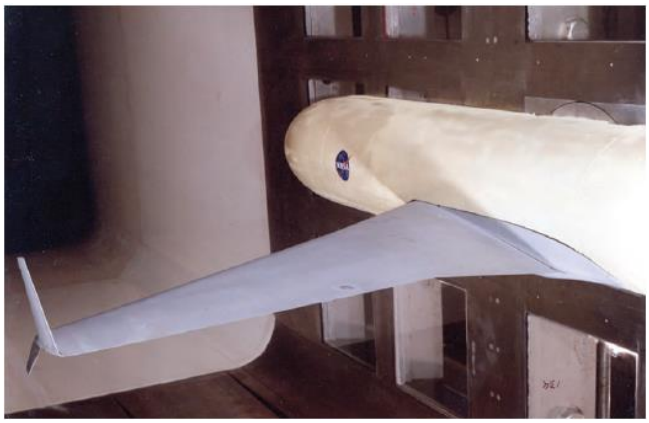

Figure 1.8 Whitcomb winglet on DC-10 model during winglet studies in Langey 8-foot transonic pressure tunnel [7]

Lift induced drag forms 40% of total drag of a commercial aircraft at cruise condition [8]. In this aspect, winglets have great importance to reduce induced drag effect. Studies have been done to show that winglet increases aircraft's range as about 7% at cruise condition [9]. Vari-Eze is the first aircraft that fly with winglets shown in *Figure 1.9*. It is homebuilt aircraft and designed by Burt Rutan in 1974.

Figure 1.9 Vari-Eze homebuilt aircraft is the first aircraft that fly with winglets [10]

Figure 1.10 shows the first jet aircraft, Learjet Model 28 that fly with winglet. Flight test showed that winglets increased range of Learjet Model 28 by about 6.5%.

Figure 1.10 Learjet 28/29, first jet aircraft that fly with winglet [7]

Boeing and Airbus are also use winglet technology in order to improve aerodynamic efficiency of aircrafts'. These companies have tried a lot of different models over the years. *Figure 1.11* and *Figure 1.12* show new generation of aircrafts with winglets of that companies.

Besides the commercial aircraft, winglets are also used on UAVs. *Figure 1.13* illustrates different kinds of UAVs with different winglets. In *Figure 1.13*a, Predator XP was represented. It is high aspect ratio and long endurance (35 hours) UAV that operates at 25.000ft. *Figure 1.13*b demonstrate Scan Eagle UAV. It has 24+ endurance and operate 19.500ft. In *Figure 1.13*c solar powered UAV, Sky Sailor was showed. It has 24 hours endurance.

Figure 1.11Boeing Next-Generation 737 with winglet [11]

Figure 1.12 Airbus A 350 XWB with circular winglet [12]

a) Predator XP [13]

b) Scan Eagle [14]

c) Sky Sailor [15]

Figure 1.13 Winglets on UAVs

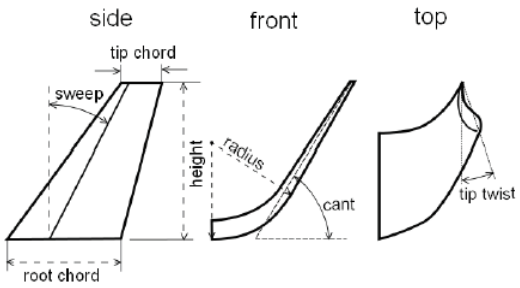

Figure 1.14 Parameters that constitute winglets shape [16]

Cant angle, sweep angle, taper ratio, toe angle, twist angle, airfoil section, height, span, blend radius (for blended winglet) are the parameters that constitute winglets shape shown in *Figure 1.14.* Studies are still continue about the winglets in order to find best design for specific flight conditions. Winglets benefits and drawbacks were listed below.

Benefits of Winglet:

- Induced drag reduction
- Fuel burn reduction
- Takeoff distance reduction
- Carbon emission reduction
- Noise effect (due to vortex) reduction
- Maximum range is increased (more payload)
- Cruise speed and cruise altitude is increased
- $C_{L\,max}$ is increased

Drawbacks of Winglet:

- Wetted area is increased
- Weight is increased
- Structure (static loads, flutter and fatigue)
- Cost

1.2. The Unmanned Air Vehicle

Figure 1.15 TİHAS drawing without winglet

TÜBİTAK Unmanned Aircraft System, TİHAS, which has been designed and built in TÜBİTAK UZAY, uses a solar panel to contribute battery power for flight. It also has auto-landing, automatic navigation, way point and takeoff system. TİHAS has a camera device for different issues like thermal and hyperspectral. It is designed to make an observation for social utilities such as agricultural application, boarding security, forest fire control, city planning and etc. at a low altitude (under 2 kilometers). TİHAS is controlled by remote-control system (autopilot). Components of this system are IMU (inertial measurement unit), Main Control PCB Board, altitude and pressure sensors, telemetry, servo-motors, RF receiver and remote control transmitter. Its technical and physical specifications are presented in *Table 1.1*

Table 1.1 TİHAS specifications

Tihas Specifications	
Chord	0.35 [m]
Wing span	4.5 [m]
Body Length	2.5 [m]
Weight	12 [kg]
Max Ceiling	2000 [m]
Cruise AOA	0° [deg]
Cruise Speed	14 [m/s]
Takeoff distance	100 [m]
Endurance	3-4 hours
Aspect Ratio	12.86

1.3. Motivation

Winglets are small wing like structures at the wingtip used to enhance aerodynamic efficiency of aircraft by decreasing the induced drag. Without adding great structural stress and weight, winglets increase effective aspect ratio of a wing. Motivation of this research is to explore efficient shapes of winglets by using multiple winglet parameters for specific conditions of TİHAS. There are many researches about conventional winglets and some for other types of winglets such as spiroid and blended. However, there are few researches about elliptical winglets. Besides, while there are many studies about the aerodynamic effects of winglets on large aircraft, there are little works about Unmanned Air Vehicles (UAVs). Therefore, using various winglet parameters, 39 different elliptical winglets were designed and analyzed at Reynolds number 309507 to increase the aerodynamic efficiency of TİHAS. Aerodynamic analyses of winglet were performed in ANSYS Fluent by using k-ω turbulence model. It is important to make this research because there is no plenty of works about low altitude UAVs about using multiple winglet parameters.

1.4. Objectives

This research has two objectives, finding best elliptical winglet design which has highest L/D value according to design parameters and numerically performing a CFD analysis on the base wing and wing with elliptical winglet at various AOA and velocities. Hence, aerodynamic performance of TİHAS is enhanced. In design approach, cant angle, sweep angle and taper ratio parameters are used in a triple combination with each other (27 models). Then, toe and twist parameters are applied to winglet separately which has best L/D values in the first 27 models. The analysis were performed on rectangular wing of 2.25 m span and 0.350m chord and wing with elliptical winglet 2.5 m span at low subsonic region. MH 114 airfoil was used both wing and winglet. Aerodynamic characteristics such as C_L, C_D, and L/D were obtained and compared.

CHAPTER 2

LITERATURE SURVEY

2.1. Brief History of Wingtips

The idea of using wingtip on aircraft was first put forward by, a British engineer, Lanchester [17] towards the end of the 1800. According to his idea, using vertical surfaces located at the wingtips can decrease the induced drag effects. He received the first patent of this concept named as “wingtip” in 1897 [18]. Then, in 1910 United States, Scottish born engineer Somerville [19] got a patent for the upward curved wingtips.

Figure 2.1 Somerville biplane with upward curved wingtips [20]

Burnelli [21], American aeronautics engineer, patented the use of end plates. It is demonstrated that using end plates at the wingtip increases the aileron effectiveness by reducing the tip vortex [18]. First implementation of Hoerner-style downward-angled wingtip devices was seen on Heinkel He 162A Spatz jet light fighter. Following the end of the Word War 2, Dr. Hoerner was the first person has done experimental research about dropped wingtips. In this research, tip vortices mechanism was

investigated by doing experiments. Also, different wingtip shapes' aerodynamic characteristics (lift to drag ratio) are studied. Dropped wingtips was named as "Horner tips" because of his honor. In that time, Horner type wingtips were used a lot because of easy construction to wingtips and not increasing the aircraft manufacturing coast. After that, in 1970s, Whitcomb [6], an aeronautical engineer at the NASA Langley Research Centre, made researches about installation of small vertical fins on aircraft's wingtips. This small vertical extension is called as "winglet" by Whitcomb. This winglet designs were tested in 1979-1980 using KC-135 Stratotanker aircraft at Dryden Flight Research Center. Also, a Lockheed L-1011, McDonnell Douglas DC-10 and Boeing KC-135A were used for tests. According to wind tunnel test results, winglet increased the L/D ratio roughly 9% and enhanced the aircraft's range as 7% at cruise condition [6], [22]. Then, Peter et al. [23] showed that using single winglet on biplanes increased the endurance as 13%. Towards the end of 1980s, Peter [24] was the first person researching and applying winglet to a competition sailplanes and had successful results [18]. In the early 1990s, Gratzer [25] patented spiroid and blended winglet. Spiroid winglet improved by Aviation Partners and first seen on a Gulfstream 2. In 1997, Boeing patented the controllable winglet concept [26]. There are also a few types of wingtips (elliptical, scimitar, raked, wingtip fence etc.) other mentioned above used by airlines such as Boeing and Airbus, *Figure 2.2*. Today, wingtip technology continues to develop and besides large aircraft, wingtips are used on UAVs.

Figure 2.2 Airbus A340-400 with conventional winglet

2.2. Studies about Wingtips

About the blended winglet, Nicolas et al. [27] have done research for Dassault Falcon 10 business jet aircraft. Winglet span and cant angle were investigated as a design parameters. Vortex lattice method (VLM) was used to optimize and obtain best winglet configuration calibrated with respect to wind tunnel data. To form aircraft drag polars, RANS model was also used. In order to forecast structural reinforcement, finite element model of wing box was created. In design methodology, Whitcomb-style blended winglet with 0.35 taper ratio, 40° leading edge sweep and twelve combinations of cant angle and winglet span were analyzed. According to results, winglet 1545 shown in *Figure 2.3* was found to be best configuration. This configuration reduced the drag by about 4.8% at Mach 0.7 and reduced by about 2.5% at Mach 0.8. Also, weight was increased as 127lb. At 0.8 Mach, range was increased as 4.3% and fuel burn is reduced by 3.9%. Finally, it is observed that maximum range increased by about 3.3% and fuel is saved by about 3.8%.

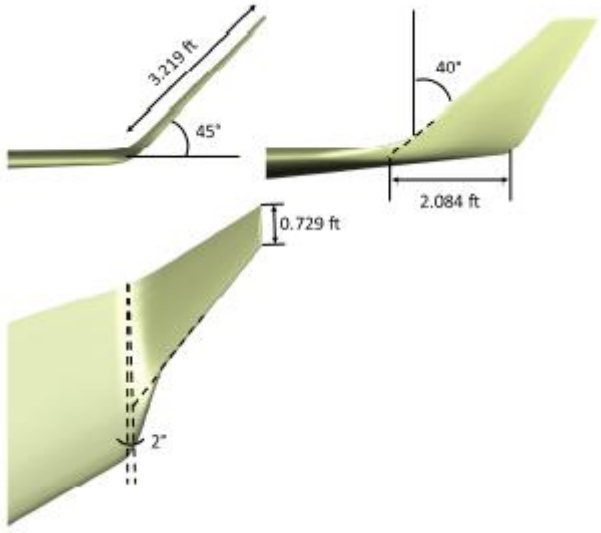

Figure 2.3 Winglet 1545 geometry [27]

Travis et al. [28] have done multi-objective optimization study to evaluate split-winglet design for Standard Cirrus sailplane in terms of benefits and drawbacks. High order potential flow method was used to evaluate the flight performance of designed winglets. Final design of split winglet, *Figure 2.4*, and simple canted winglet (previous work) were compared in terms of aerodynamic efficiencies. Results showed that optimized split-winglet design increased the average cross-country speed of Standard Cirrus sailplane by 8.9% with respect to clean wing configuration. When compared with simple canted winglet (6%), split-winglet had better result. Also, lower surface of split-winglet provides 37% benefit at low speed but at high speed there is parasite drag penalty causes decrease in performance.

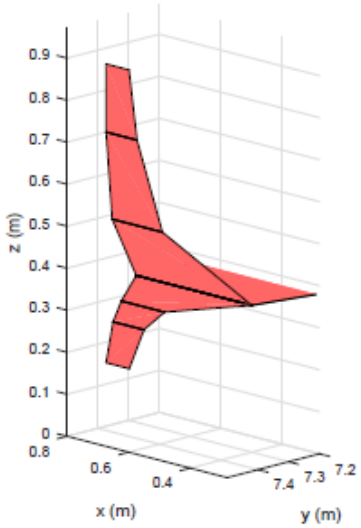

Figure 2.4 Final split winglet design [28]

Designing of a morphing wingtip, Cooper et al. [29] has done a different work. By using chiral-type internal structure, adaptive wingtip concept was improved enabling controlled cant angle, chamber and twist along the flight envelope. The aim of this study was to get optimal configuration at different flight phase in an adaptive manner by parameterizing the cant angle, twist angle and chamber profile. Viscous coupled VCFlite3D code was performed to determine aerodynamic characteristic of models.

Also it was studied that how chiral structure ease the required shape adjustment in terms of cant, twist and chamber. Results showed that, using the morphing wingtip, 2% fuel reduction is provided.

Shahriar et al. [30] have done a numerical optimization study on winglet. They interested in aero structural optimization of wing with winglets. Winglet up, winglet down and raked wingtip designs were studied and compared to optimized planar wings of same span. Boeing 737-900 wing with the RAE 2822 supercritical airfoil was used as a baseline wing geometry. They concluded that winglet down configuration was the most competitive design and it had drag improvement approximately 2%. About the optimization process, Frank et al. [31] made a different approach. Single objective and multi objective evolutionary algorithm optimization methods were used together. During the multi objective optimization study, minimizing drag at cruise condition and thermal flight and reducing the bending moment were aimed. Janus B sailplane a 1978 aircraft shown in *Figure 2.5* was used for winglet design. Winglet height and root chord were discussed as a design parameters. It was concluded that, selected winglet showed the performance by about 3.4% for thermal drag reduction and 0.35% for cruise drag reduction but bending moment is increased as 0.17%.

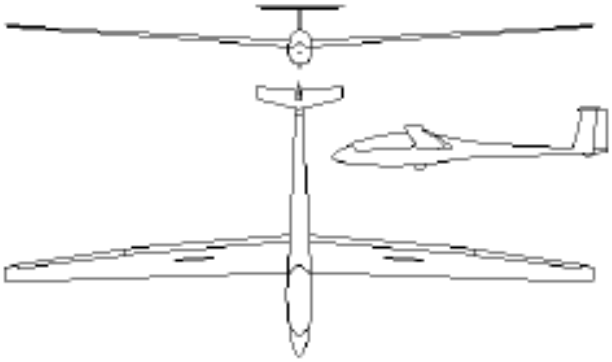

Figure 2.5 Janus B sailplane [31]

Unlike the other morphing winglet studies, Gomes et al. [32] has done some extensive researches about morphing winglet mechanism. In the study of design and analysis of an adaptive wingtip, variable orientation wingtip device was analyzed. By using multidisciplinary optimization procedure, five different scenarios were investigated (maximum endurance, maximum range, minimum stall speed, minimum turn radius and maximum top speed) for varying cant and toe angle parameters. Results demonstrated that 20% reduction for takeoff ground roll was provided. Related to articulated winglet mechanism [33], to investigate viability of variable orientation winglet design, some tests have been done about the actuation capabilities and the system response. Test design consists of wing and winglet with NACA 0012 airfoil connected each other from their spars' with two electric servo actuators (*Figure 2.6*), each one rotating one axis to adjust the winglet's toe and cant angles. As an actuation performance, deflection speed and accuracy were tested and measured after repeated deflection cycles by high definition video captures to evaluate the mechanism's reliability and repeatability. To perform and evaluate the dynamic response of system, dynamic load with a hand-held vibration exciter was used and wing and winglet's motion velocity was measured by laser Doppler velocimetry. Results revealed that the system capabilities are fulfill the intended characteristic.

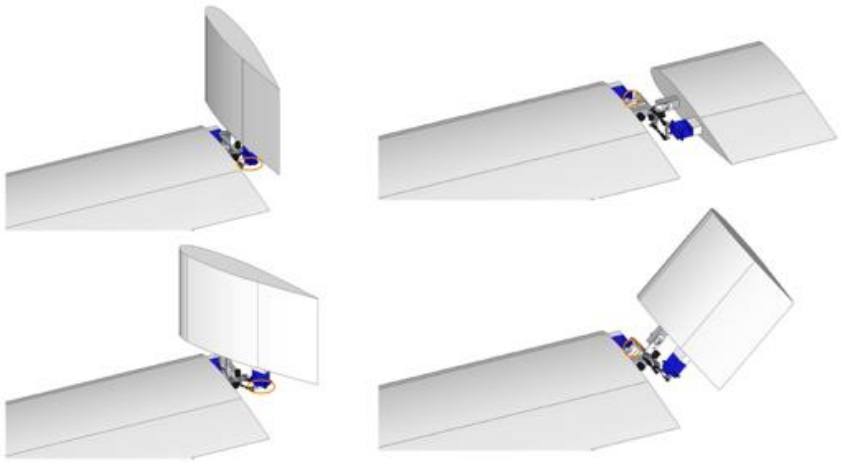

Figure 2.6 Toe and cant changing mechanism [33]

Diaz et al. [34] has studied a combination of two winglet mechanism (winglet and raked wingtip) named as rakelet type winglet for KC-135 Stratotanker aircraft. The aim of this study was to make an assessment the aerodynamic benefits of rakelet wingtip for KC-135 in terms of wingtip size, cant angle, toe out angle and rakelet blending performing in wind tunnel, *Figure 2.7*.

Figure 2.7 Different wingtips model performed in wind tunnel [34]

Tests were carried out using two different scaled models shown in *Figure 2.8*, at Mach number 0.4 and AOA from 0-5 degrees (1° increment) in wind tunnel. 1/76 scaled model was used for size, cant angle and toe out angle optimization. 1/27 model was used for assessment of the effect of blending between the raked wingtip and winglet. At the first stage, five variations of size, cant angle and toe out angle were investigated. Then, four blending configurations were performed. Eventually, optimal configuration were compared to KC-135 without wingtip. Results showed that rakalet configuration of winglet root chord of 100% of the raked wingtip tip chord, 15° cant angle, -2° toe-out angle was optimal configuration. It increased C_L/C_D ratio by about 9.85% and increased $C_L^{1/2}/C_D$ ratio about 7.51% according to baseline wing. Also, about 35% blending assured performance development for endurance and range.

Figure 2.8 1/76 and 1/27 KC-135 scale models in wind tunnel [34]

About the comparison of raked wingtip and blended winglet in terms of investigation of vortices in the wake region, Ryan et al. [35] Hayashibara have done a research. At 0.85 Mach, these two configurations were studied by using Spalart–Allmaras turbulence model in fluent and results compared to clean wing. Results demonstrated that wing with raked wingtip had lowest vorticity vector in vortex wake region and reduced induced drag more than blended winglet. Also, Joram et al. [36] have done a research about comparison of wingletted wing and C wing with planar wing related to drag characteristic. Results revealed that wingletted wing has great performance than C wing.

Andrew et al. [37] have done investigation about both the effects of performance improvement and maneuvering characteristic of active multiple winglets for UAV performance shown in *Figure 2.9*. Several winglet span sizes (4, 8 and 12 inches) and assorted dihedral angle are studied at different AOA and compared with baseline wing in terms of aerodynamic characteristic. In order to assess cruise performance of UAV with and without winglet, PMARC-12 (aerodynamic panel code) and neural network-based analysis were performed. Results showed that the using winglets (passive and active multiple winglets) increased both range and endurance of UAV. A further point, these winglets may be employed in place of control surfaces.

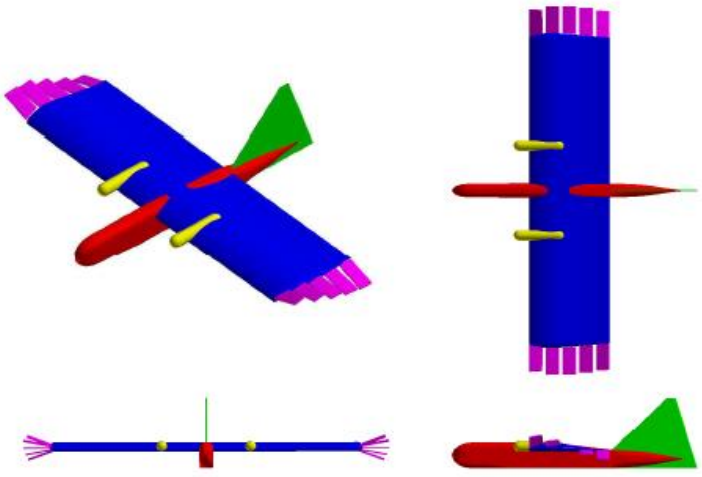

Figure 2.9 Dragon eye configuration with winglets [37]

David et al. [38] have done different research about winglets. As can be seen from the *Figure 2.10*, three different winglet configurations (1 inch up, 3 inches up and 1 inch down) were studied with and without ground effect (2 inches, 4 inches and 6 inches height) at various AOA and three different Reynolds number (Re 1:189.310, Re 2: 231.705, Re 3: 299.202) in wind tunnel. Results showed that 3 inches up winglet has greatest benefit in terms of aerodynamic features. Also 2 inches height showed better values in terms of ground effect.

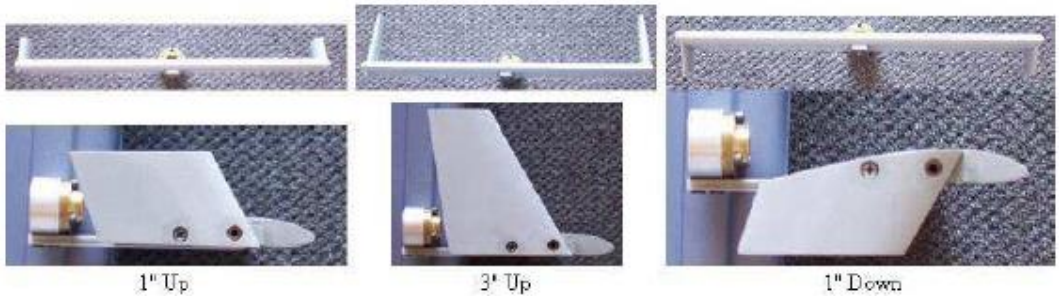

Figure 2.10 Different winglet configurations tested in wind tunnel [38]

Norm [39] has done a research about winglet toe-out angle optimization for the Gates Learjet Longhorn Longhorn wing. Winglet toe out angle effect was investigated on Longhorn model 28 and 55 by testing it in low speed and transonic wind tunnel (*Figure 2.11*). Results showed that, winglet with -2 ° toe out angle has optimum performance. Also, winglet with toe out angle -5° decreased the flow separation in the winglet root at high Mach number.

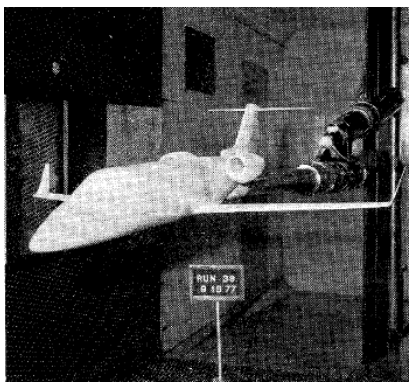

Figure 2.11 Model 55 at Calspan Boeing transonic wind tunnel [39]

About the winglet optimization study for Medium Altitude Long Endurance (MALE) UAV, Panagiotou et al. [40] have done investigation. Five different blended winglet types were designed using PSU 94-097 airfoil shown in *Figure 2.12*. These designs were compared to clean wing in terms of aerodynamic efficiencies. Numerical analysis was performed in CFD at loiter conditions (140 km/h and 2000 m) and Spalart-Allmaras turbulence model was used at various AOA (-8 to 16). According to the results, winglet with cant angle 60° has best aerodynamic efficiency (configuration 5) and increased the flight time 1 hour (10%). Moreover, winglet affects the longitudinal stability of UAV positively but provided no effect on stall angle.

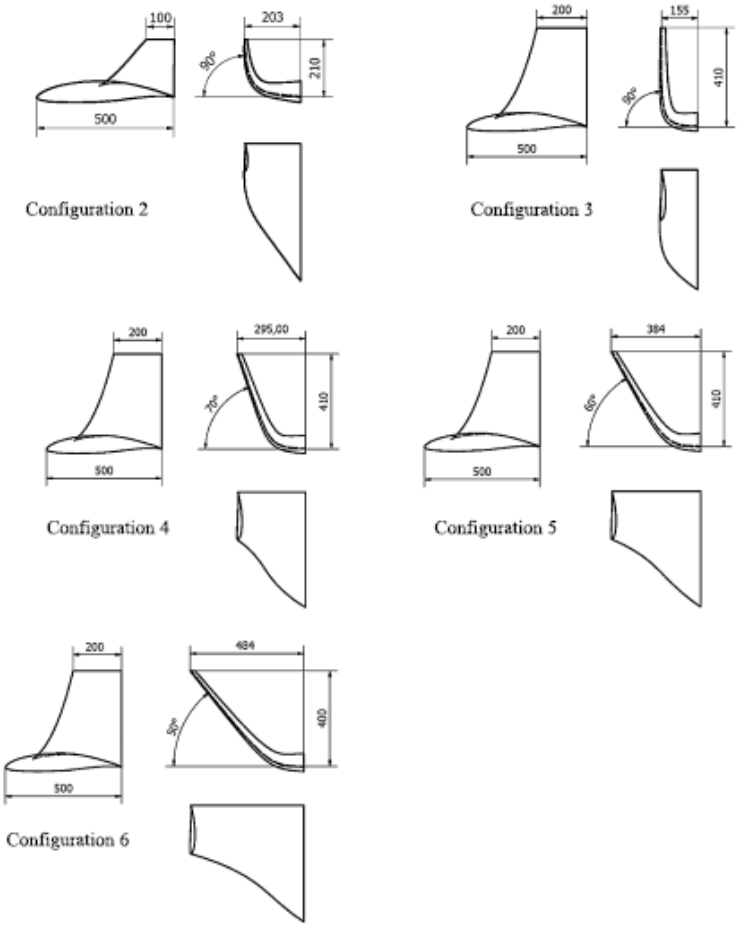

Figure 2.12 Different winglet designs [40]

Bourdin et al. [41] has done research on application of variable cant angle winglets for morphing aircraft control. The system works pair of winglets with adaptive cant angle. Winglets are independently actuated and mounted at the tips of a flying wing. They can take different cant angle between -90° and +90° independently from each other. By modifying cant angle, winglets affect aircraft control. For instance, as it shown below the *Figure 2.13*, changing right winglet cant angle upward and unchanging left winglet position as a planar to wing plane, model has a rolling moment because of lift reduction from the right wing. Also, according to winglets different cant angle, they affect rolling, pitching and yawing moments.

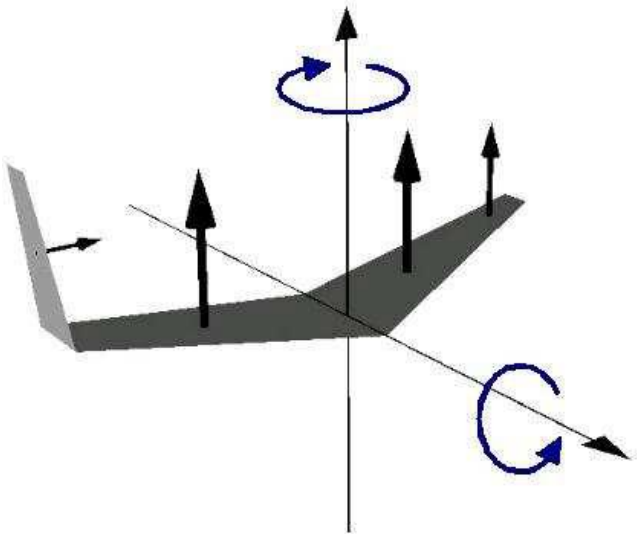

Figure 2.13 An unsymmetric wing-tip arrangement for a sweptback wing to initiate a coordinated turn [41]

In terms of the investigation of effects of variable cant angle winglets on aerodynamic characteristics of aircraft, Beechook [42] has done research for 0°, 30°, 45°, 60° cant angles winglets.

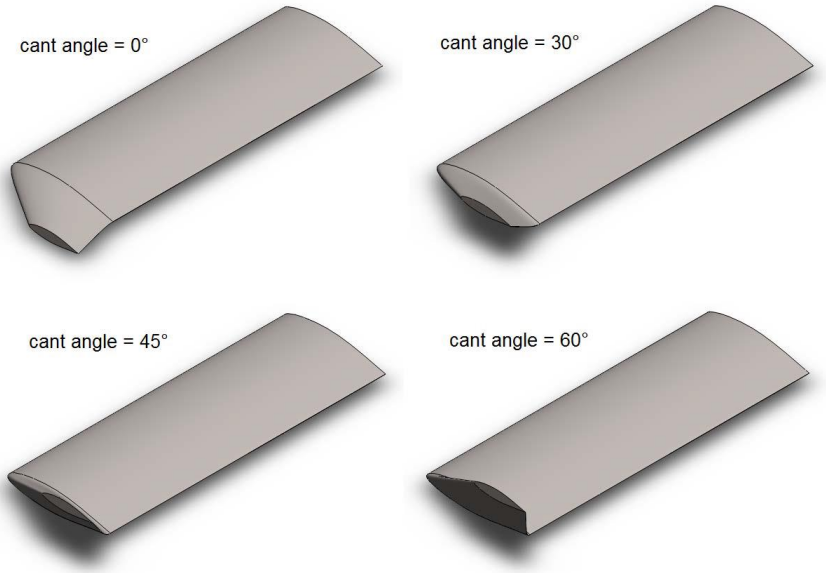

Figure 2.14 Winglet with different cant angle [42]

As can be seen from the *Figure 2.14* above, 4 different wing-winglet configuration were performed using NACA 65_2218 airfoil section. In this study, both experimental (wind tunnel tests, at sea level condition and free-stream velocity of 35 m/s) and computational analysis (ANSYS CFX, Spalart Allmaras tubulence model) have done and results were compared. According to these results, elliptical winglet at 45° cant was found the most efficient configuration and produced highest lift. It improved the lift curve gradient by 8%. Moreover, winglet with cant angle 60° produced less lift as 12% than winglet with cant angle 45° according to CFD results.

Using multiple winglets configurations to reduce wing induced drag and increase L/D ratio is another design approach. Smith [43] made investigation about multi-winglet using a NACA 0012 airfoil section for the untwisted, rectangular wing and flat plates for the winglets. As can be seen from the *Figure 2.15*, wing-winglet configurations have been tested in wind tunnel over a range of Re number from 1.61×10^5 to 3.0×10^5.

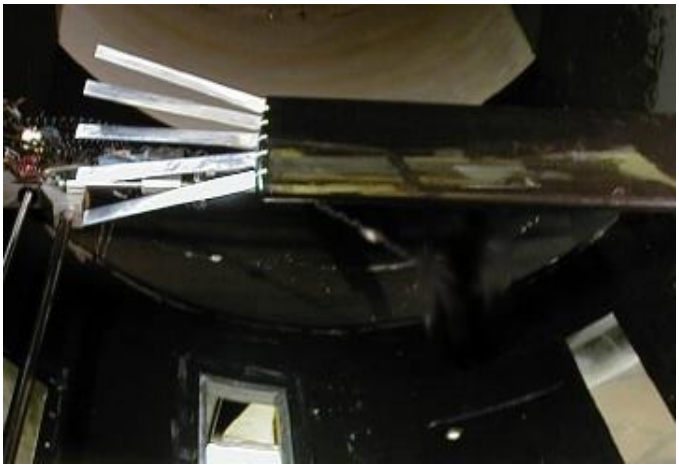

Figure 2.15 Multiple winglet configurations [43]

According to experimental results, L/D ratio was increased 15-30% compared with the baseline wing. Also, negative incidence and twist of the winglets has positive effect to L/D ratio by decreasing the induced drag. At zero incidence, flat plate winglets develop the lift curve slope and produce more lift when comparing the equivalent area of the baseline wing. Moreover, dihedral spread of the winglets increases lift by redistributing the tip vortex into multiple vortices.

Jacob [16] has done a research about investigation of method for designing and optimizing winglet geometry for UAVs at Reynolds number 1 x 10^6. Vortex Lattice Method (VLM) was used and developed as a design methodology. To define optimal winglet geometries, Matlab based TORNADO VLM code was used. Optimized designs were also tested in wind tunnel. Whitcomb and blended type winglets were compared to base design.

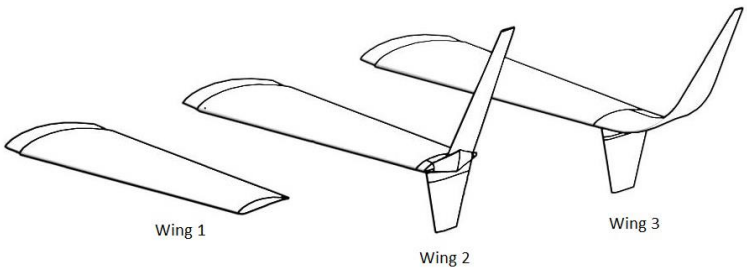

Figure 2.16 Base wing, whitcomb winglet and blended winglet [16]

According to VLM results, blended winglet was found better than Whitcomb winglet. The maximum value for $C_L\backslash C_D$ was increased %28 using optimized blended winglets. As a result of this, endurance is increased 71% and range is increased 28%. However, root bending moment for the blended winglet is greater than the Whitcomb winglet about 5%. As can be seen from the *Figure 2.16*, 3 wing configurations compared about aerodynamic performance. Wing 1 is base wing, wing 2 is wing with lower winglets and a straight upper winglet, wing 3 is wing with lower winglets and blended upper winglets. Based on the results of VLM, wing 1 has $(C_L\backslash C_D)_{max}$=23.46, wing 2 has $(C_L\backslash C_D)_{max}$ =25.43, and wing 3 has $(C_L\backslash C_D)_{max}$ =23.00 values. This trend is not changed according to wind tunnel experiments but results are less than VLM because of the higher drag coefficients. VLM does not model viscous effect, it can only approximate surface drag. In terms of aerodynamic performance, wind tunnel results show that, optimized blended winglet increases the range 31.85% and endurance 38.7%. Whitcomb winglet increases the range 14.49% and the endurance 18.8%.

About the performance investigation of an aircraft wing at various cant angles of winglets, Myilsamy [44] has done a research. As can be seen from the *Figure 2.17* , 3 different wing-winglet configurations are compared in terms of aerodynamic performances.

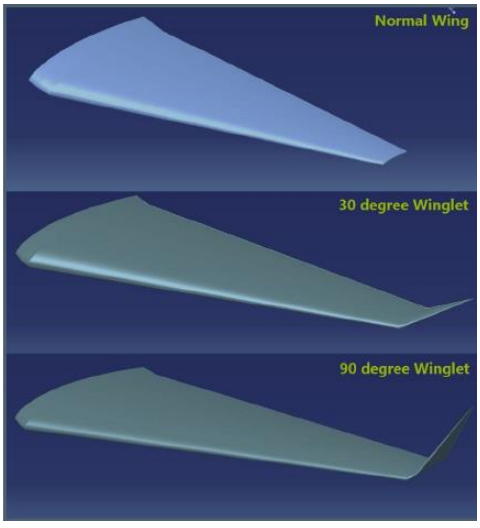

Figure 2.17 Base wing and wing with different cant angle [44]

In design point, just winglet cant angle parameter was used and other parameters are not mentioned. 0° (base wing), 30° and 90° degree cant angle winglets were performed by using NACA 4412 airfoil at different angle of attack from -2° to 10°. Unlike programs used in other studies, AcuSolve CFD program was used for numerical analysis. 3-D steady state pressure based k-ω turbulence model was chosen for calculations. According AcuSolve results, winglet has 90° cant angle gave highest lift coefficient between -2° to 10° AOA. However, aerodynamic performance of winglet cant angle 30° was better up to 2° AOA because of low drag coefficient. Considering takeoff and landing performance, it was resulted that low cant angle at low AOA and high cant angle at high AOA give better results.

Unlike other winglet designs, Hossain et al. [45] has done research about aerodynamic characteristics of bird feather like winglet. In this study, three configurations, wing without winglet, wing with horizontal winglet and wing with 60° degree inclination winglet were tested in wind tunnel for Re $1.66x10^5$, $2.08x10^5$ and $2.50x10^5$ and at various AOA (0°-14°). NACA 65_3218 airfoil was used for wing and winglet structure. According to results, bird feather like winglet increased the lift coefficient by 10-20% and decreases the drag coefficient by 25-30% for at AOA 8°.

Figure 2.18 Bird feather like winglet in wind tunnel [45]

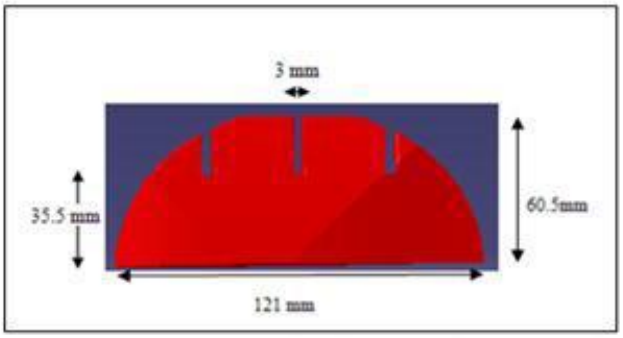

Figure 2.19 Bird feather like winglet [45]

Arora [46] also has done research about elliptical winglet. Aerodynamic performances of winglet configurations were performed again wind tunnel for Re $1.7x10^5$, $2.1x10^5$ and $2.5x10^5$ at various AOA (0°-14°). As can be seen from the figure below, for wind tunnel test, cylindrical body with NACA 65_3218 airfoil rectangular wing was used. Results show that, elliptical winglet 60° inclination has best aerodynamic performance. It increased lift curve slope by 6% compared to wing without winglet configuration. Also, it has best L/D ratio.

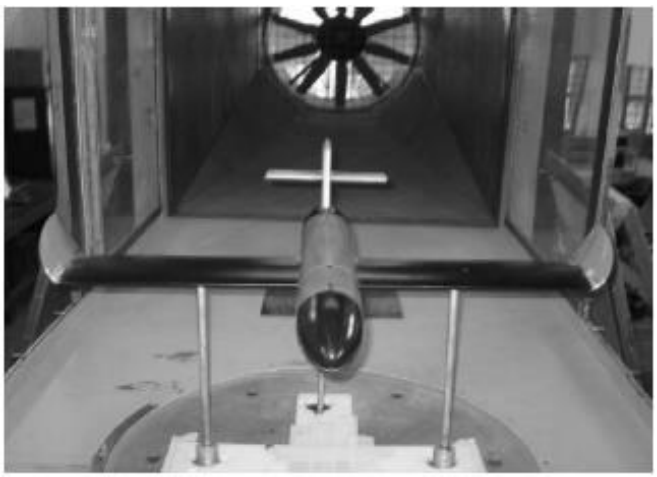

Figure 2.20 Elliptical winglet in wind tunnel [46]

Elliptical and semicircle winglets were close to each other in terms of design approach. Azlin [47] compared the aerodynamic characteristic of these two types of winglet. In this study, NACA 65_3218 airfoil was used for wing and winglets. Computational simulation was done by using Fluent 6.2. Spalart-Allmaras turbulenbce model and coupled implicit solver was used. Analysis performed for four different AOA (0°, 4°, 8°, and 12°) and at three different velocities 40 m/s, 45 m/s and 50 m/s. CFD results showed that elliptical winglet with 45° cant angle gives highest lift coefficient and lowest drag values. Also, compared with others, winglet with 45° cant angle reduced trailing vortices more seen in *Figure 2.21*.

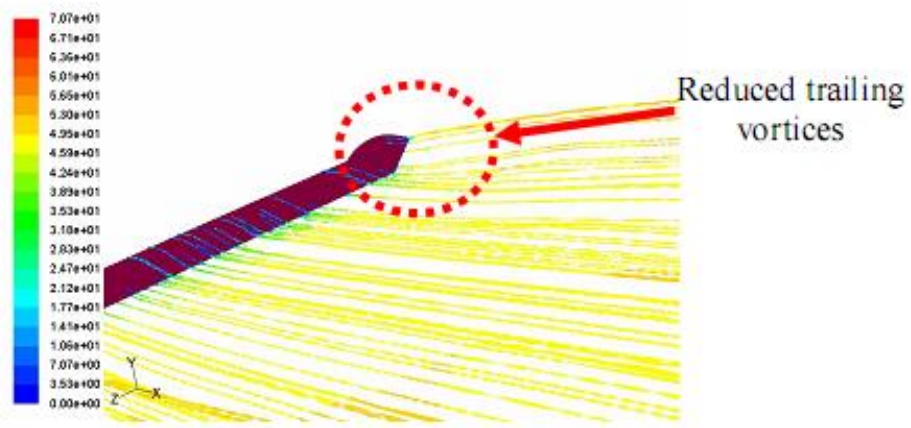

Figure 2.21 Streamline of elliptical winglet [47]

Considering the lift induced drag, winglet usage is very crucial for commercial aircrafts. Lift induced drag constitutes 40% of total drag at cruise conditions and 80-90% at takeoff for typical transport aircraft. To reduce this effect, Nikola [48] made research about effects of several types of winglet configurations on commercial aircraft. Blended winglet, wingtip fence, MAX winglet concept and spiroid winglet are investigated (*Figure 2.22*).

a) Blended winglet

b) Wingtip fence

c) Max winglet

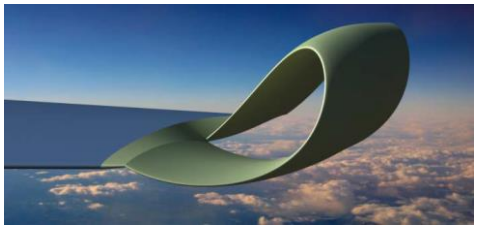

d) Spiroid winglet 1

e) Spiroid winglet 2

Figure 2.22 Blended winglet, wingtip fence, max winglet, spiroid winglet 1 and spiroid winglet 2 [48]

Approximately 100 winglet shapes were analyzed using two geometric parameters height and angle. Numerical simulations were done by using ANSYS Fluent and realizable k-ε turbulence model at Mach number 0.8. According to results, strength of induced drag and vortices was reduced by using winglet. This is very important for the performance of takeoff and landing. When comparing the aerodynamic characteristics of winglet among them, Maxi winglet had the highest improvement but spiroid winglets had poorest improvement. It is because of the wetted surface and larger parasite drag. After 100 analysis, optimized winglet shape was obtained as represented in *Figure 2.23*, by using optimization software Non-Dominated Sorting Generic Algorithm-NSGA 2 in modeFRONTIER.

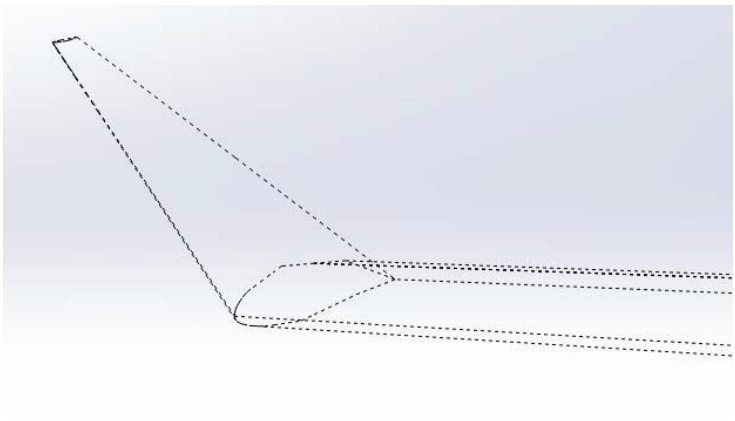

Figure 2.23 Optimized winglet shape in modeFRONTIER [48]

CHAPTER 3

METHODOLOGY

3.1. Winglet Design

To obtain the intended aerodynamic performance over the wide range of operation of an aircraft, it is important to design a new winglet for every application [3]. To reach the desired performance goal, all important winglet parameters must be determined. Cant angle, sweep angle, toe angle, twist angle, taper ratio, height, span and airfoil section are the parameters that determine the aerodynamic characteristic of winglet (*Figure 3.1*).

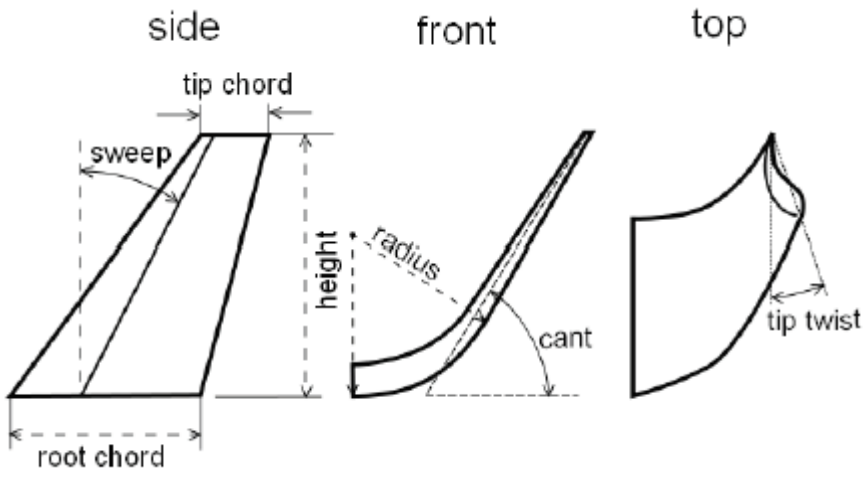

Figure 3.1 Winglet design parameters [16]

It is very complicated problem to find winglet having the desired performance by using all parameters. In this aspect, all winglet parameters should be tried in a different combinations or special optimization tools must be used to get optimum design.

In this study CATIA is used as a design tool. Blended and elliptical winglet shapes are used in a different manner. In blended winglet, there is a radius between wing and winglet and transition region between wing and winglet is not smooth shown in *Figure 3.2*. In elliptical winglet, transition region between wing and winglet is smooth because it uses one ellipse and it cuts from acute angle from ellipse center shown in *Figure 3.3*.

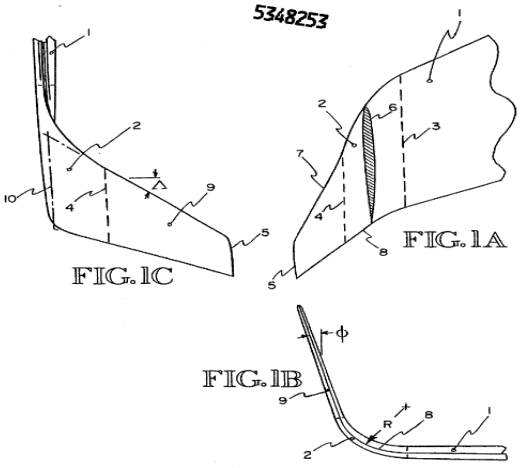

Figure 3.2 Blended winglet [49]

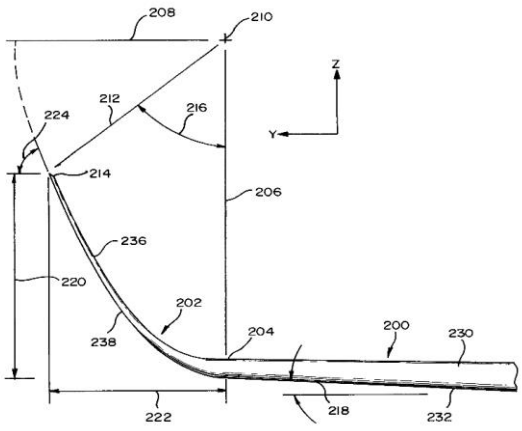

Figure 3.3 Elliptical winglet [50]

This thesis shows a different design approach. As can be seen from the *Figure 3.4*, two same ellipses are used to obtain guide curves of winglet. First ellipse center is intersected with wing tip as a height of chord (350mm) and 250 mm span is a vertical ellipse. Second ellipse center is also intersected with wing tip and constrained to move on the vertical line between first ellipse center and wing tip. Then second ellipse is rotated to left according to XY plane. After that, to achieve the intended winglet guide curve, rotated ellipse is trimmed and joined first ellipse in a design constraint. Unlike the other design, this obtained guide curve is a driving point in the design of a winglet. Compared to blended and elliptical winglet with this design, it differs at some points. For example, there is no fixed bending radius. Instead of this, vertical ellipse (fixed ellipse) forms transition region between wing and second curve (rotated ellipse) in a variable radius. A further point, rotated ellipse build the second region of curve and adjusts the perpendicularity of it in a different way. Hence, according to vertical eclipse rotation or cant angle, consecutive lines being formed. This formed curve constitutes winglet's front and rear guide curves and takes final shape depending on the other parameters. Winglet span and height have dominant effect with cant angle to determine reference area and winglet shape. Also taper ratio adjust winglet root and tip Reynolds number (also affect reference area). Toe and twist angle have less effect compared with them.

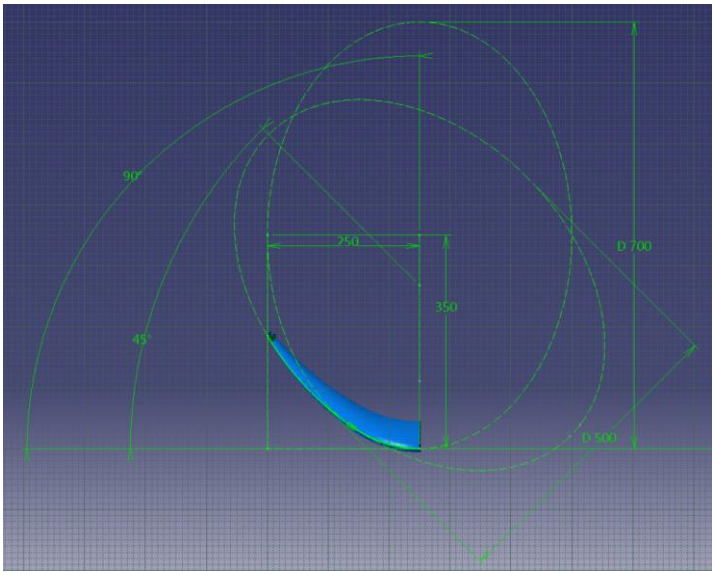

Figure 3.4 Winglet design with two ellipses

According to winglet design parameters mentioned above, 39 different winglets are designed. First of all, three different cant angles (59.4°, 69.3° and 90°), three different sweep angles (0°, 15° and 30°) and three different taper ratios (0.2, 0.3 and 0.4) were handled in a triple combination with each other (27 models). After that, winglet which has the best L/D ratio is chosen to apply toe and twist parameters. Then, six different toe angles (-5°, -3°, -1°, 1°, 3°, 5°) and six different twist angles (-5°, -3°, -1°, 1°, 3°, 5°) are deployed separately as represented in *Figure 3.5*. Ultimately, winglet has best L/D is picked out to compare aerodynamic efficiency with clean wing. Ongoing sections, it will be explained that how winglet parameters are generated in detail.

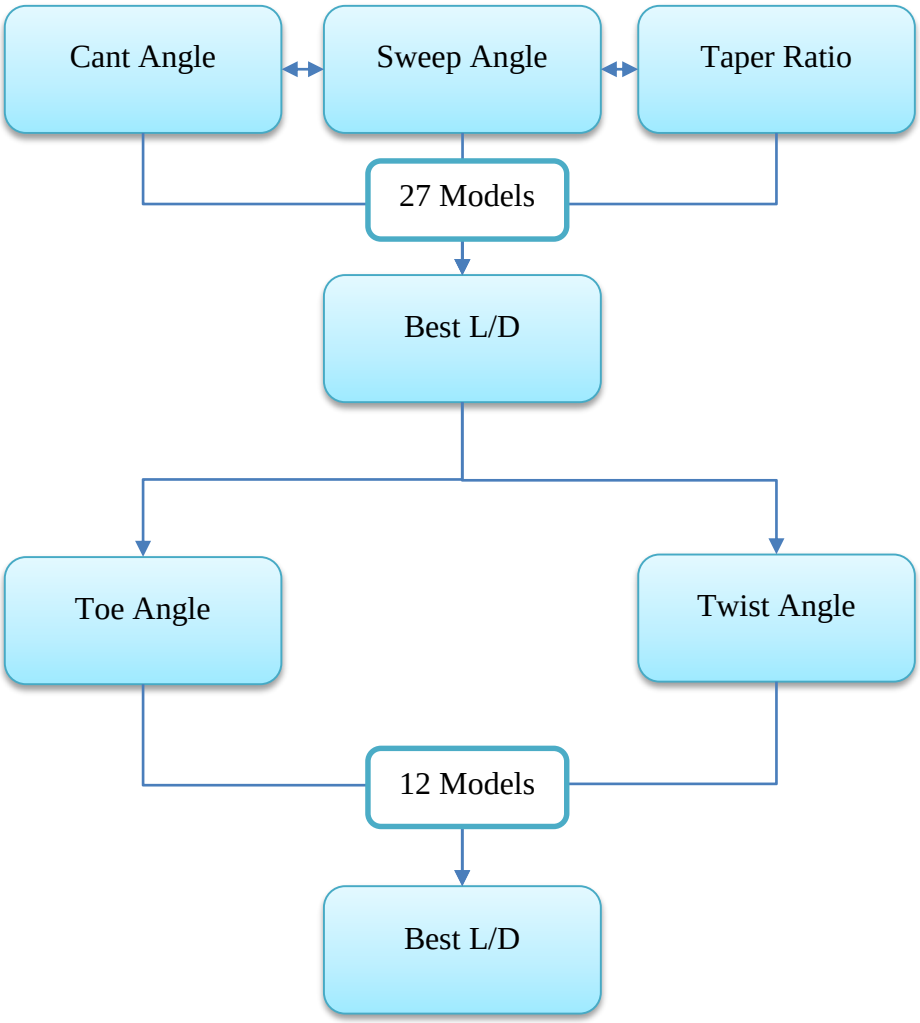

Figure 3.5 Design flow chart

3.1.1. Airfoil

Since the winglet does not work as the wing does, airfoil section is one of the most important part of the winglet design. Because of this, according to aircraft operational condition, selection of airfoil determines the performance of winglet for different Reynolds number. Maughmer et al. [51] investigation's states that winglet airfoil must work a wide range of Reynold number because winglet's small chord makes Reynold number low. As a result of his study, PSU 94-097 airfoil was designed for low Reynolds number regime ($2.4x10^5$ – $1.0x10^6$).

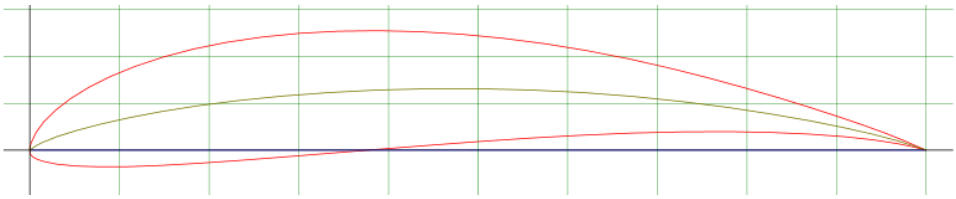

Figure 3.6 MH 114 13.02% (mh114-il) airfoil [52]

Since the TİHAS's wing operates at low Reynold number regime ($3.1x10^5$) and wing airfoil was selected for low speed conditions, airfoil design and selection have not been performed. Therefore, airfoil which was used in wing, *Figure 3.6*, was employed for winglet root and tip shown in *Figure 3.7*.

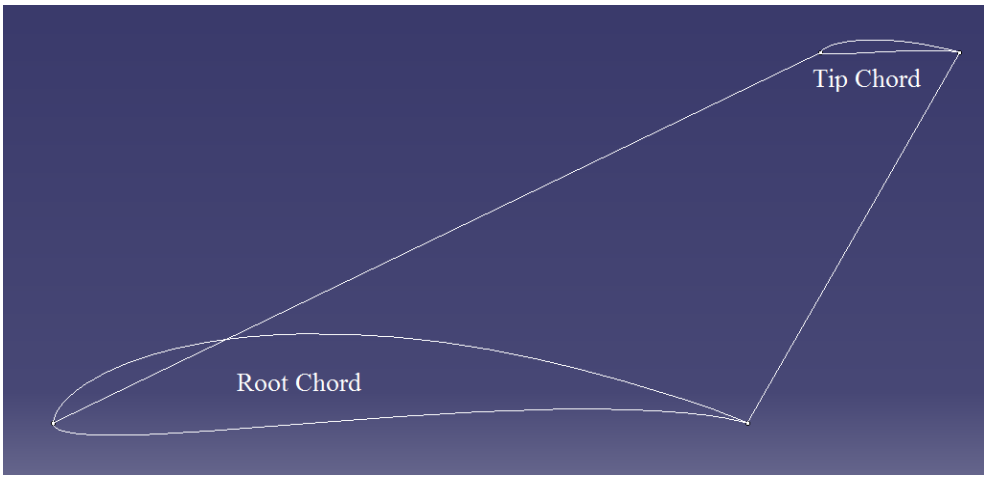

Figure 3.7 Winglet root and tip airfoil

3.1.2. Winglet Height and Span

Height and span are one of the most important parameters of the winglet. If there is a span limitation or an existing wing must be modified for high performance, winglets may provide a major advantage [16]. Also, according to Jansen et al. [53] when considering aerostructural optimization approach if there is a span constraint, wing with winglet is the optimal design. In TİHAS specifications, there is a wing span constraint up to 5 meters. Because of this, winglet span was set as the maximum value to 250 mm (wing span of TİHAS is 4.5 meters). Unlike other design parameters, winglet span is kept constant for all conditions even if other parameters change. Thus, winglet span is being a limiting parameter in this study according to others illustrated in *Figure 3.8*.

Because of structural weight, parasite drag and solar cells (shadow effect), winglet height was not adjusted so much. It was set 350 mm (as chord length) as a maximum value and it varies depending on change of cant angle (vertical eclipse rotations). As mentioned in winglet design part 3.1, three different cant angle were formed. Winglet height takes its maximum value when cant angle is 90° and takes minimum value when cant is 45°. Winglet span is also becoming limiting factor in this regard.

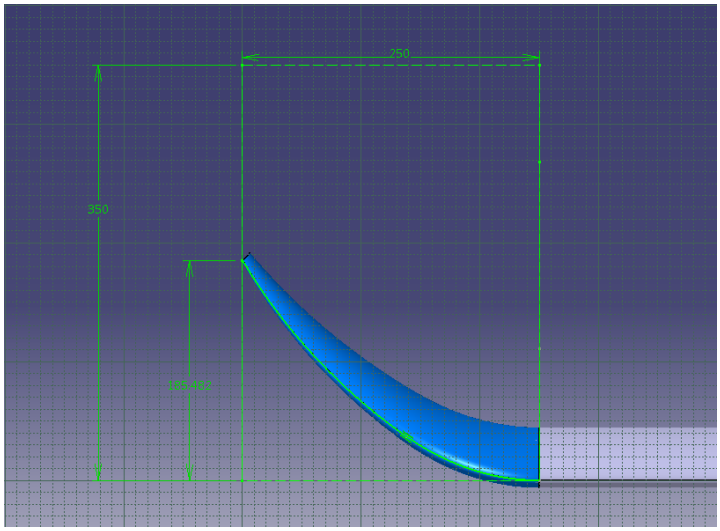

Figure 3.8 Winglet height and span

3.1.3. Cant Angle

Cant angle is determinative and the most important winglet parameter to assess about aerodynamic efficiency of wing and winglet. As Takenaka et al. [54] stressed in his work, cant angle and span length (explained previous section) have dominant effect for drag reduction.

In this study, cant angle is decisive parameter that determines the shape of the winglet. To form winglet cant angle, two similar ellipses is used. First ellipse center is intersected with wing tip as a 350 mm height and 250 mm span is a vertical ellipse and it is fixed this point. Second ellipse center is also intersected with wing tip and constrained to move on the vertical line between first ellipse center and wing tip. Then second ellipse is rotated to left according to XY plane. After that, to achieve the intended winglet guide curve, rotated ellipse is trimmed and joined first ellipse in a design constraint. Thus, smooth junction region between wing and winglet is constituted. The transition area between wing and winglet is very crucial in terms of formation of wave drag especially at high cant angles [27]. Therefore, different design pattern is tried and an elliptical transition region is formed between the wing and winglet to overcome wave drag effect.

Three different cant angle is generated by rotating one of the ellipse (second ellipse) for 45°, 60° and 90° (90° means no rotation) as illustrated in *Figure 3.10*. As a result of these rotation, corresponding cant angles formed between curves and horizontal axis are 59.38°, 69.25° and 90° (*Figure 3.9)*. Also, according to these cant angle, transition region curvature, span and angle is also changed but transition region between wing and winglet remains elliptical. Because of its shape, ellipse can rotate maximum 42° while creating cant angle. After 42° degree, vertical fixed ellipse and rotating ellipse cannot intersect tangential. Therefore, 45° ellipse rotation and corresponding cant angle 69.25° can be tested as a minimum.

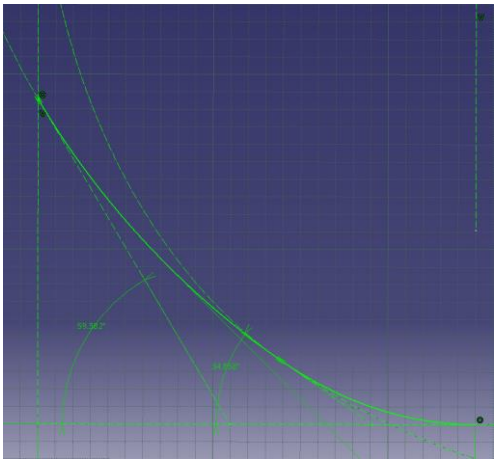

a) 45° Ellipse rotation (cant angle 59.38°)

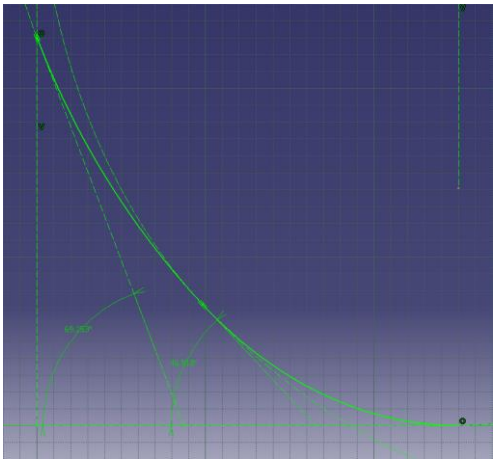

b) 60° Ellipse rotation (cant angle 69.25°)

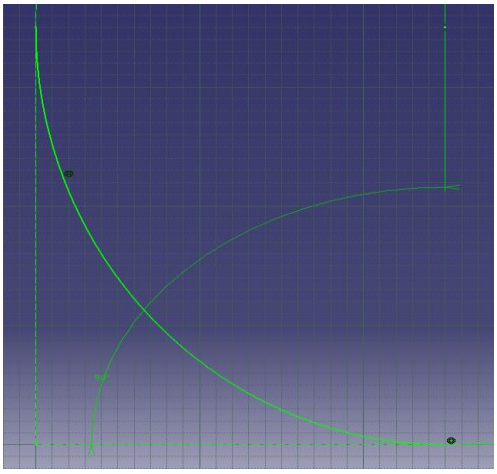

c) 90° Ellipse Rotation (Cant Angle 90°)

Figure 3.9 Winglet guide curves based on cant angles

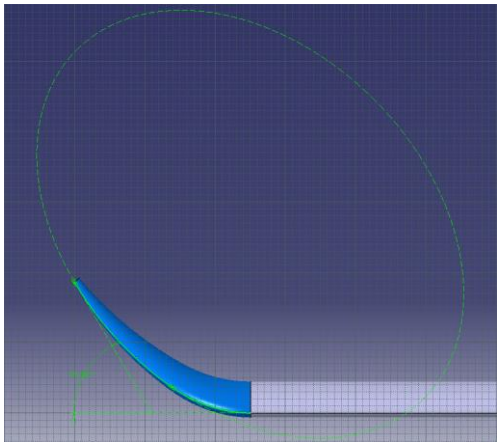

a) *Winglet Cant 59.4° according to second ellipse rotation (45° ellipse rotation)*

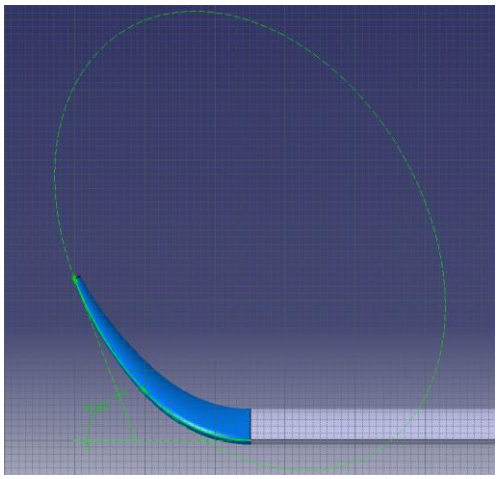

b) *Winglet Cant 69.3° according to second ellipse rotation (60° ellipse rotation)*

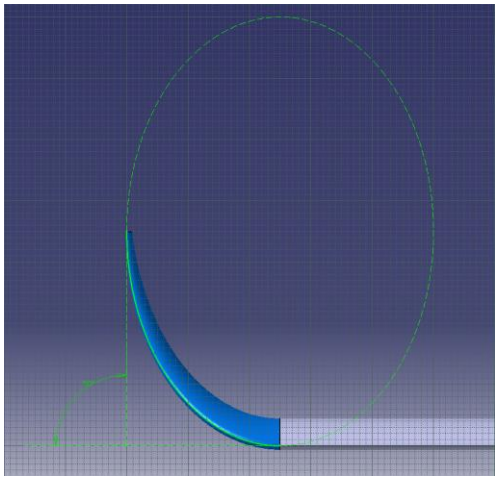

c) *Winglet Cant 90° according to second ellipse rotation (90° ellipse rotation)*

Figure 3.10 Winglet cant angles change according to rotation of ellipse

3.1.4. Taper Ratio and Sweep Angle

After determining the winglet guide curves and cant angles, taper ratio and sweep angle parameters are performed related to them. Three different taper ratios were utilized (λ= 0.2, 0.3 and 0.4) and winglet tip chord section was tapered according to trailing edge, as demonstrated in *Figure 3.11*.

Aircraft static directional stability increases with winglet sweep angle [39]. Since winglet's leading edge sweep angles change according to winglet's tip chord taper ratios change, aft sweep angle generation was preferred as shown in *Figure 3.12*. Three different sweep angles were utilized (Λ = 0°, 15°and 30°).

Since sweep angle works associated with taper ratio, after giving taper ratio, winglet tip chord section translated as sweep angle as through the backward and sweep angle was created related to it. After that, winglet guide curves are rebuild according to these parameters without adjusting the original shape.

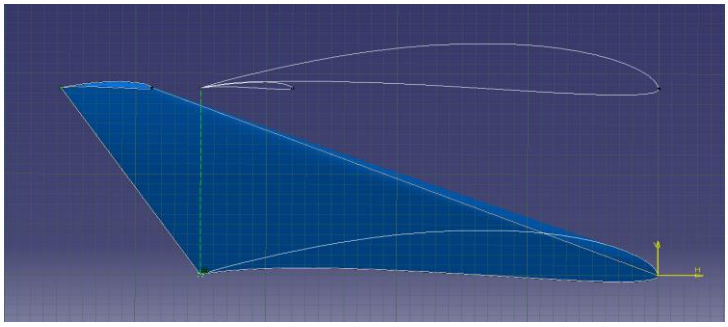

Figure 3.11 Taper ratio, λ =0.2

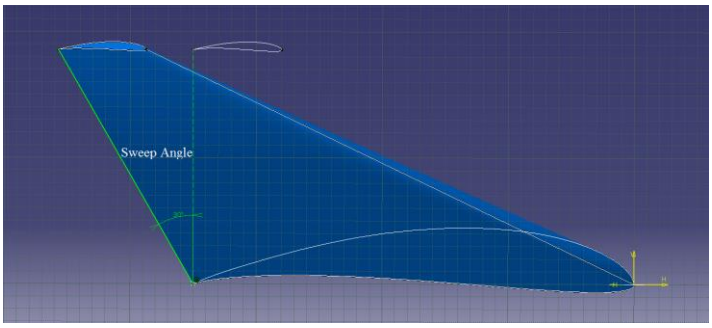

Figure 3.12 Winglet sweep angle, Λ= 30°

3.1.5. Twist and Toe Angle

After performing cant angles, sweep angles and taper ratios, twist angles and toe angles were carried out separately for winglet has best L/D. Twist angle is utilized in order to provide a uniform load distribution on winglet and toe angle varies according to different flight conditions to yield effective lift force for a wing in the horizontal position [16].

Twist angle was created by rotating the winglet tip airfoil section about the axis passing through the quarter chord of winglet tip airfoil as shown in *Figure 3.13*. Six different twist angles are utilized (-5°, -3°, -1°, 1°, 3°, 5°). After generation twist angle, the curves (rear and front guide curves formed by two ellipses) used to form shape to the winglets must be modified because winglet tip airfoil section's angle of attack is changed. Hence, the guide curves starting from wing root and joining the wingtips do not intersect winglet tip airfoil. In order to form new guide curves without adjusting the original shape of them, firstly, fifty points were created on original winglet guide curves and a hundred points were created on wing leading edge. Then, to create new guide curves, four points from wingtip side (to provide smooth transition) and first twenty points from winglet root side were taken as a starting point then joined twisted winglet tip airfoil section's leading edge and trailing edge points.

Winglet was rotated with respect to vertical lines passing through the wingtip leading edge and trailing edge points to generate toe angles. Six different toe angles were utilized (-5°, -3°, -1°, 1°, 3°, 5°). As can be seen from *Figure 3.14*, in order to generate toe in angle, winglet was rotated to wing leading edge vertical line and to generate toe out angle it was rotated to wing trailing edge vertical line. As being twist angle creation, after rotation of winglet, origin guide curves must be modified because when winglet toed in, leading edge of winglet exceeds wing leading edge horizontal line and trailing edge of winglet gets in the wing trailing edge horizontal line. To preserve original shape of guide curves, the same process was carried out (again fifty points were created on winglet guide curves and a hundred point created on wing's leading and trailing edge horizontal lines) in order to create new guide curves for toe angles as was done in twist angle.

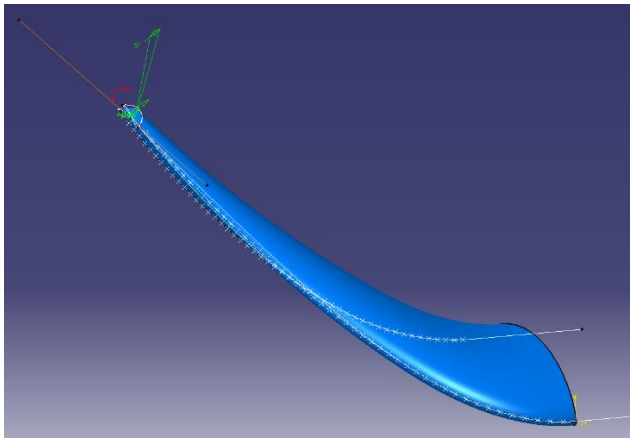

Figure 3.13 Twist angle: -5°

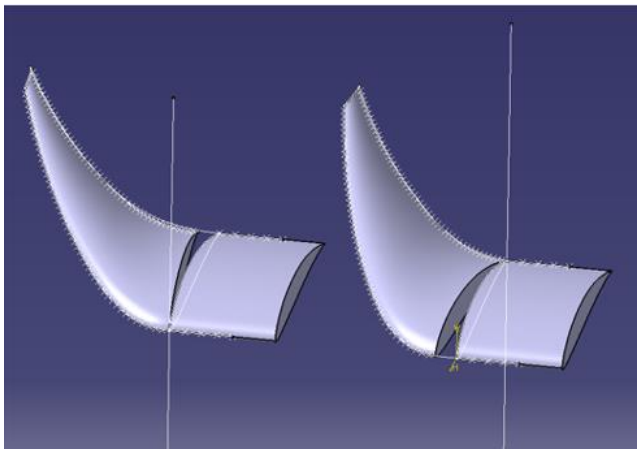

Figure 3.14 Front view of toe in 5° and toe out angle 5°

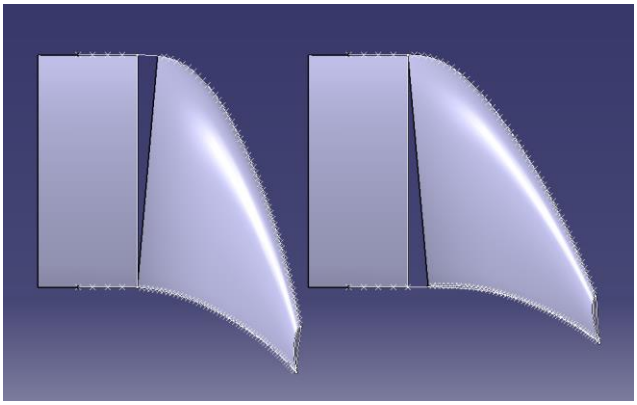

Figure 3.15 Top view of toe out 5° and toe in angle 5°

3.2. Numerical Analysis

Numerical analysis consist of 4 parts: enclosure volume creation, meshing, fluent analysis and post processing parts. The first three will be explained following parts and the post-processing results are presented in the following chapter. Analysis are performed with a high performance computer having 120 processor using 8 clusters.

3.2.1. Enclosure Volume

Instead of using ANSYS design modeler or spaceclaim, flow domain was created by using CATIA. Models are not too complex and because of this there is no need to use spaceclaim model corrections before the meshing part. Two different volumes were defined one of them was to be used in body sizing (form smaller elements around the wing and winglet). Then wing and wing with winglet models were subtracted from these two volumes to create enclosure volume around the models. As can be seen from the *Figure 3.16* enclosure volume sizes are identified according to chord size. To make a better post process and obtain a better results, rectangular enclosure volume is chosen. In order to see the wall effects on flow characteristic, four different sized flow domains are generated and one of them is used for CFD analysis.

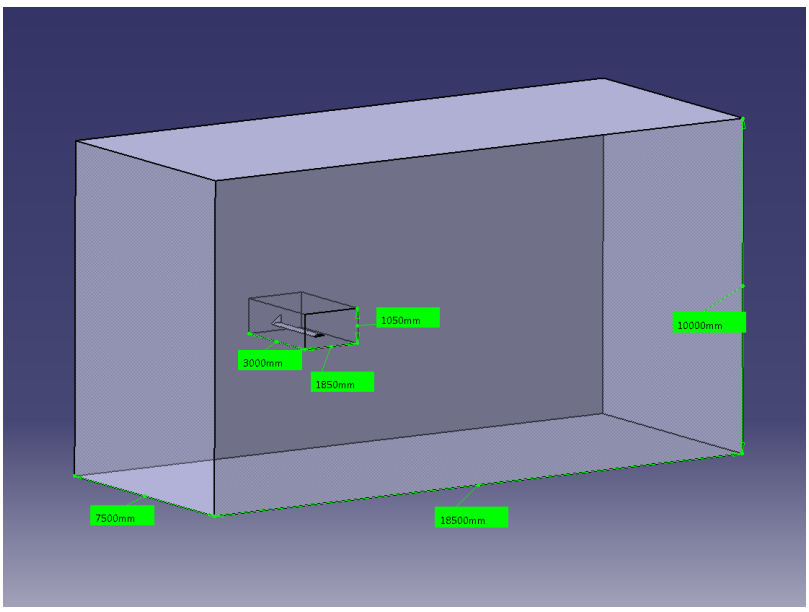

Figure 3.16 Enclosure volume from CATIA

3.2.2. Mesh

Because of the complexity of the model (in term of mesh creation), unstructured tetrahedral mesh is used. Since the airfoil has curvature shape, as an advanced size function, proximity and curvature was chosen. Advanced size function parameters (Min and Max sizes) was determined according to chord length and element number. Max size was set to 250 mm to not exceed to chord length and min size was set to 50 mm. Relevance center was defined as a fine. It allows the program to control the fineness of the mesh for whole model. To increase the element quality by moving locations of nodes with respect to surrounding nodes and elements, smoothing was adjusted to high. To obtain smooth transition between growing elements, transition was defined as slow. Curvature normal angle works with curvature advanced size function and its default value is 18°. To pass curvature regions (for example leading edge) smoothly and get fine mesh, it was reduced to 14°. Patch conforming, patch independency and defeaturing options were left to the control of program depending on the other settings. After a long term sizing iterations, these measurement that shown in *Table 3.1* were selected to get optimum mesh.

Table 3.1 Global mesh settings

Global Mesh Parameters	
Advnced Size Function	Proximety and Curvature
Relevance Center	Fine
Initial Size Seed	Acvtive Assembly
Smoothing	High
Transition	Slow
Span Angle Center	Fine
Curvature Normal Angle	14°
Num Cell Across Gap	2
Proximity Size Funciton Sources	Face and Edges
Min Size	50 mm
Proximity Min Size	50 mm
Max Face Size	250 mm
Max Size	250 mm
Growth Rate	Default (1.20)

3.2.2.1. Boundary Layer

Boundary layer creation is one of the most important part of meshing. In order to observe aerodynamic effects and obtain results accurately, first layer thickness (Y+) and total thickness (δ) must be calculated. The Schlichting skin-friction formula [55] was used to forecast the local skin-friction for a turbulent boundary layer. It is valid for Re < 10^9.

Y+ calculation:

Reynolds Number Calculation:

$$Re = \frac{\rho \cdot U \cdot L}{\mu} \tag{3.1}$$

Schlichting skin-friction correlation:

$$C_f = [2\log_{10}(Re_x) - 0.65]^{-2.3} \qquad \text{for} \qquad Re < 10^9 \tag{3.2}$$

Wall shear stress:

$$\tau_w = C_f \cdot \frac{1}{2} \rho U_{freestream}^2 \tag{3.3}$$

Friction velocity:

$$u_* = \sqrt{\frac{\tau_\omega}{\rho}} \tag{3.4}$$

Wall distance:

$$y = \frac{y^+ \mu}{\rho u_*} \tag{3.5}$$

According to equations above, estimated firs layer wall distance is 2.3e^{-5}m.

Then, laminar boundary layer thickness is determined by using eqn. 3.6 [2].

$$\delta = \frac{5.0x}{\sqrt{Re_x}} \tag{3.6}$$

According to chord length and Re number, laminar boundary layer thickness is calculated as a 3.15 mm. To reach the calculated total thickness, using first layer thickness and growth rate, maximum layers are found 18 layers. However, since the airfoil geometry shrinks at the trailing edge, boundary layer mesh height remains below the desired value at wing trailing edge. Also, last element height of inflation layer mesh is low according to element just above the inflation layer. In order to arrange the ratio between the last element height of inflation layer and first element above the inflation layer, maximum layers value was taken 25.

Table 3.2 Boundary mesh settings

Inflation Mesh Parameters	
Scoping Method	Geometry Selection
Geometry	1 Body
Boundary Scoping Method	Named Seleciton
Boundary	Wing
Inflation Option	Firts Layer Thickness
First Layer Height	2.3e-002mm
Maximum Layers	25
Growth Rate	1.2
Inflation Algoritm	Pre

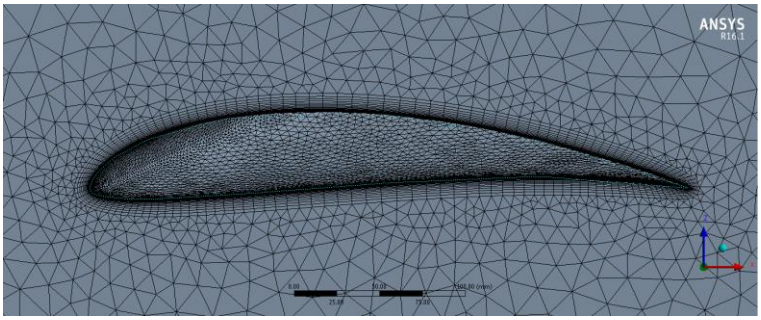

Figure 3.17 Mesh around the airfoil

3.2.2.2. Edge Sizing

To capture the full geometry of wing and winglet (airfoil) with creating elements, edge sizing is used locally. 4 edges were selected for baseline wing and 6 edges was selected for wing with winglet (root and tip). To get smaller elements at leading and trailing edge, bias type sizing is used as shown in *Figure 3.18*. Smooth transition was used as a bias option and growth rate is adjusted 1.04 to get fine cell distribution from leading to trailing edge. Sizing values were chosen as 5 mm for maximum and 2 mm for minimum and behavior was set to soft. This provides to mesh algorithm ease to create fine and small cells at curved and difficult sides.

Table 3.3 Edge sizing settings

Edge Sizing Parameters	
Scoping Method	Geometry Selection
Geometry	4 Edges
Type	Element Size
Element Size	5 mm
Behaviour	Soft
Curvature Normal Angle	Default (14°)
Growth Rate	Default (1.2)
Bias Type	– ––– ––––– ––– –
Bias Option	Smooth Transition
Bias Growth Rate	1.04
Local Min Size	2 mm

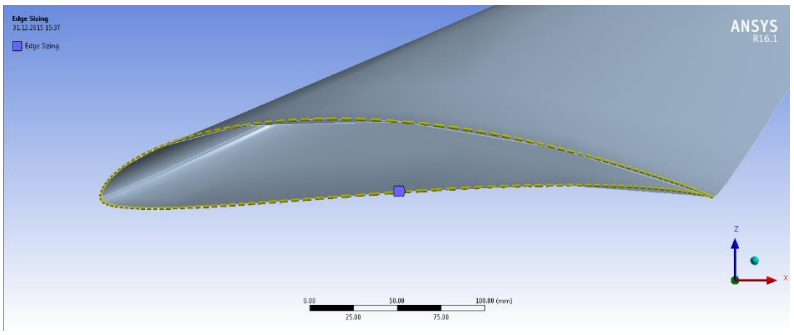

Figure 3.18 Edge sizing with bias factor

3.2.2.3. Face Sizing

After edge sizing performed, to divide more qualified cells to surface of the wing and winglet, face sizing was used. Since the wing and winglet geometry shrinks at trailing edge, it is hard to generate fine elements for mesh algorithm. Therefore, in addition to the edge sizing, it is needed to dimension surface sizing. As being in the edge sizing, 5-2 mm sizing was selected and element creation behavior was chosen soft.

Table 3.4 Face sizing

Face Sizing Parameters	
Scoping Method	Named Selection
Named Selection	Wing
Type	Element Size
Element Size	5 mm
Behaviour	Soft
Curvature Normal Angle	Soft
Growth Rate	Default
Local Min Size	2 mm

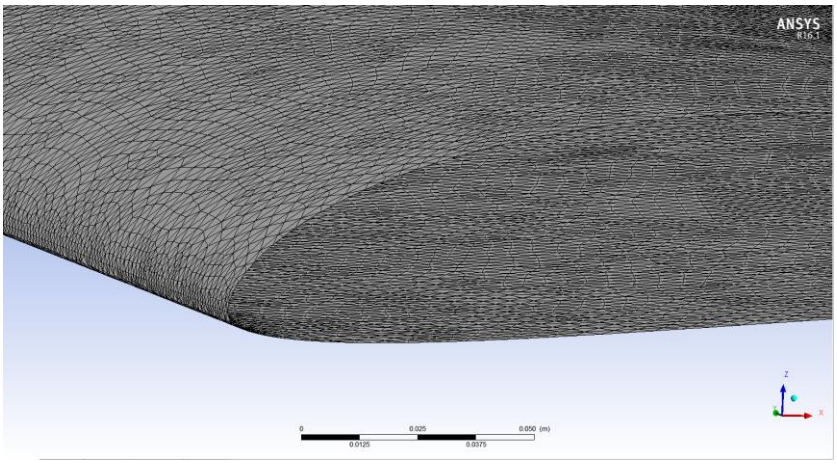

Figure 3.19 Face sizing of the wing

3.2.2.4. Body Sizing

Since the convergence and run time mostly depend on mesh number, it is crucial to operate with adequate elements. Other than mesh refinement, it is important to create fine elements around the wing and winglet to obtain better results and hold the convergence time short. Hence, to keep the number of element in the optimum and work with less cells, body sizing function was used. *Table 3.5* shows body sizing parameters used in domain. As indicated *Figure 3.20*, elements start to grow with minimum size (2 mm) from wing and winglet surface to end of the border line of first body. Then, elements continue to grow from first body with 50 mm to second body's end of the border line to be 250 mm maximum size.

Table 3.5 Body sizing

Body Sizing Parameters	
Scoping Method	Geometry Selection
Geometry	1 Body
Type	Body of Influence
Bodies of Influence	1 Body
Element Size	50 mm
Growth Rate	Default
Local Min Size	2 mm

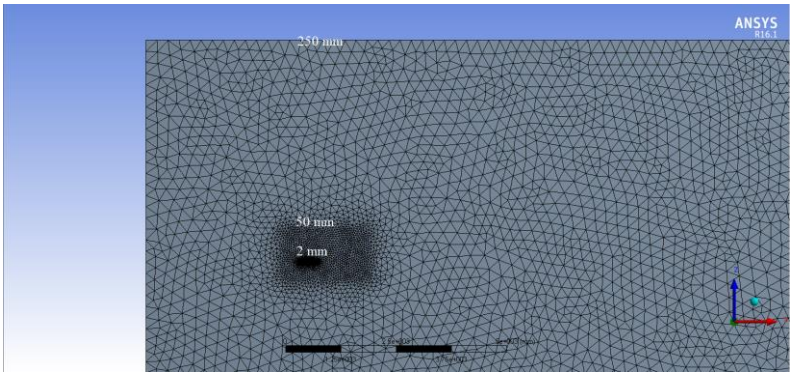

Figure 3.20 Elements grow form the wing surface with 2mm and reach the first maximum value at first body wall as 50 mm. Then they continue to grow and take the maximum value at outer wall as 250 mm

3.2.2.5. Mesh Metric

After mesh generation, mesh quality was evaluated by using mesh metric options. Regard with the convergence criteria, mesh skewness was checked. In ANSYS equations solvers assume that cells are relatively equilateral or equiangular (*Figure 3.21*). For this reason, highly skewed face and cells are unacceptable and cannot be solved. According to skewness definition, represented in *Table 3.6*, "0" value shows that an equilateral cell (best) and "1" shows a completely degenerate cell (the worst). In this study, skewness value of cells is measured approximately between 0.95 - 0.96. Ansys can solve the equations where the skewness value is up to 0.98 but convergence time is getting longer.

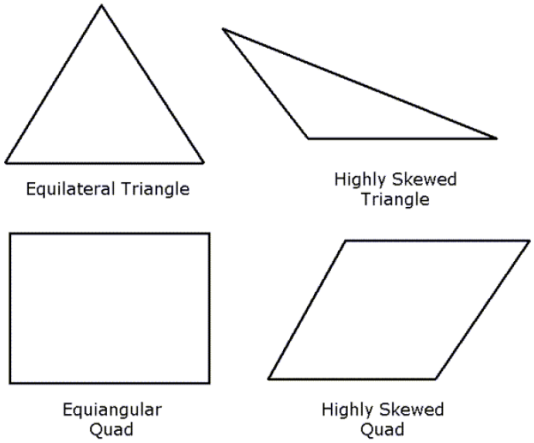

Figure 3.21 Skewness [56]

Table 3.6 Skewness Quality table [56]

Value of Skewness	Cell Quality
1	degenerate
0.9 — <1	bad (sliver)
0.75 — 0.9	poor
0.5 — 0.75	fair
0.25 — 0.5	good
>0 — 0.25	excellent
0	equilateral

3.2.2.6. Mesh Refinement

Mesh refinement calculations were done on baseline wing. As can be seen from the *Table 3.7*, four different sizing were performed. Face and edge sizing parameters were just altered. Body sizing and global mesh sizing settings were not adjusted while making mesh improvement operations because they had insignificant effects on C_L and C_D values.

When face and edge size are reduced and number of elements are increased, mesh refinement curve shows an asymptotic behavior and close to convergence *Figure 3.22*. After CFD runs, middle mesh was selected for all calculations to keep short duration for solutions. *Figure 3.23* shows detailed volume mesh quality from course mesh to fine mesh that analyzed in CFD.

Table 3.7 Mesh refinement values (clean wing)

Mesh Refinement				
	Course-1	Course-2	Middle	Fine
Elenement Number	1853099	2958732	7010005	21690457
Face and Edge Values	20 - 8 mm	10-4mm	5 - 2 mm	2.5 - 1 mm
C_L Values	0.71352	0.67664	0.64344	0.63646

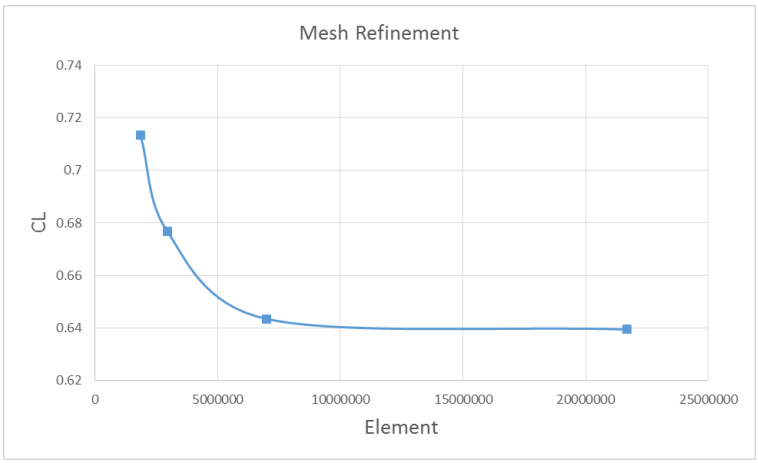

Figure 3.22 Mesh convergence curve

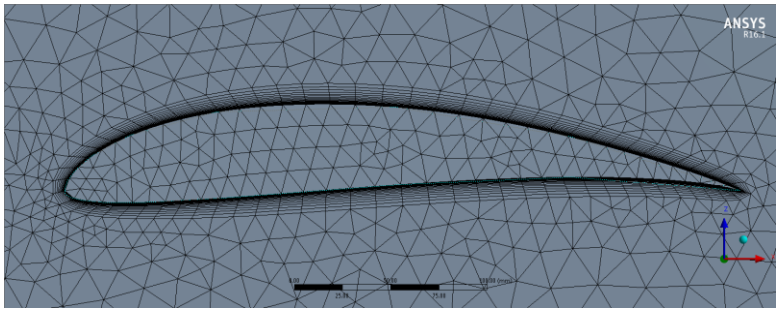

a) Course mesh-1 (1.9M elements)

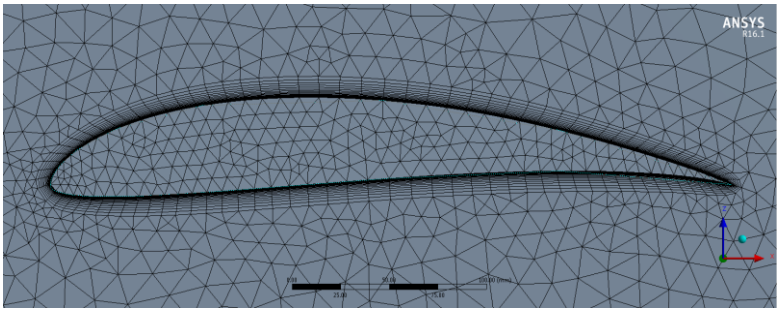

b) Course mesh-2 (3M elements)

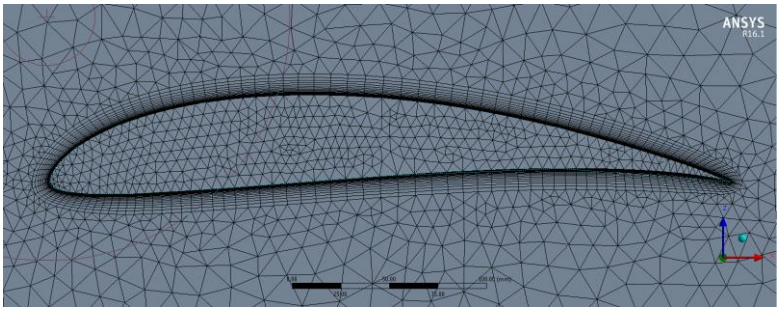

c) Middle mesh (7M elements)

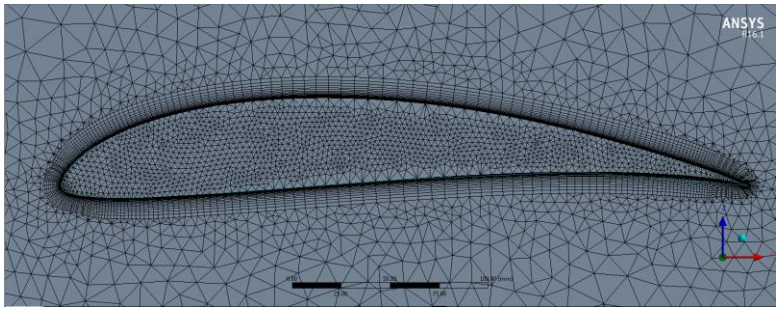

d) Fine mesh (21.6M elements)

Figure 3.23 Different mesh sizes from course to fine

3.2.3. CFD

Numerical calculations have been carried out with the help of 3-D steady state pressure based SST *k-ω* turbulence model by using Fluent. (This turbulence model is also widely used in external aerodynamics and flows close to wall [27]). This model uses control volume based technique to convert the governing equations to algebraic equations. Air was selected as a fluid type material. Related to it, density and dynamic viscosity values were entered for 1000 meters (ρ =1.1117 kg/m^3 and μ = 1.75x10^{-5} kg/m-s). Operation cell zone conditions was set to 89876 Pa. Inlet 1 and inlet 2 were defined as velocity inlet with 14 m/s velocity. Outlet was defined as pressure outlet. Turbulence intensity was adjusted to 1% (open air conditions) to prevent reversed flow across the computational flow domain during the solutions. Simple scheme was chosen concerning about the Pressure-Velocity Coupling. To get fine results, Green-Gauss Node Based is selected for Spatial Discretization. Under-Relaxation Factors settings remains as a program controlled (default). One analysis convergence took approximately 1 hour for different winglet models and positive AOA but it took 6-7 hours for negative AOA for both clean wing and wing with winglet (1500 iterations for positive AOA and 6000-7000 iterations for negative AOA). No convergence criterion was used. It was observed from monitors with C_L and C_D values until C_L and C_D converges.

Table 3.8 Fluent Parameters

Fluent Parameters	
General	Pressure Based, Steady
Models	SST k-omega
Materials	Air
Area	depends each case
Density	1.1117 [kg/m^3]
Length	0.35 [m]
Pressure	89876 [Pa]
Temperature	281.7 [K]
Velocity	14 [m/s]
Viscosity	1.76e-5 [kg/m-s]
Solution Method	Simple (2nd order)
Initialization	Hybrid and FMG

CHAPTER 4

RESULTS

4.1. Best Winglet Design Analysis

As mentioned in winglet design part, first 27 analysis were done depending on three parameters cant angle, sweep angle and taper ratio. According to CFD results, winglet has cant angle 59.4° (rotation 45°), sweep angle 30° and taper ratio 0.2 was found to be best designed configuration has the best L/D value and it is 23.762. Among the these 27 analysis, another design gives the closest L/D value compared to the best design is cant angle 69.3° (rotation 60°), sweep angle 30° and taper ratio 0.2 which has 23.760. These two designs have almost the same L/D values but due to the surface wetted area (winglet height increases with high cant angle and hence surface area), easy production (small cant angle) and solar panels (high cant angle cause shadow effect because of winglet height), winglet has cant angle 59.4° (rotation 45°), sweep angle 30° and taper ratio 0.2 was selected to apply toe and twist angle.

After performing first 27 analysis, toe and twist angle were implemented to this winglet model. CFD results showed that, toe out angle 3° has the best L/D value (23.867) among others. Toe out angle 5° and negative twist angle -5° follow this design with L/D ratios 23.856 and 23.800 as closest values respectively.

As a result, as can be seen from *Figure 4.1* and *Figure 4.2*, cant Angle 59.4°, sweep angle 30°, taper ratio 0.2 and toe out angle 3° was chosen as the best designed (has highest L/D) winglet when compared with clean wing.

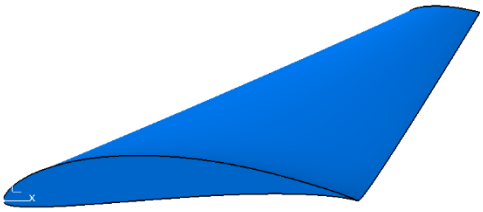

a) Side view

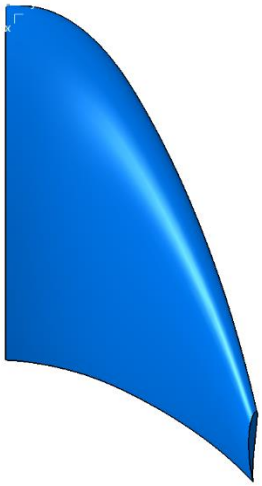

b) Top view

Figure 4.1 Side and top view of winglet has the best L/D value. Cant angle 59.4°, sweep angle 30°, taper ratio 0.2 and toe out angle 3°

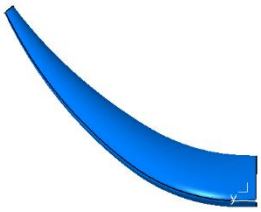

a) Front view

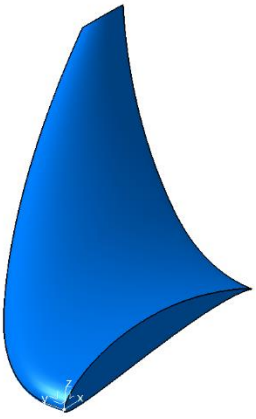

b) Isometric view

Figure 4.2 Front and isometric view of winglet has the best L/D value. Cant angle 59.4°, sweep angle 30°, taper ratio 0.2 and toe out angle 3°

4.2. Comparison of Aerodynamic Forces

Comprehensive numerical studies have been performed to investigate the aerodynamic performance of different winglet designs and clean wing using Ansys 16.1 Fluent 3D steady state pressure based SST k-ω turbulence model. Instead of using Spalart Allmaras or k-ε turbulence model, SST k-ω was preferred although it increases the solution time to obtain better results (C_L and C_D). Analysis were carried out for different designs and clean wing at zero AOA and Re=309507 for TİHAS cruise conditions (V=14 m/s, 1000 meters altitude, ρ =1.1117 kg/m^3 and μ = 1.75e-5 kg/m-s). To examine stall characteristic, best winglet design and clean wing were compared at various AOA and various speed (flight envelope).

In order to make more analysis and get results in a short time, computers with different properties (CPU speed) were used. For example, negative and high AOA wing and wing with winglet designs were run in high performance computer (HPC) with 120 CPU and simple and easy computable models (clean wing configurations) were run in desktop computers have 4 CPU. Also, some clean wing models which had been solved in desktop computers were performed again in HPC to reach better and accurate results (especially high velocities). There were two different results found for the same models. All the analysis made in the HPC always gave the lowest C_L and C_D values (approximately 1%) compared to desktop computers' results. According to Ansys documents [56], flow domain is divided according to number of processors that computers have and each divided volume is solved with a certain amount of error margin. The more partitions mean the more error occurs. That's why, desktop computer with 4 CPU gives high values. As a result of this, all models were analyzed in HPC merely to make an accurate comparison among the models.

As mentioned Enclosure Volume part, flow domain was determined according to wing chord length (0.35m). However, to investigate whether the enclosure volume sizes have effects on results or not, 4 different sizes of them were analyzed. Flow domain consisting of the body that small and inside of the outer body has the dimensions of 1.85m x 3m x 1.05m and the outer body has the dimensions of 18.5m x 7.5m x 10m was taken as a base enclosure volume, *Figure 3.16*.

The other three models were created by increasing the sizes of the previous model about 20% for each sizes and for each case. Modifications were done on clean wing flow domain and analysis of them were performed at zero AOA and cruise conditions. Then C_L values were compared for different sized enclosure volumes. It is evident from *Figure 4.3*, results show that modification or increasing of enclosure volume sizes has insignificant effect on C_L values (0.15%-0.21% change). Thus, the smallest (base) flow domain was chosen for all CFD runs to work with less element number.

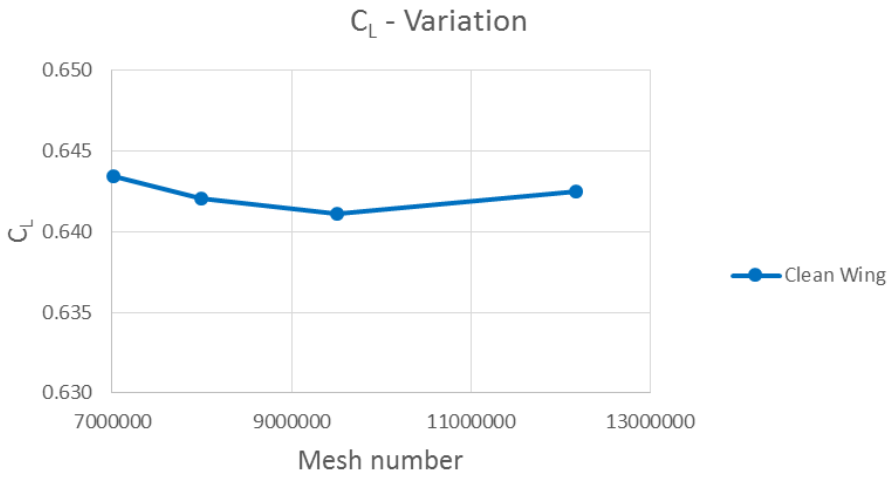

Figure 4.3 C_L Variations according to flow domain adjustment for different mesh numbers

A further point related to flow domain is its shape and boundary conditions. Rectangular enclosure volume was used to make better post-processing and observation of flow behavior around the wing and winglet instead of using pressure far field. As a boundary conditions, front and rear part of enclosure volume were defined as velocity inlet (inlet-1) and pressure outlet and symmetry plane wall defined as symmetry. Top, side and bottom parts of flow domain were defined as inlet-2 and velocity magnitude and direction of them were inserted parallel to the surfaces, means adjusted to the same direction as in inlet-1. These boundaries also have been named in different ways at some research [42] such as free slip wall. For this reason, top, side and bottom parts were defined separately both as a "wall" and "symmetry" to

investigate effects of them on C_L and C_D. Then analysis were performed for three different boundaries but a significant change was not observed (0.07%-0.09%).

After determination of enclosure volume shape and sizes and mesh number, models were solved respectively. According to design flow chart, firstly, cant angle, sweep angle and taper ratio were investigated in a triple combination in terms of aerodynamic efficiencies. Totally 27 different wing with winglet models were studied as a first section. Then toe and twist angle were applied in second part.

It is demonstrated from *Figure 4.4* that C_L varies depending on variable cant angles, sweep angles and taper ratios. Variation of sweep angle affected to C_L negatively for all taper ratios and cant angles. At λ=0.2, when sweep angle kept growing from 0° to 30°, C_L values showed decreasing trend for each three cant angles. While C_L was reducing at cant angle 90° and 69.3° as 0.9%, cant angle 59.4° was less affected with 0.35% reduction. When taper ratio becomes λ=0.3, the negative effect of the sweep angles were unchanged. In this case, increasing of sweep angle caused a greater C_L decline at cant angle 59.4°. While C_L reduced by 1.27% at cant angle 59.4°, a small amount of decrease was observed at cant angle 90° and 69.3° as 0.8%-0.3%. If the taper ratio λ=0.4 will be evaluated for variable cant and sweep angles' effects on C_L, again variation of sweep angle continued to maintain its negative effects on C_L. As in the taper ratio λ=0.2, cant angle 90° was affected more than others in terms of C_L reduction. C_L of cant angle 90° reduced by 1.2% while cant angle 59.4° (has minimum reduction) reduced as 0.2%.

According to other parameters (cant and sweep angles), if it is evaluated that the effects of variation of taper ratios (λ=0.2, λ=0.3, λ=0.4) on C_L variation, no significant change was observed. Model with cant angle 59.4°, sweep angle 30° and taper ratio 0.3 only has significant C_L reduction as 0.78% according to other taper ratios.

If these there parameters are evaluated among each other, cant angle demonstrated more dominant effect (C_L increases by about 2.36% when cant angle changes to 59.4° to 90° at sweep angle 0° and taper ratio 0.4) on C_L. When the cant angle was increased from 59.4° to 90°, C_L always showed positive increment even if other parameters were changed.

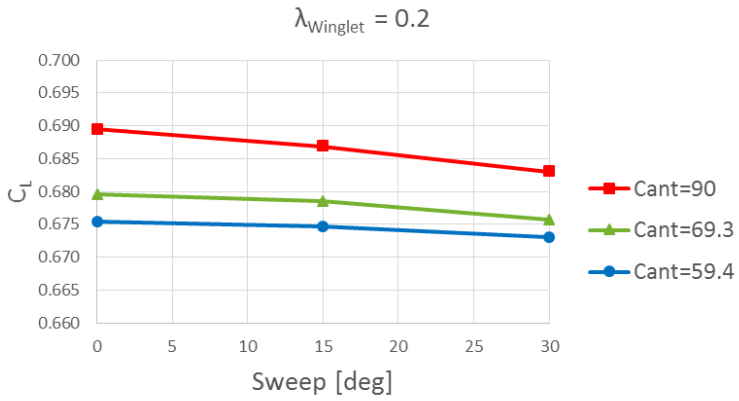

a) Cant and sweep angle effects on C_L at λ= 0.2

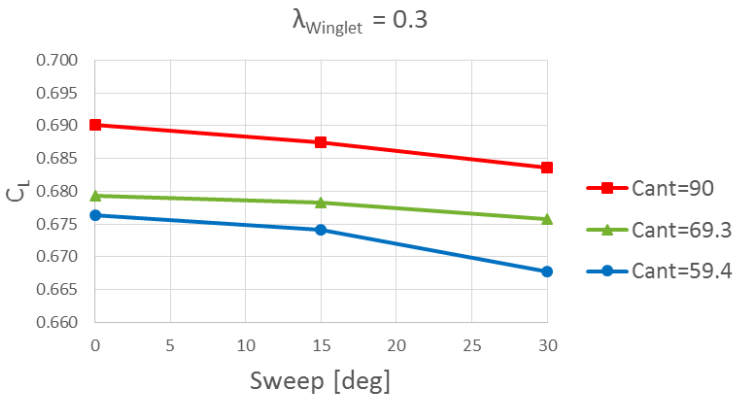

b) Cant and sweep angle effects on C_L at λ= 0.3

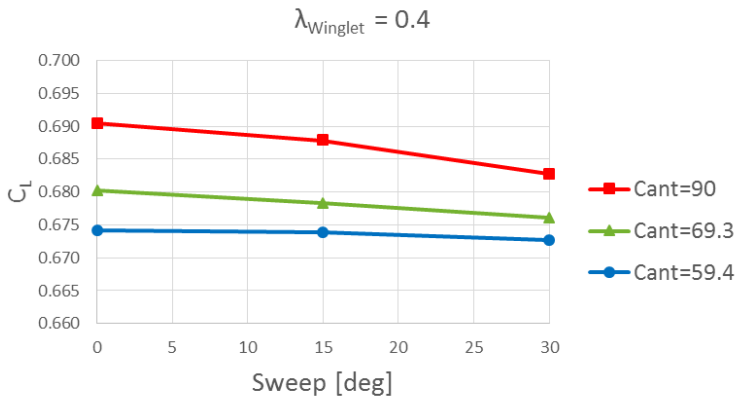

c) Cant and sweep angle effects on C_L at λ= 0.4

Figure 4.4 Cant and sweep angle effects on C_L at different taper ratios

Effects of the variation of the parameters (cant angle, sweep angle and taper ratio) that in first 27 analysis on C_D values are showed in *Figure 4.5*. At each taper ratios (λ=0.2, 0.3, 0.4) and cant angles, increase of sweep angle caused reduction of C_D. C_D values revealed decrescent behavior for all cant angles while sweep angle change from 0° to 30° at taper ratio λ=0.2. With the sweep angle increment, C_D was decreased by 1.31% at cant angle 90°, by 0.9% at cant angle 69.3° and by 0.53% at cant angle 59.4°. At taper ratio λ=0.3, reducing effect of sweep angle variation on C_D did not changed. In this case, C_D decreased further at cant angle 59.4° when comparing with the cant angle 69.3° according to taper ratio λ=0.2. C_D reduction was calculated as 1.57%, 0.99% and 1.39% at cant angle 90°, 69.3° and 59.4° respectively. When taper ratio becomes λ=0.4, reducing effect of sweep angle variation on C_D kept to continue. Compared with taper ratios λ=0.2 and λ=0.3, sweep angle showed the highest C_D drop at taper ratio λ=0.4 with the reduction of 1.75%. As in previous taper ratios, reduction of C_D at cant angle 69.3° was calculated around the 0.9% and C_D decline of cant angle 59.4° was recorded as 0.55%.

When the effect of different taper ratios (λ=0.2, λ=0.3, λ=0.4) on variation of C_D is evaluated according to other parameters (cant and sweep angles), crucial alteration was observed. C_D value of cant angle 90°, 69.3° and 59.4° increased as 2.35%, 1.71% and 1.19% respectively when taper ratio changes to 0.2 to 0.4. The reason of while taper ratio has no significant effect on C_L, it has crucial increase on C_D is due to the wetted area increase. Surface area of winglet is increased by increasing the taper ratio. A further point, increase of cant angle caused wetted area increment because while span of winglet remains constant, height of it increased with cant angle increment. Thus, besides the increment of drag due to increase of C_L, additional parasite drag was also added due to the increase of wetted area.

When three parameters (cant angle, sweep angle and taper ratio) are evaluated among each other, cant angle has the dominant effect (C_D increases by about 3.51% when cant angle changes to 59.4° to 90° at sweep angle 0° and taper ratio 0.4) on C_D compared with others.

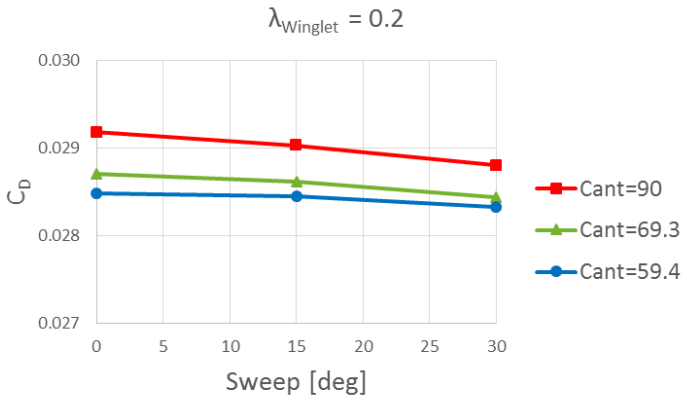

a) Cant and sweep angle effects on C_D at λ= 0.2

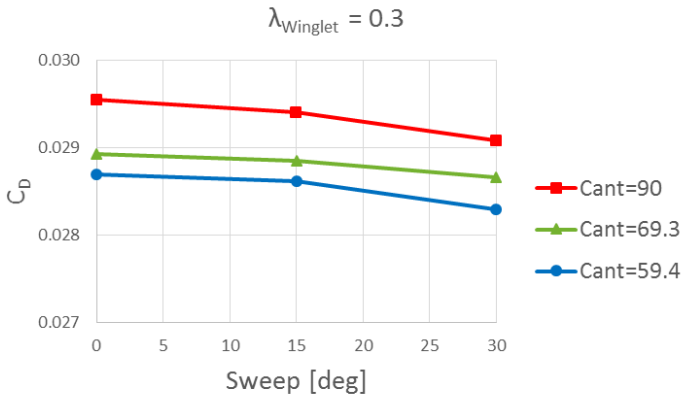

b) Cant and sweep angle effects on C_D at λ= 0.3

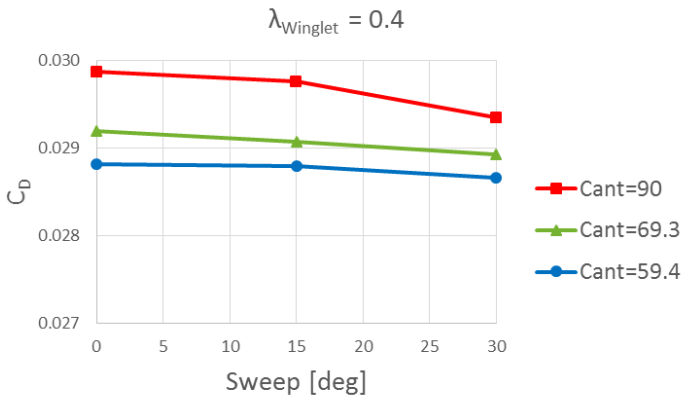

c) Cant and sweep angle effects on C_D at λ= 0.4

Figure 4.5 Cant and sweep angle effects on c_d at different taper ratios

It is indicated in *Figure 4.6* that, variation of sweep angle from 0° to 30° affected to C_L/C_D positively for all taper ratios and cant angles (except at λ=0.3 and cant angle=59.4°). The effect of variation of sweep angle was examined for all taper ratios and cant angles. At taper λ=0.2, C_L/C_D increased as 0.38%, 0.34% and 0.19, at cant angles 90°, 69.3° and 59.4° respectively. When taper ratio becomes λ=0.3, change of sweep angle from 0° to 15° caused C_L/C_D reduction as 0.09% then it increased as 0.21% at sweep angle 30°. C_L/C_D was increased at cant angle 90° and 69.3° as 0.64% and 0.38%. When evaluation is done, for taper ratio λ=0.4, it was observed that as 0.64%, 0.30% and 0.34% increment occurred on C_L/C_D for cant angle 90°, 69.3° and 59.4° respectively. The increase of taper ratio from 0.2 to 0.4 affected negatively to C_L/C_D. It is because of increase of C_D was created more according to increase of C_L due to the increase of surface area. The highest C_L/C_D values was observed at λ=0.2 and it was increased with other parameters variation that cant angle and sweep angle.

Figure 4.7 shows lift force variations according to change of cant and sweep angles at different taper ratios. It is concluded that, lift force is increased with increasing taper ratios from λ=0.2 to λ=0.4 because of surface are increment. While the increase of sweep angle from 0° to 30° affected to lift force negatively at cant angle 90°, very small change occurred at cant angle 69.3° and no significant effect observed for cant angle 59.4°. Also, increase of cant angle (increase of cant angle cause surface increase) has positive effect on it.

Figure 4.8 demonstrates the drag force variation according to change of cant and sweep angles at different taper ratios. The same effects were observed according to variation of parameters as in lift force.

It is concluded that, cant angle has major effect according to others on C_L, C_D, lift and drag force. Also, 27 models were compared in terms of lift and drag force with clean wing in *Figure 4.7* and *Figure 4.8* and it was found that all wing with winglet models revealed better efficiency as expected. As a result, cant angle 59.4°, sweep angle 30° and taper ratio 0.2 demonstrated the highest L/D value and it was selected for investigation of effects of toe and twist angles variations.

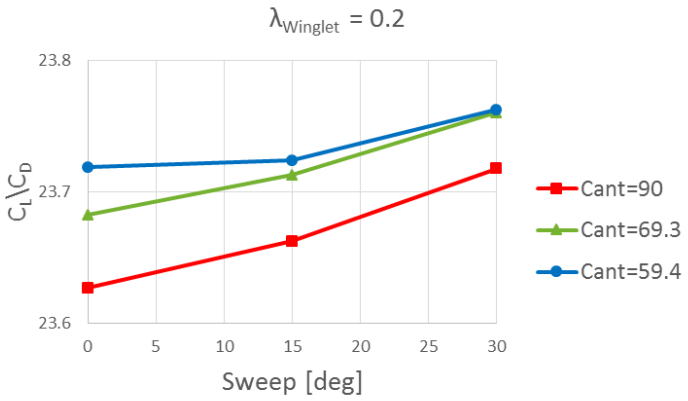

a) Cant and sweep angle effects on C_L/C_D at λ= 0.2

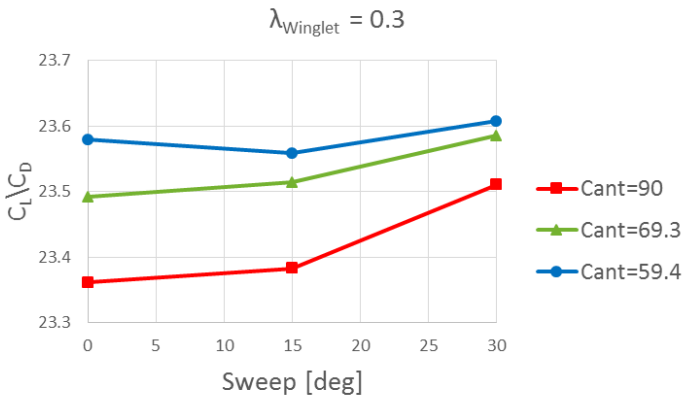

b) Cant and sweep angle effects on C_L/C_D at λ= 0.3

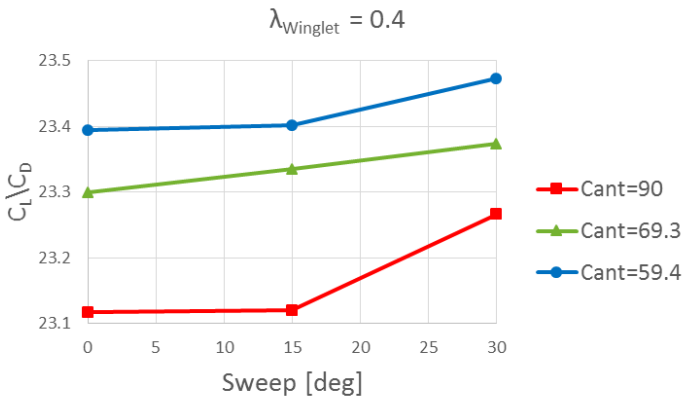

c) Cant and sweep angle effects on C_L/C_D at λ= 0.4

Figure 4.6 Cant and sweep angle effects on C_L/C_D at different taper ratios

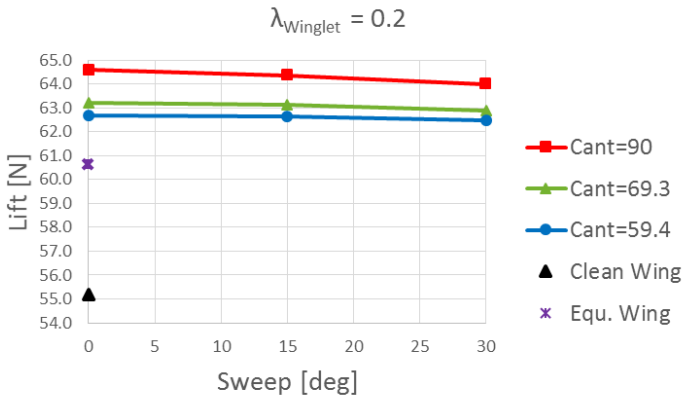

a) Cant and sweep angle effects on lift force at λ= 0.2

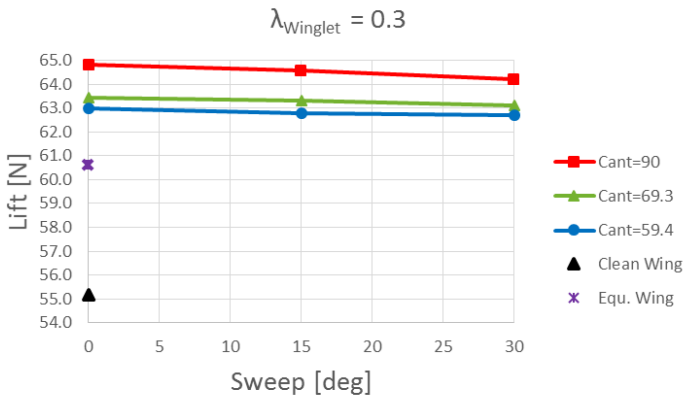

b) Cant and sweep angle effects on lift force at λ= 0.3

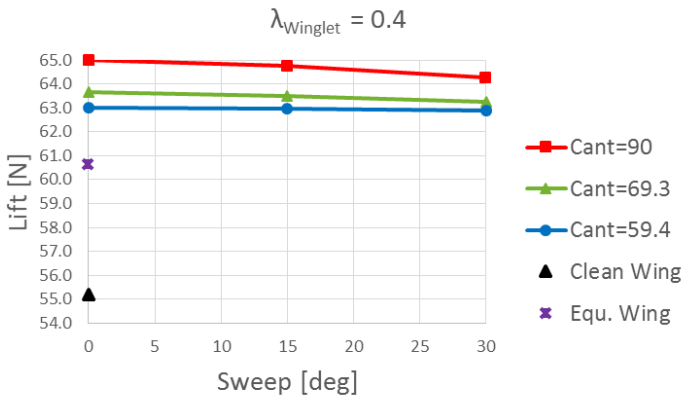

c) Cant and sweep angle effects on lift force at λ= 0.4

Figure 4.7 Cant and sweep angle effects on lift force at different taper ratios

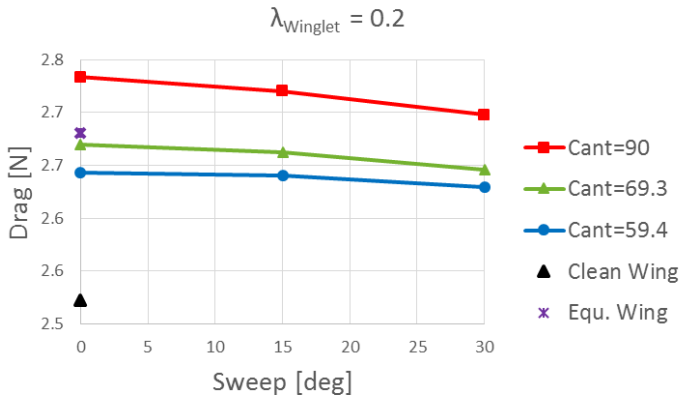

a) Cant and sweep angle effects on drag force at λ= 0.2

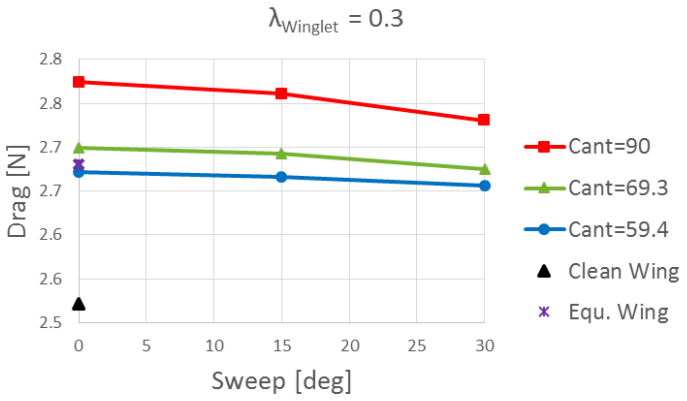

b) Cant and sweep angle effects on drag force at λ= 0.3

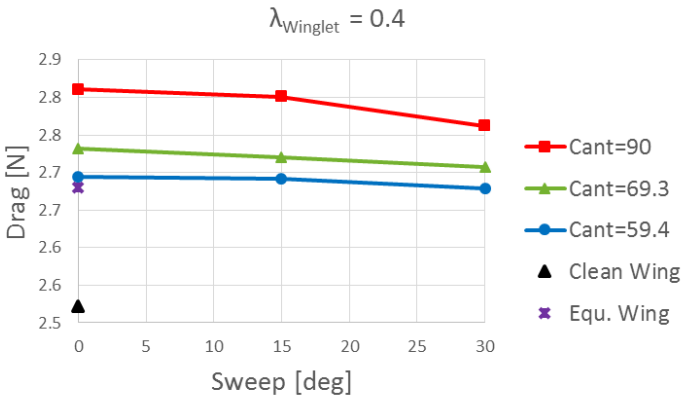

c) Cant and sweep angle effects on drag force at λ= 0.4

Figure 4.8 Cant and sweep angle effects on drag force at different taper ratios

In first 27 analysis, cant angle, sweep angle and taper ratio were investigated according to aerodynamic efficiencies and cant angle 59.4°, sweep angle 30° and taper ratio λ=0.2 was found best designed winglet configuration in terms of the highest L/D value. As a second analysis part, toe and twist angle were implemented separately to this was chosen winglet configuration. Results are as follows.

Figure 4.9 shows variation of toe in and toe out angles' effect on C_L, C_D, and L/D. C_L demonstrated decreasing behavior from toe angle in (-5°) to toe out (5°). While toe in (-5°) angle forms maximum C_L with the increase of 2.54% according to zero toed winglet, toe out (5°) angle causes C_L reduction as 2.44%. Likewise, C_D also reduced when toe angle changes from -5° to 5°. C_D received the highest value with the increase of 4.21% at toe in (-5°) angle and took the minimum value at toe out (5) angle with the 2.08% reduction. However, L/D ratio decreased from 0° toe angle to toe in angle (-5°) and took the lowest value with 1.71% reduction. Also, L/D increased with toe out angle increment and received the highest value at toe out angle 3° with 0.43% increase. Toe out angles improved L/D ratio better than toe in angles because while toe in angles increase the trailing edge surface of winglet (turbulence flow), toe out angles increases the leading edge surface of winglet (laminar flow) and this causes more drag reduction at toe out angles. Moreover, with the toe out angle, negative incidence occur according to flow direction and this also affects to drag reduction.

Depending on the twist angle variation, change of wing with winglets' C_L, C_D, and L/D values demonstrated in *Figure 4.10*. C_L and C_D increased with the increase of negative twist angles and decreased with the increase of positive twist angle (except twist angle 1°). C_L and C_D received the highest value at twist angle -5° as 0.32% and 0.92% and took the lowest value at twist angle 5° as 0.07% and 0.23% respectively. L/D value received the highest value at twist angle 5° as the increase of 0.16% and took the lowest value at twist angle -5° as 0.61 % reduction.

As a result, toe out angle 3° showed better improvement in terms of L/D increase. Thus, according to design algorithm, winglet has 59.4° cant angle, 30° sweep angle, 0.2 taper ratio and 3° toe out angle was found the best designed configuration in terms the highest L/D.

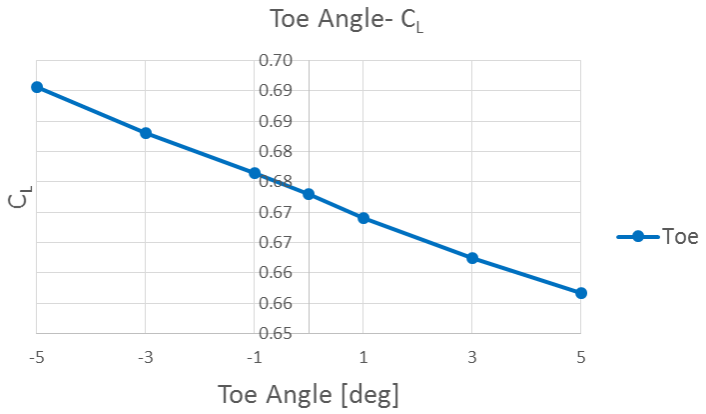

a) Toe in and toe out angle effect on C_L

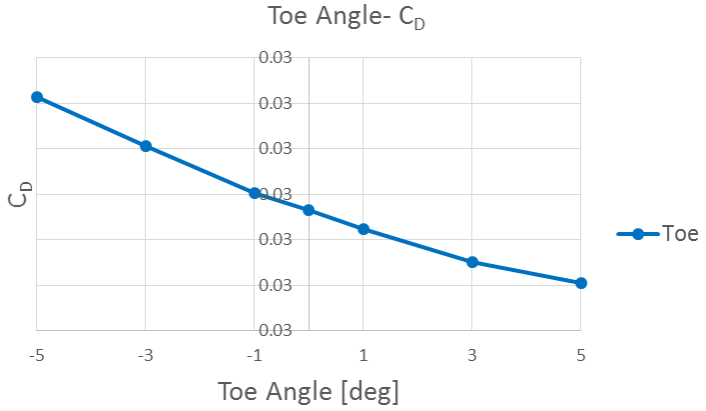

b) Toe in and toe out angle effect on C_D

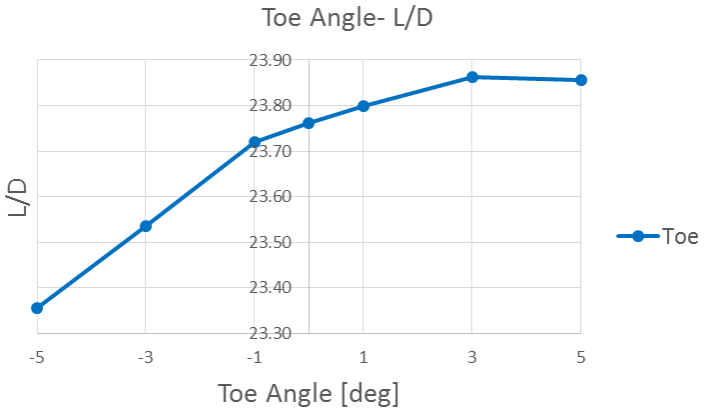

c) *Toe in and toe out angle effect on L/D*

Figure 4.9 Toe angle effects on winglet having the best L/D among the 27 analysis

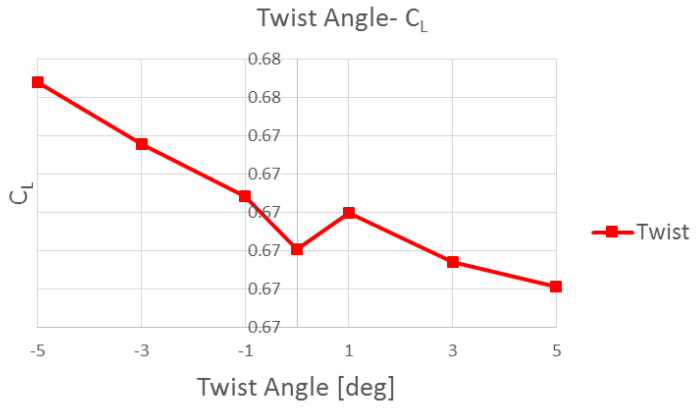

a) Positive and negative twist angle effect on C_L

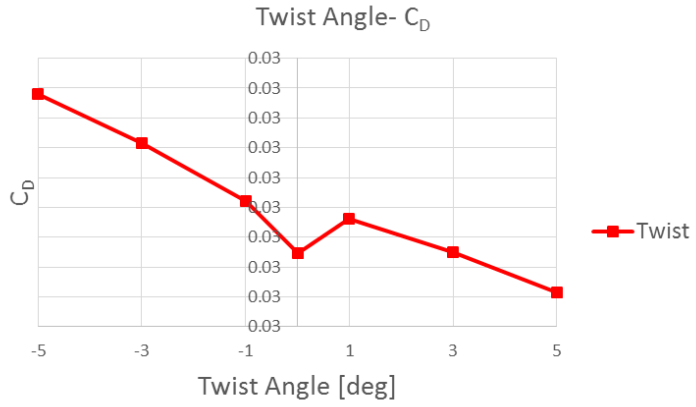

b) Positive and negative twist angle effect on C_D

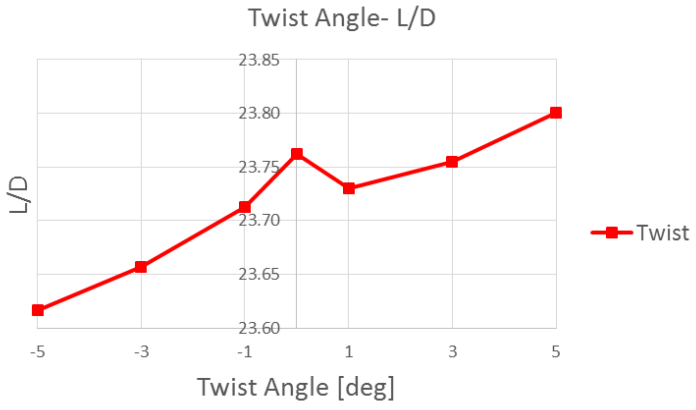

c) *Positive and negative twist angle effect on L/D*

Figure 4.10 Twist angle effects on winglet having the best L/D among the 27 analysis

After analyzing all winglet parameters and selecting best designed winglet configuration, wing with winglet which has the best L/D was compared clean wing, equivalence surface area wing and equivalence span wing in terms of aerodynamic efficiencies. Results were explained as follow and showed in *Table 4.1* respectively.

According to fluent results, the best case improved lift force as 10.59%. Besides the effect of winglet, span extension and surface area increment was also affected on it. Also, C_L was developed as 2.86% and C_D was reduced by about 5.62%. C_D has more improvement according to C_L because winglet increase effective span and effective AR of wing approaching elliptic lift distribution by reducing wingtip vortex and induce drag effect. Thus, L/D was increased as 8.32% when compared with clean wing.

In order to understand winglet efficiencies according to clean wing, the best case was compared with clean wing has same reference area. To do this, clean wing semi span was adjusted to 2.44m to equalize reference areas. Results reveals that, the best case has better efficiencies by about 1.76% lift and C_L increase and also, L/D value is higher as 5.21% due to the better C_D value by 3.51%.

A further point, the best case was also compared same semi span clean wing (2.5m) to observe what would happened if 2.5m wing had been used instead of using wing with winglet. Fluent results showed that, the best case again showed great improvement according to same span clean wing in terms of aerodynamic efficiencies. Although lift force is less than same span wing as a small amount (0.93%), the best case has the better C_L, C_D, and L/D values as 1.36%, 3.13%, and 4.45%.

Table 4.1 Comparison of the best case with other configurations in terms of aerodynamic properties

	Clean wing	The Best Case	Equivalence Wing	Same Span Wing
b/2 [m]	2.25	2.5	2.44	2.5
S_{ref} [m^2]	0.787	0.855	0.855	0.875
Lift Force [N]	55.17	61.7	60.62	62.29
C_L	0.6434	0.6624	0.6508	0.6534
C_D	0.0294	0.0278	0.0288	0.0287
L/D	21.88	23.86	22.62	22.80
AR	12.87	14.62	13.93	14.29

In order to investigate the behavior of C_L, C_D, and L/D variation and stall characteristic of clean wing and the best case (wing with winglet), analysis were done at different AOA. As indicated in *Figure 4.11*, L/D received the highest value at 2° AOA both for clean wing and the best case. After 2°, it began to decrease when AOA goes to 20° and -5°. As can be seen from *Figure 4.12*, 14° found as a stall angle for both cases. Wing extension due to the winglet had no effect on stall angle characteristic. As expected, wing with winglet model has positive effect on C_L and C_D. Best case has the highest C_L and the lowest C_D (except -5°AOA) for all AOA.

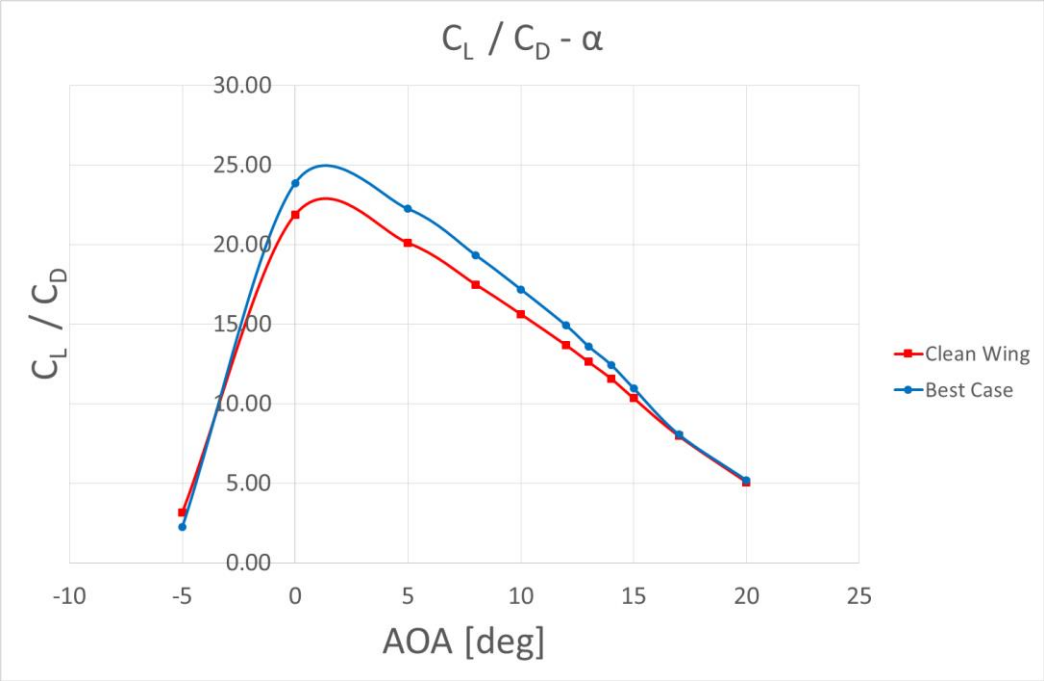

Figure 4.11 C_L/C_D variations of clean wing and wing with winglet (the best case) at different AOA (-5° to 20°)

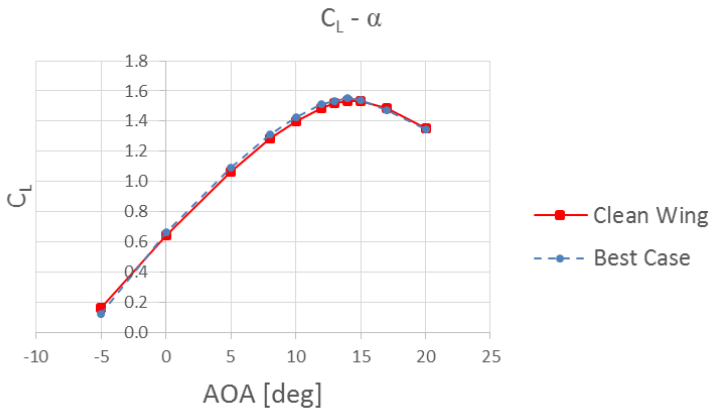

a) Clean wing & best case C_L-α curves

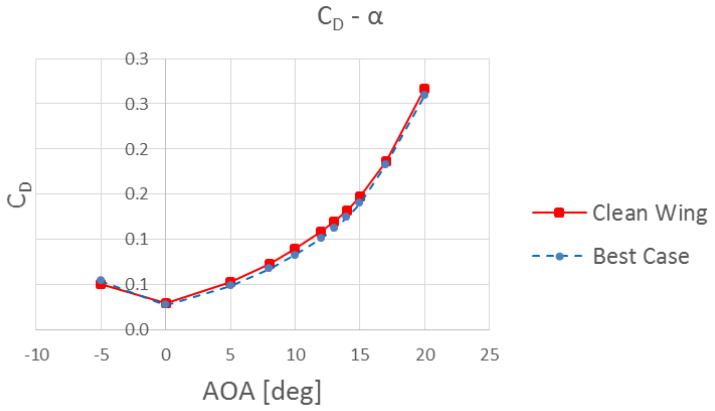

b) Clean wing & best case C_D-α curves

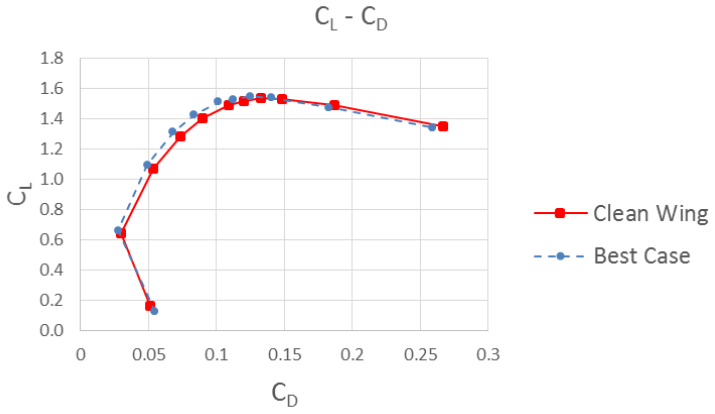

c) Clean wing & best case drag polar curves

Figure 4.12 Clean wing & best case C_L-α, C_D-α and drag polar curves

After analysis converge, fluent also gives lift and drag force in terms of pressure and viscous effect. In order to see the contribution of winglet to pressure and viscous drag forces and lift forces, clean wing and the best case's wing with winglet were examined and compared as follow.

Figure 4.13 and *Figure 4.14* shows drag and lift force components for best case at different AOA. As expected, pressure has dominant effect on both drag and lift forces. For the best case's wing at 0° AOA, viscous drag force constitutes 34.92% of the total drag force of the wing and viscous lift force constitutes 0.8% of the total lift force of the wing. For the best case's winglet, viscous drag force constitutes 43.14% of total drag force of winglet and viscous lift force constitutes 0.24% of the total lift force of the winglet. Viscous and pressure components of drag and lift forces for the best case's wing and winglet were demonstrated in *Figure 4.15* to *Figure 4.18* in detail. As can be seen, viscosity has less effect both on lift and drag force compared to pressure effect. In *Figure 4.18* and *Figure 4.19*, various effects of viscous and pressure lift and drag force to total drag and lift force of the best case were revealed. While viscous lift force change total lift force by about 0.9%, viscous drag force constitute by about 35.6% of total drag force.

Viscous and pressure effect of lift and drag force of clean wing were showed in *Figure 4.21* and *Figure 4.22*. As shown, pressure has dominant effect on both lift and drag force. At 0° AOA, viscous drag force constitutes 33.02% of total drag force and viscous lift force constitutes 0.08% of the total lift force of clean wing.

Interestingly, while AOA increase, viscous drag effect reduced but pressure drag effect increased in drag force distribution, *Figure 4.23*. Pressure lift force effect increased up to stall angle 14° and reduced to 20 °AOA. However, viscous lift force effect remained same for all AOA *Figure 4.24*.

When clean wing and wing of best case compared, although viscous drag force remained same in both cases, pressure drag force was reduced in wing of best case by about 8.23%. Again although viscous lift force effect remained same for both cases, pressure lift force was increased for wing of best case by about 4.95%.

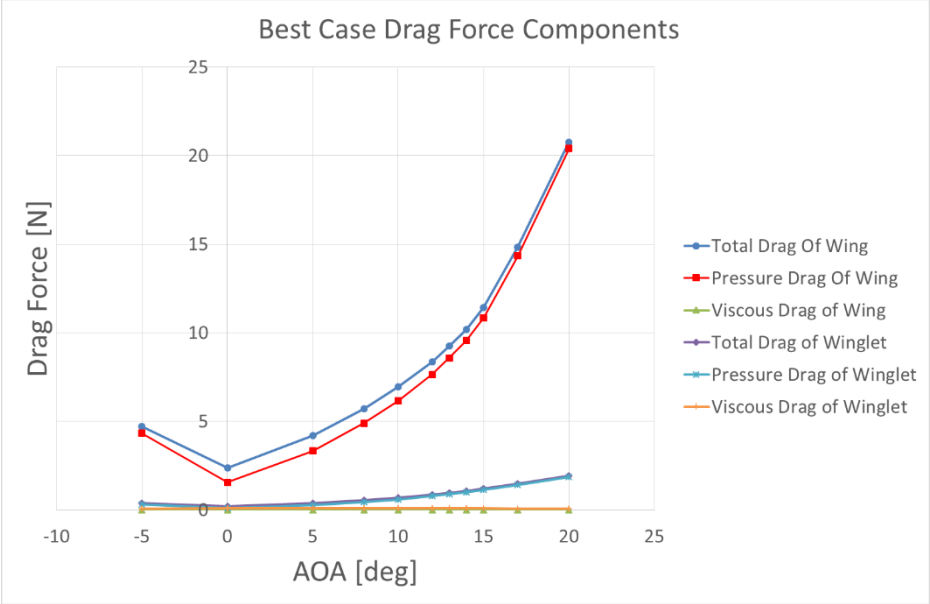

Figure 4.13 Best case drag force components

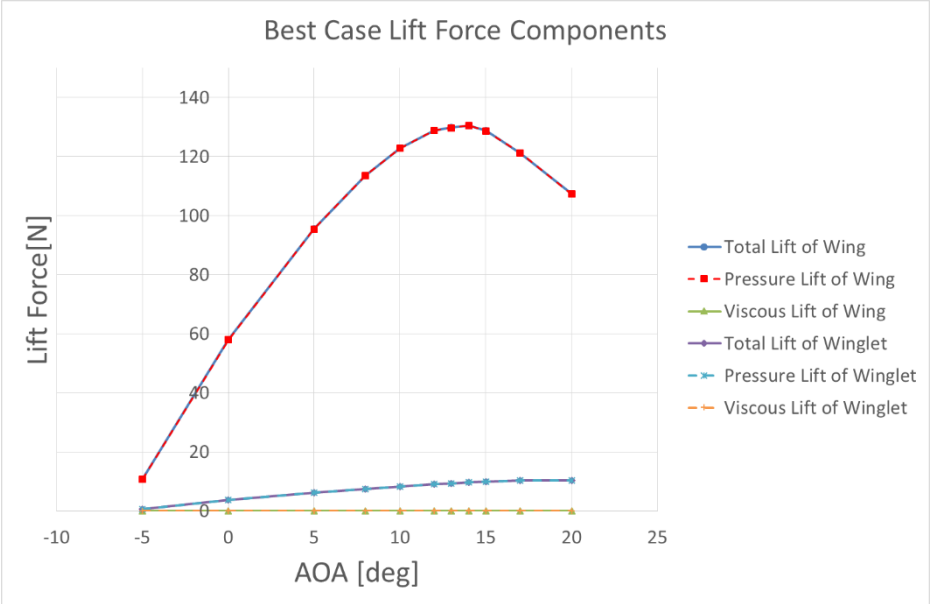

Figure 4.14 Best case lift force components

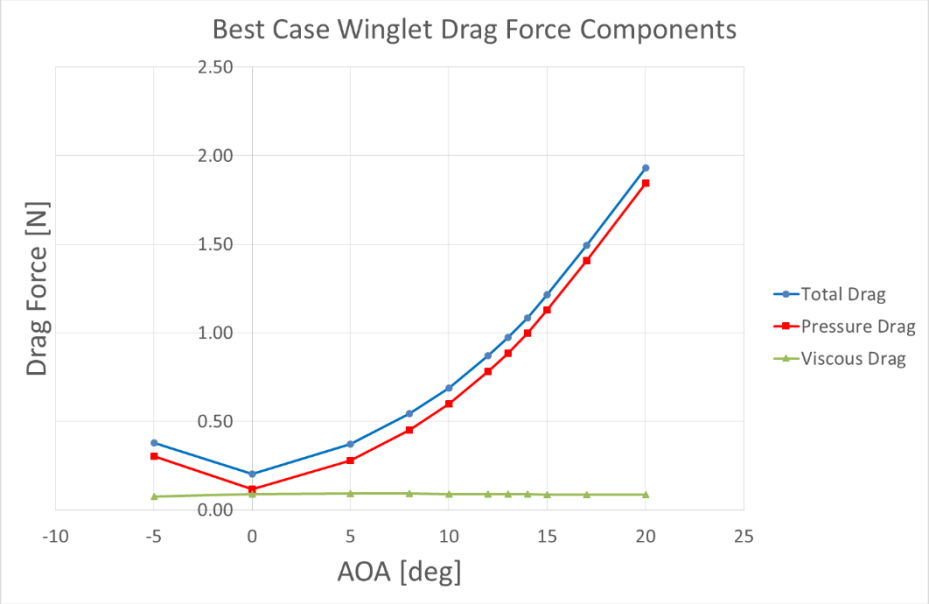

Figure 4.15 Best case winglet drag force components

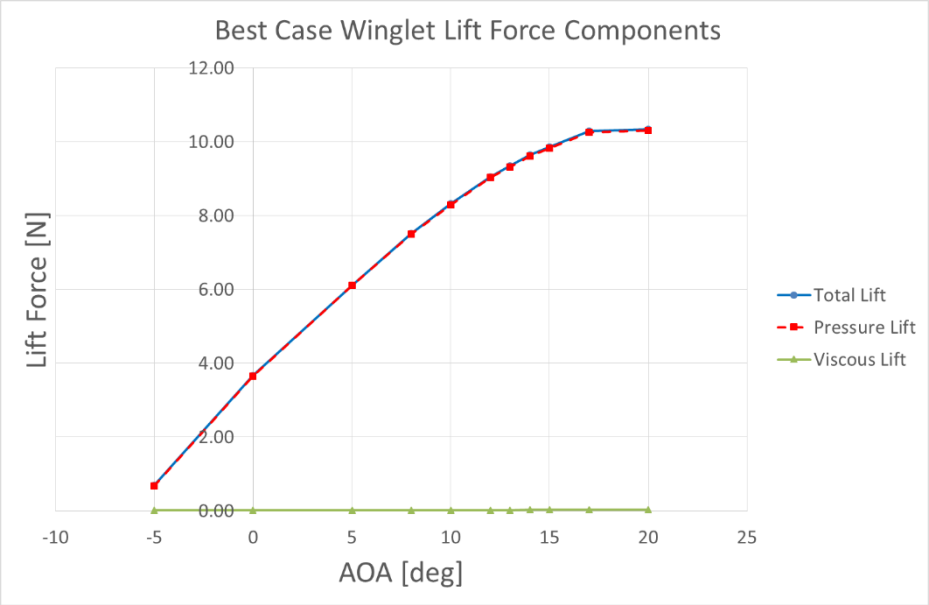

Figure 4.16 Best case winglet lift force components

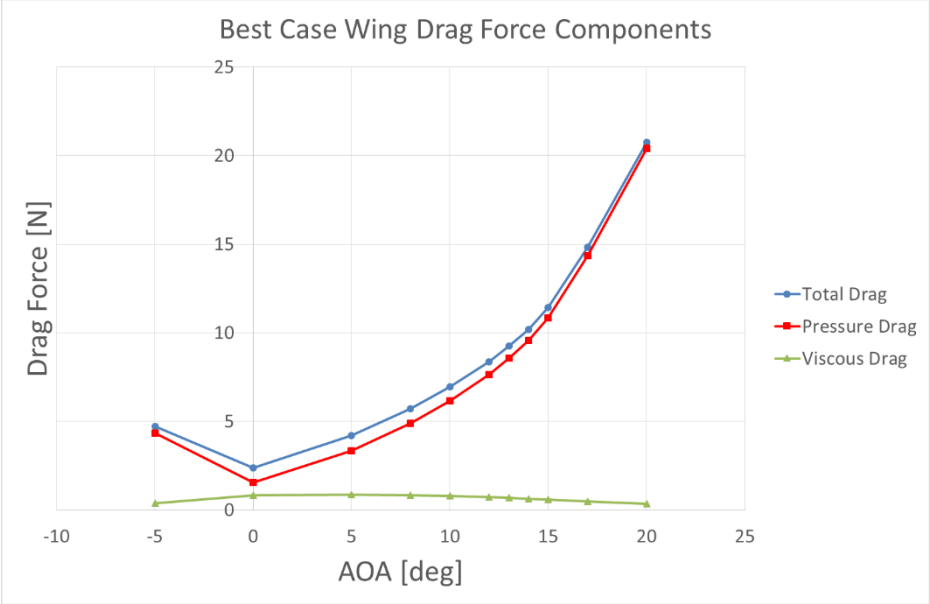

Figure 4.17 Best case wing drag force components

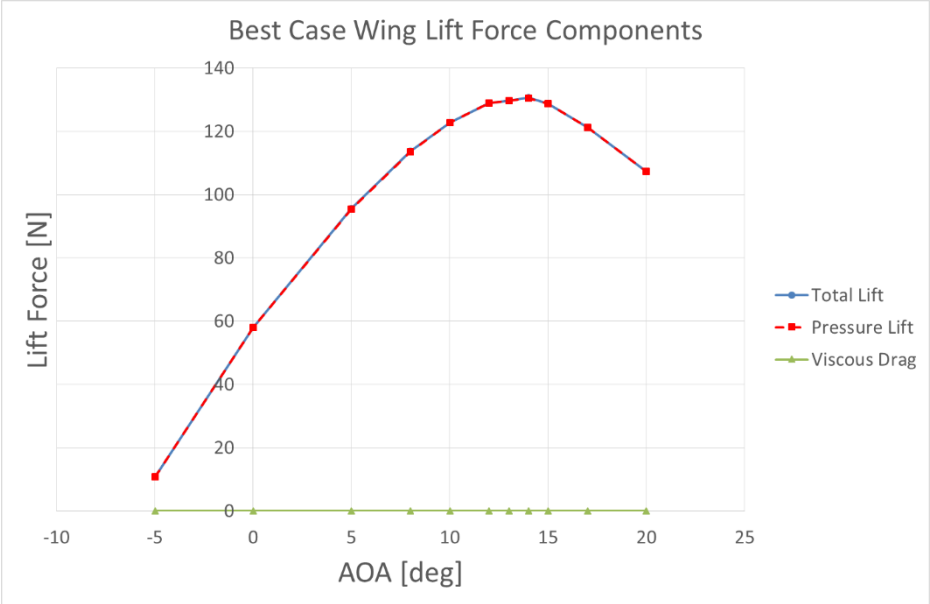

Figure 4.18 Best case wing lift force components

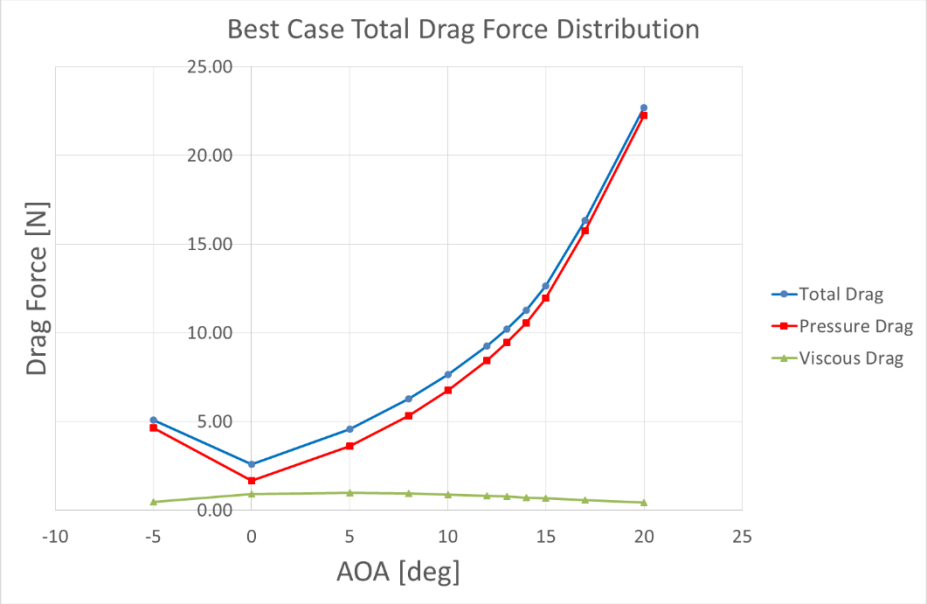

Figure 4.19 Best case total drag force distribution

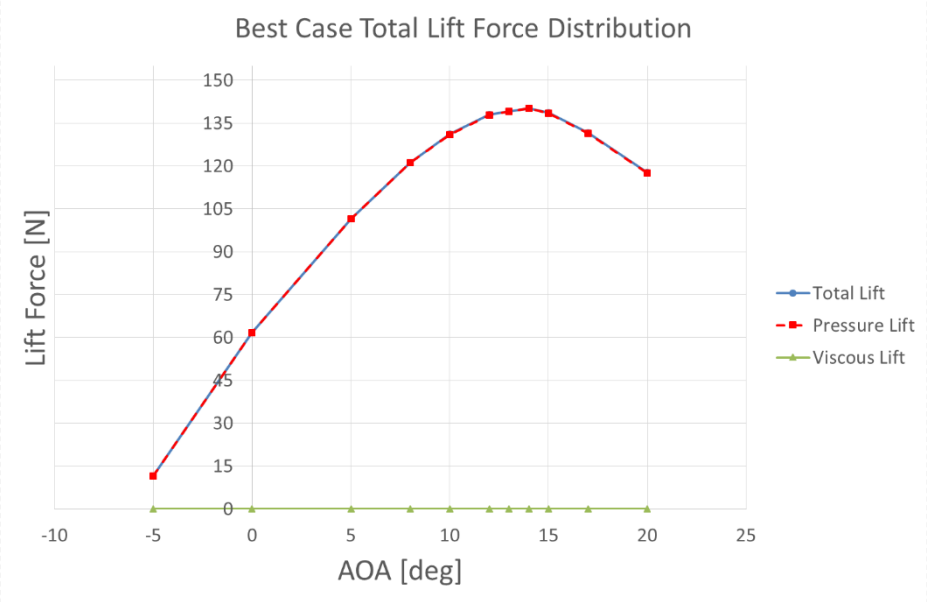

Figure 4.20 Best case total lift force distribution

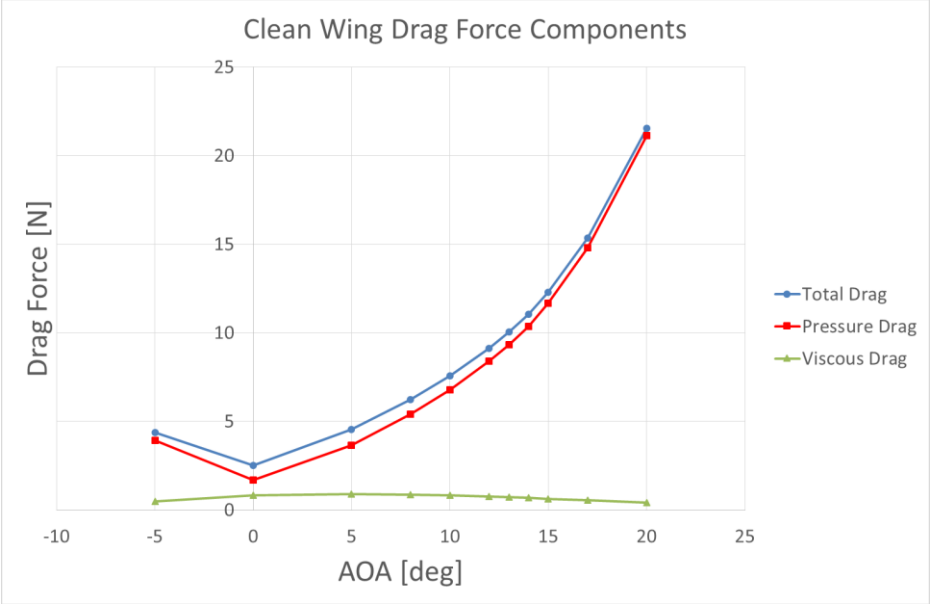

Figure 4.21 Clean wing drag force components

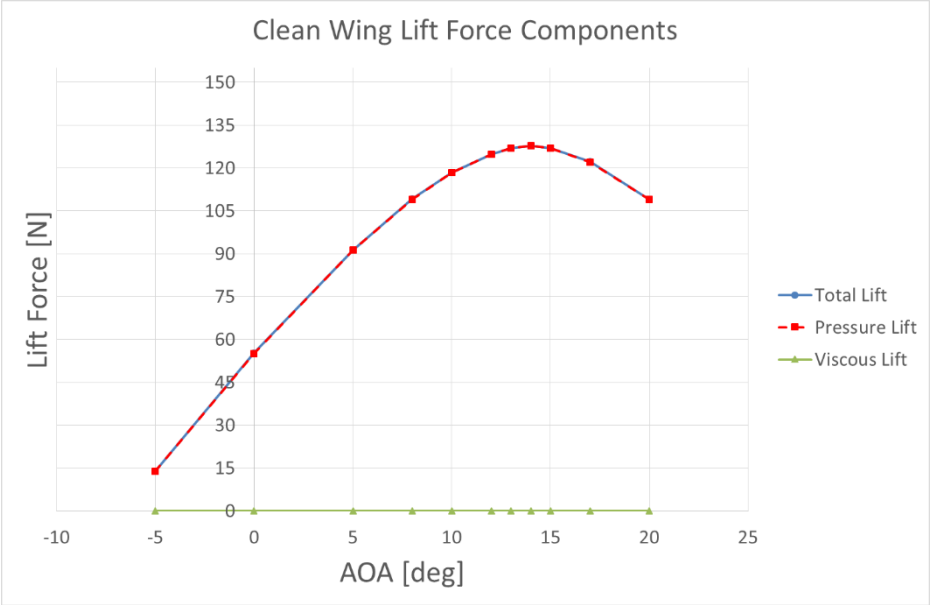

Figure 4.22 Clean wing lift force components

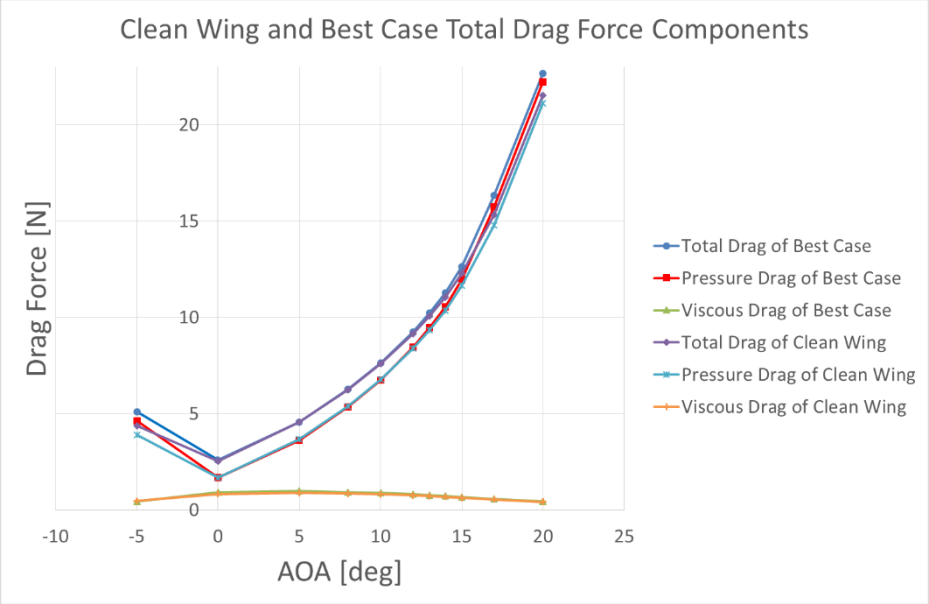

Figure 4.23 Clean wing and best case total drag force components

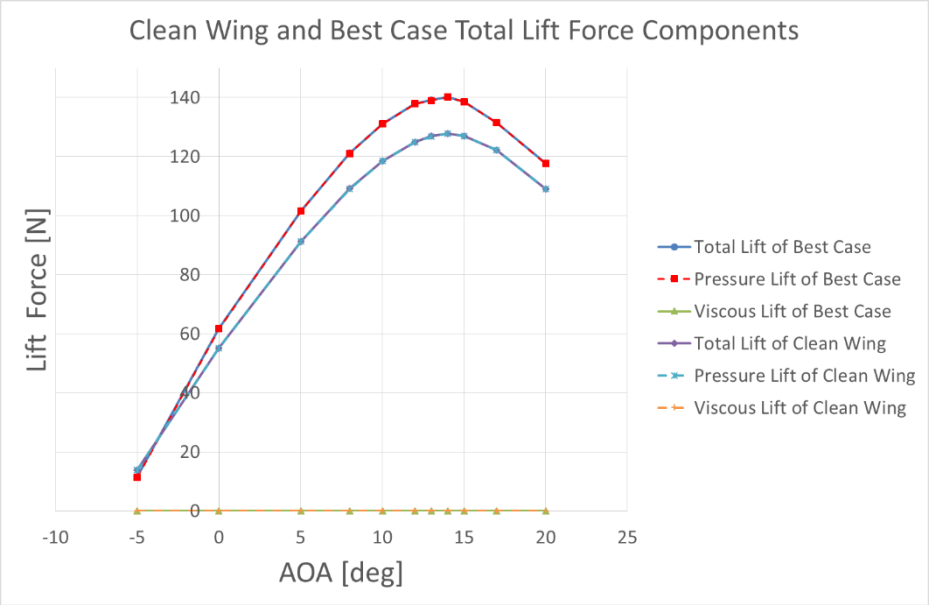

Figure 4.24 Clean wing and best case total lift force components

4.3. Flowfield Analysis

FLUENT was used for post processing of the results to examine flow behavior of clean wing and the best case. Y+ distribution, pressure contours, velocity streamlines, and vorticity magnitude were investigated.

Figure 4.25 indicates that, maximum Y+ value on the wing is 1.26. ANSYS can solve the SST k-ω equations if Y+ is between 1 and 5. It is also important to convergence of analysis.

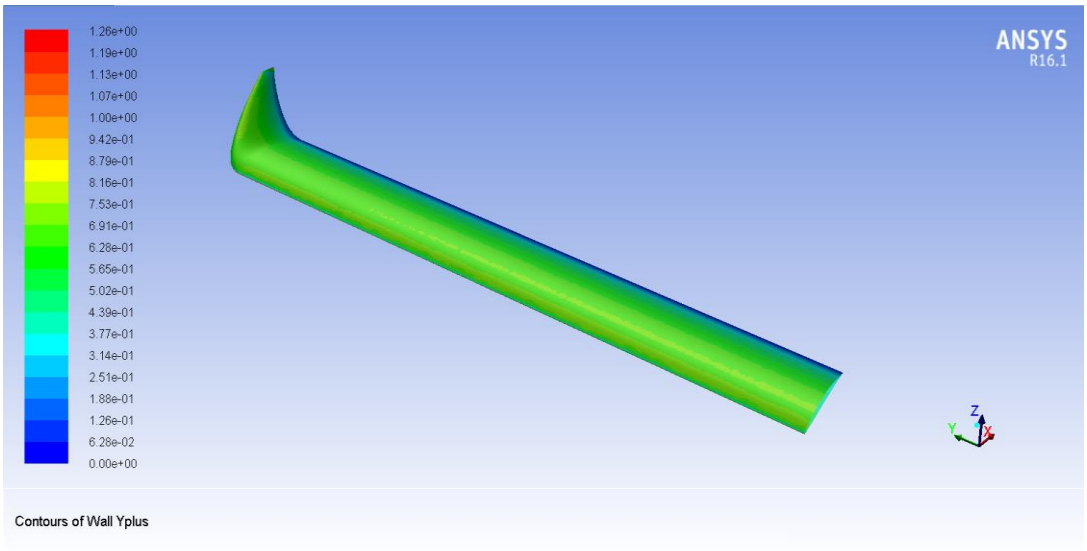

Figure 4.25 Y+ Distribution on wing with winglet, the best case

Figure 4.26 and *Figure 4.27* show the pressure variation on clean wing and the best case. Depending on wingtip vortex, lift distribution was reduced on clean wing wingtip while it approaches elliptic lift distribution on the best case.

Velocity streamlines around the wingtip of clean wing and best case were demonstrated in *Figure 4.28* and *Figure 4.29*.

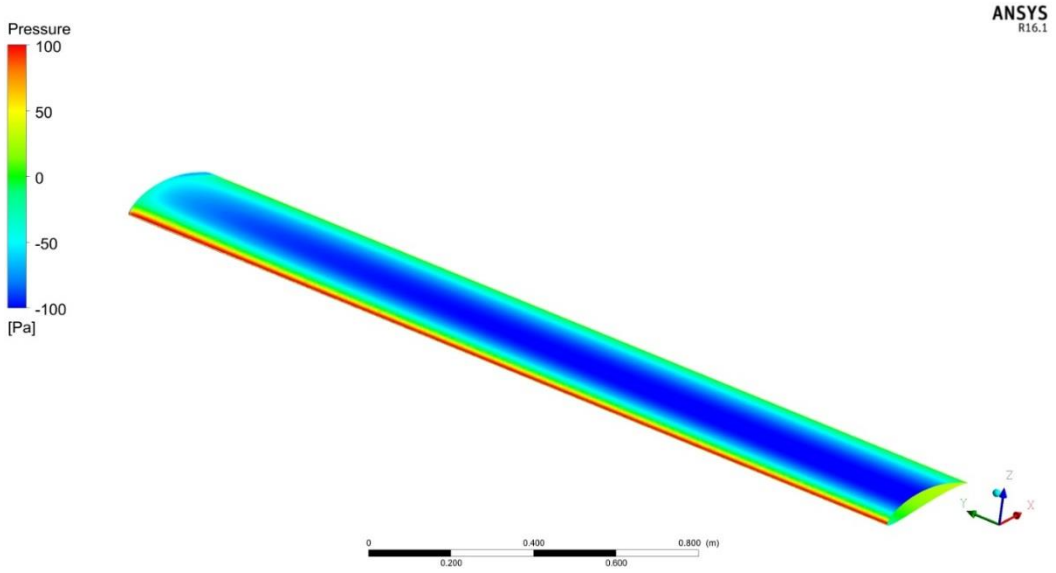

Figure 4.26 Pressure contour on wing

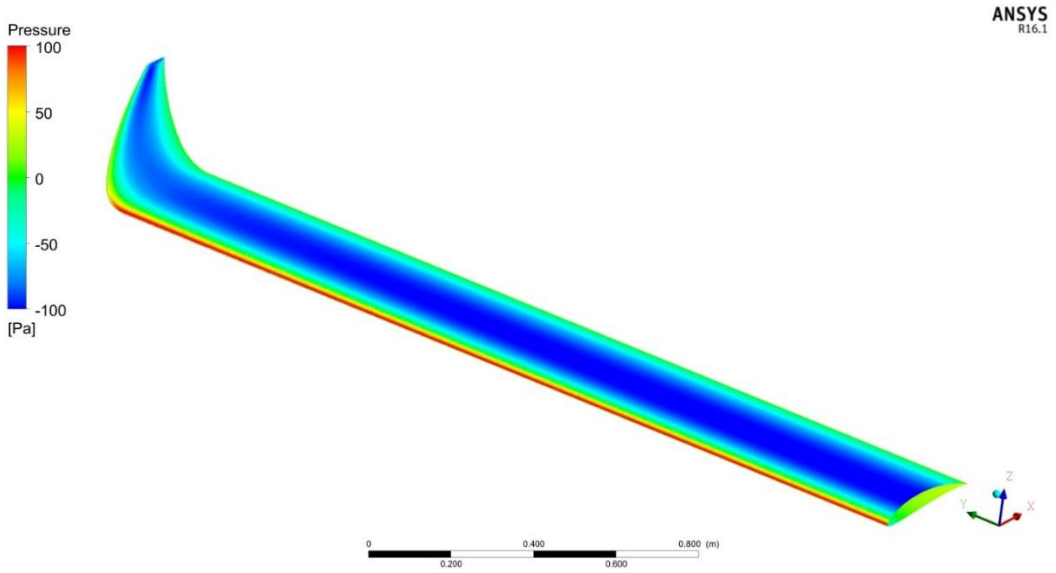

Figure 4.27 Pressure contour on the best case

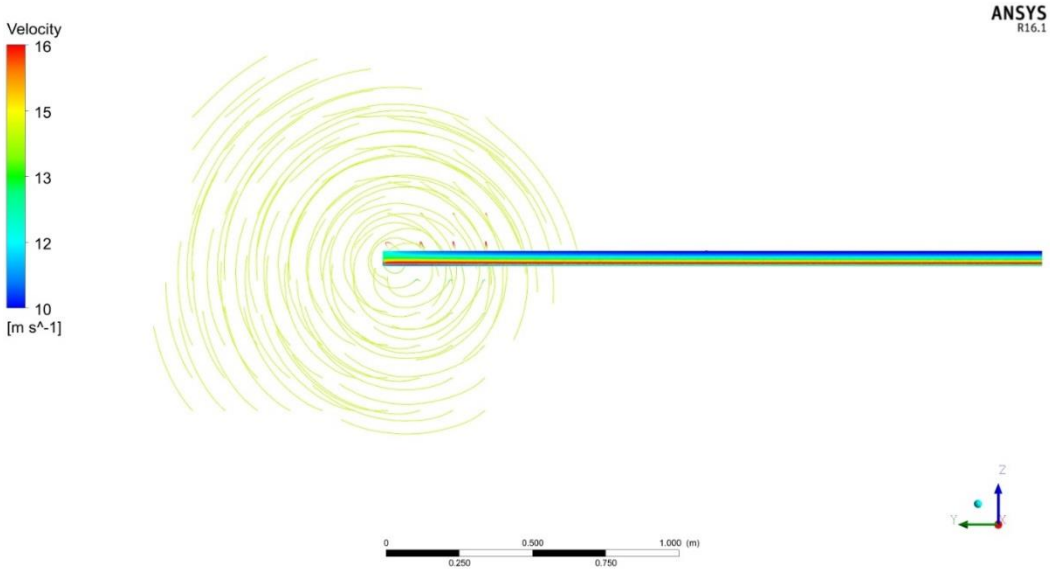

Figure 4.28 Tip vortex on the wing

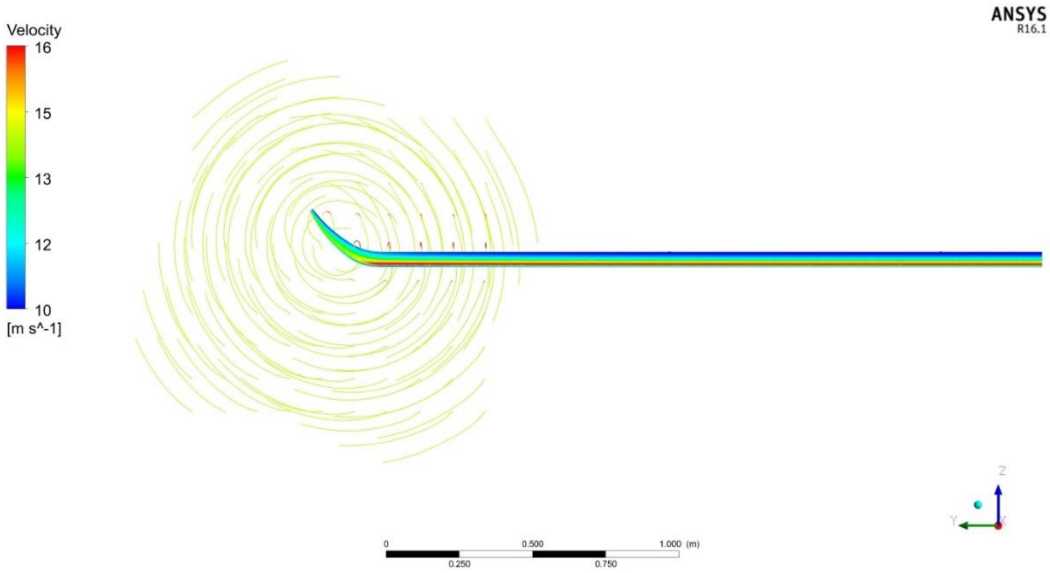

Figure 4.29 Tip vortex on the best case

Vorticity magnitude in the vortex wake region of the flow was visualized by generating different planes at different distances. *Figure 4.30* and *Figure 4.31* shows contours of vorticity magnitude in s^{-1} for clean wing and the best case. The color red represents magnitude of vorticity behind the wing at 25 s^{-1}. When magnitude of vorticity decreases, colors change from red to blue and blue represents 0 s^{-1} means freestream velocity. *Figure 4.30* shows that clean wing had the highest vorticity magnitude at all planes behind the clean wing when comparing wing with winglet configuration was shown in *Figure 4.31*. Plane at 0.5m behind the wing revealed that strength of vorticity is so high both in clean wing and best case. The strength of vorticity began to decrease with distance from the wing and comparing the clean wing, the best case had the lowest vorticity strength on plane at 2m. This shows that flow was normalized in a short distance by using winglet according to clean wing.

Figure 4.32 and *Figure 4.33* shows planform view (XY plane) of vorticity magnitude for clean wing and the best case. As expected, the vorticity magnitude in the wake region of clean wing and the best case is highest just behind of the wingtip and it reduces as the distance flow direction increases. Clean wing has a higher vorticity magnitude both in the direction of the flow and in the spanwise direction. However, the best case has a lower vorticity magnitude both in spanwise and flow direction.

Side view of the contour of vorticity magnitude were also examined and represented in *Figure 4.34* and *Figure 4.35*. It is again clearly seen that clean wing has a greater vorticity magnitude comparing to the best case. The most important result in this figure is the trailing vortex length of clean wing is larger than the best case. The flow was normalized to the longer distance downstream according to the best case.

When a general evaluation is done, with the aid of winglet, wingtip vortex was moved away from the wing and strength of vorticity was reduced. Thus, induced drag was minimized and effective AR of the wing was enhanced.

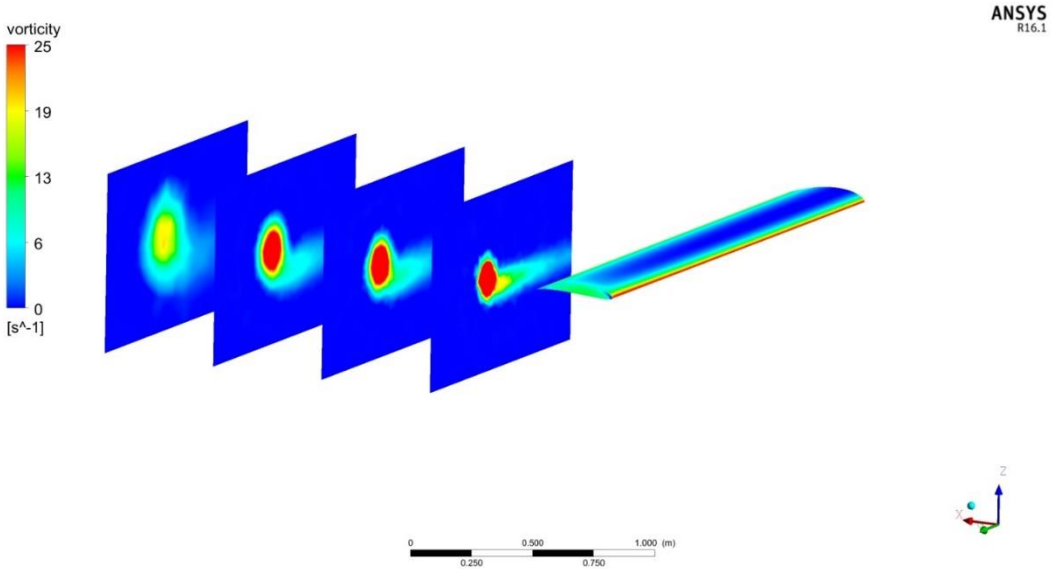

Figure 4.30 Clean wing vorticity variation at the wake region at planes 0.5m, 1m, 1.5m and 2m behind the wing

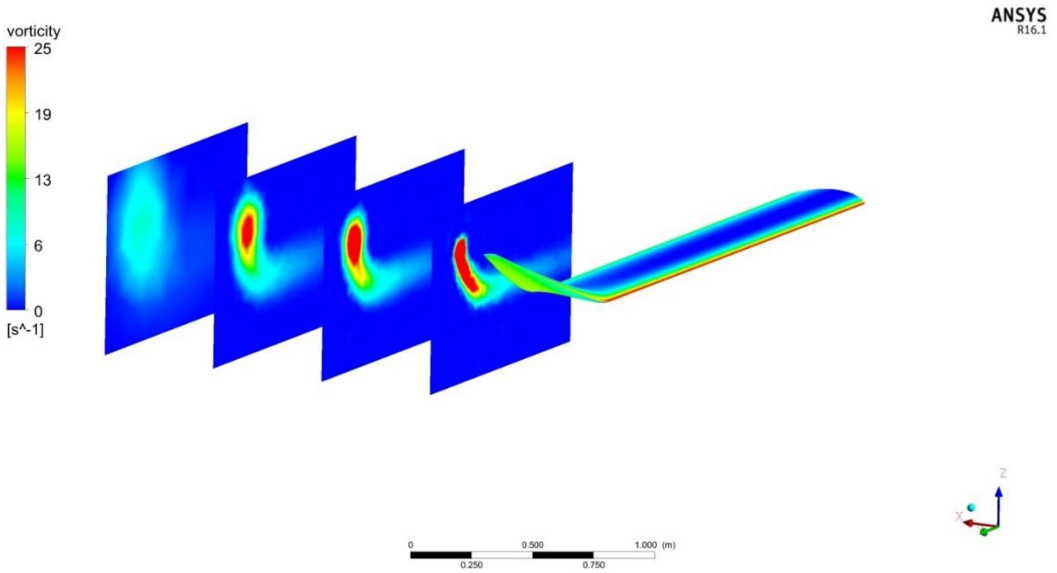

Figure 4.31 Best case vorticity variation at the wake region at planes 0.5 m, 1 m, 1.5m and 2m behind the wing

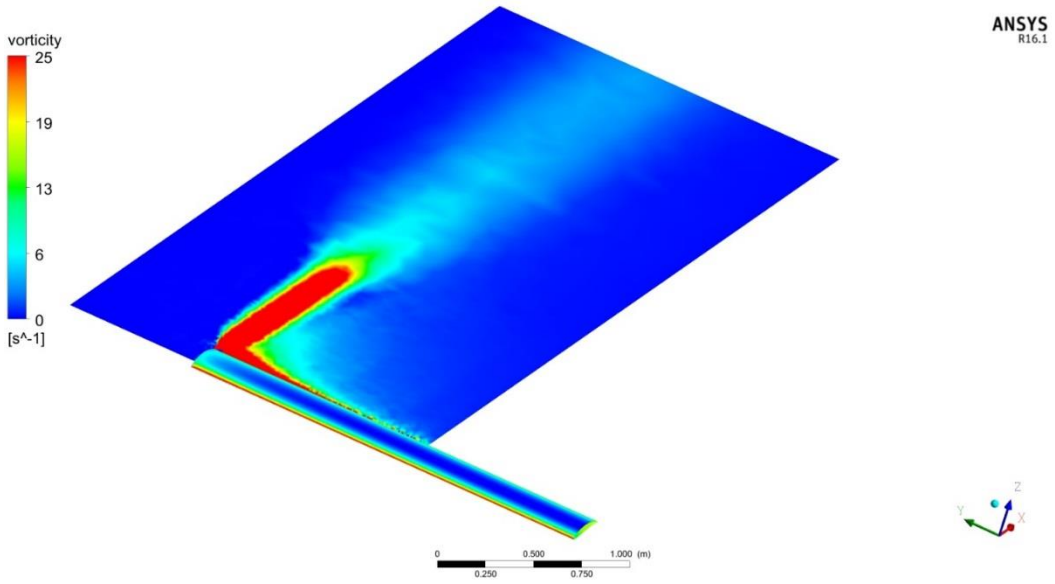

Figure 4.32 Clean wing vorticity variation at the wake region behind the wing

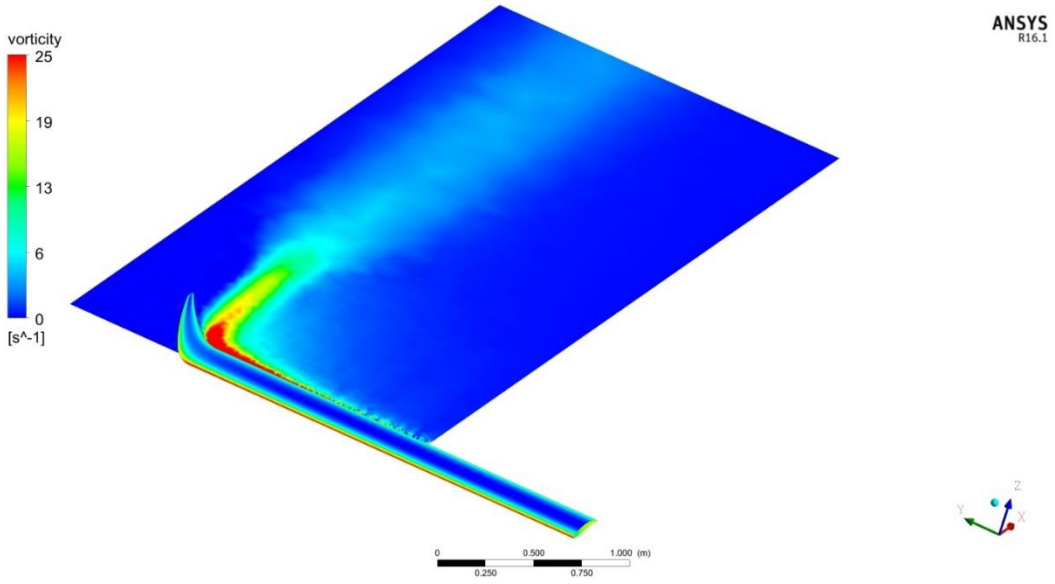

Figure 4.33 Best case vorticity variation on wake region behind the best case

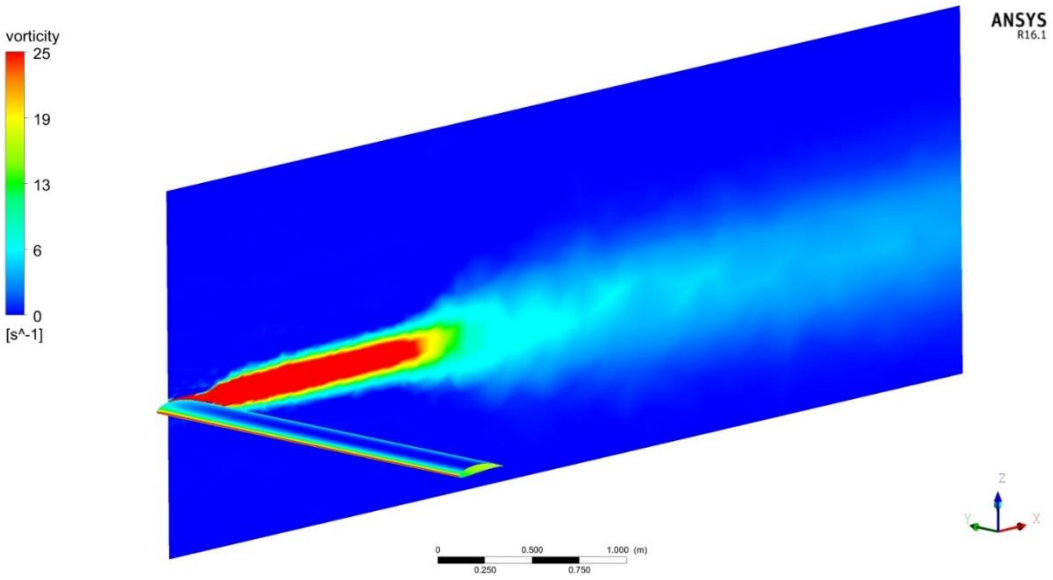

Figure 4.34 Clean wing vorticity variation on wingtip xz plane

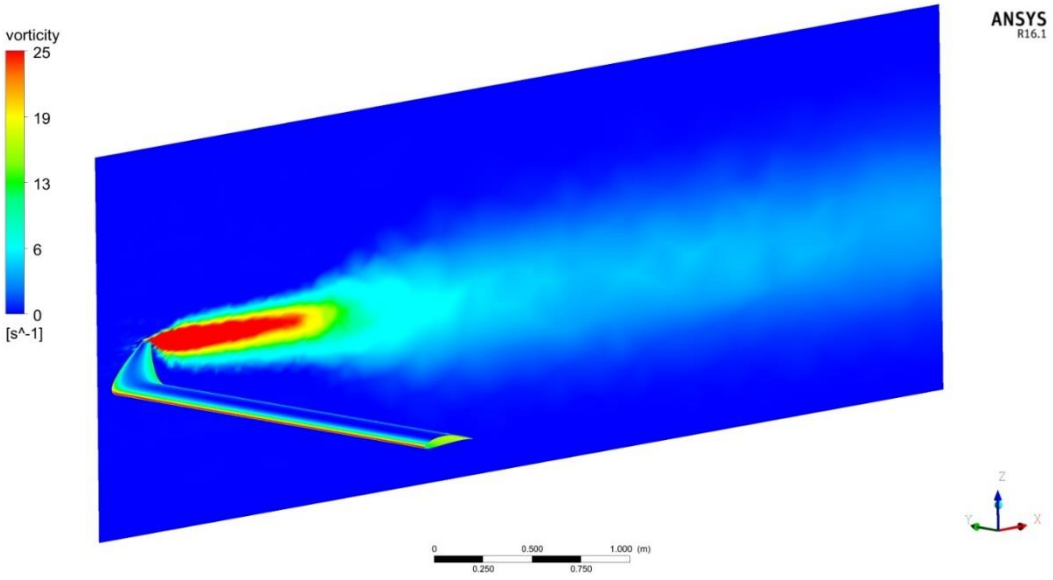

Figure 4.35 Best case vorticity variation on winglet tip xz plane

4.4. TİHAS Performance Evaluation

Figure 4.36 TİHAS, final version of modified wing with winglet

After installation of the best designed winglet to TİHAS, wing span was increased to 5m. Accordingly, AR and S_{ref} was increased to 14.62 and 0.855m^2 respectively. Since the TİHAS is battery powered UAV, the Breguet equations were not used to calculate endurance and range because during the flight, weight of the TİHAS does not change. Lance [57] has done work about calculation of electric powered aircraft's endurance and range. In order to calculate performance of TİHAS, these equations were used.

Endurance equation for battery powered aircraft is:

$$E = t = Rt^{1-n}\left(\frac{\eta_{tot}\ VxC}{P_R}\right) \tag{4.1}$$

Where P_R is the power required and it is:

$$P_R = \frac{1}{2}\rho U^3 S C_{D0} + \frac{2W^2 k}{\rho U S} \tag{4.2}$$

Rt: Battery hour rating in hours (h)

$\eta_{tot:}$ Total efficiency of motor driver, motor and propeller

V: Battery voltage in volts (V)

C: Battery capacity in ampere hours (Ah)

t: Discharge time in hours (h)

n: Battery discharge rate

ρ: Density

S: Reference area

C_{D0}: Zero lift drag

U: Velocity

Performance calculations were performed for cruise conditions and it was assumed that weight of TİHAS remained 12 kg (unchanged). According to Lance's formula, TİHAS endurance was increased as 7.81% according to clean wing with the usage of winglet.

Range was calculated according to endurance:

$$R = E \; x \; U \tag{4.3}$$

Then range was also increased as 7.81% comparing to clean wing.

In order to investigate aerodynamic effect of winglet during the flight of TİHAS, variation of C_L, C_D and L/D are performed at different velocities (stall velocity 8 m/s to maximum velocity 22 m/s). *Figure 4.37* demonstrates that, in flight envelope, the TİHAS with wing with winglet has better performance in terms of C_L, C_D and L/D values. From stall velocity to maximum velocity, wing with winglet configuration showed great improvement.

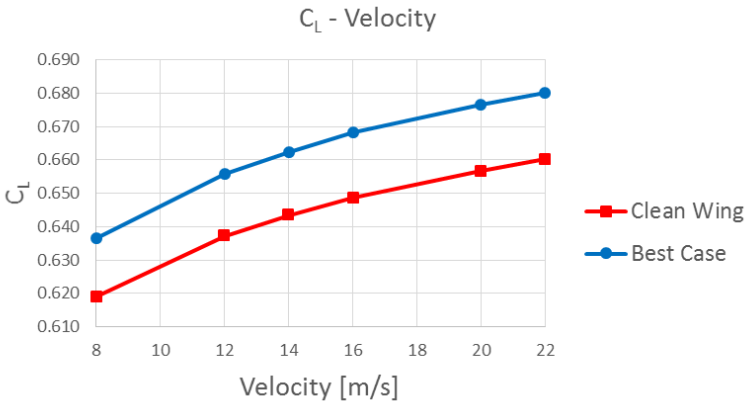

a) C_L Variation of clean wing and the best case at different velocities

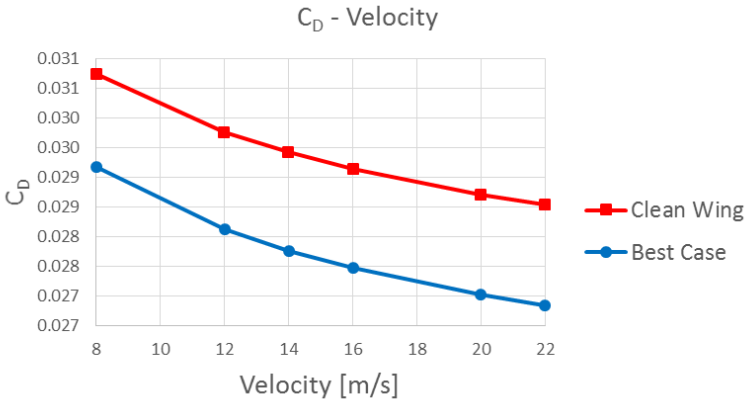

b) C_D variation of clean wing and the best case at different velocities

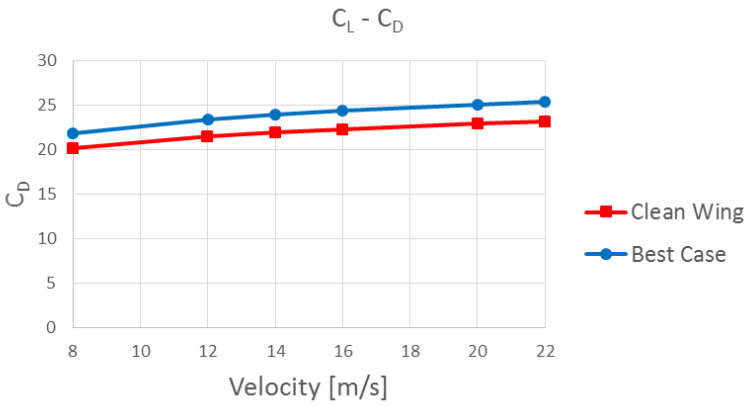

c) C_L variation of clean wing and the best case at different velocities

Figure 4.37 C_L, C_D and C_L/C_D behavior of clean wing and the best case in flight envelope

CHAPTER 5

CONCLUSION

A winglet design for TİHAS is presented. Winglet design parameters such as cant angle, sweep angle, taper ratio, twist angle and toe angle were investigated in an iterative process. Winglet span kept constant because of the span limitation and winglet height was limited as chord length, as 0.35m. As an airfoil section for winglet MH 114 was used. Numerical calculations have been carried out with the help of 3-D steady state pressure based k-ω SST turbulence model by using ANSYS (16.1), Fluent. Structural and stability effects of winglet were not performed because these are beyond the scope of this study.

Design procedure consists of two parts. First, cant angle (90°, 69.3° and 59.4°), sweep angle (0°, 15° and 30°) and taper ratio (0.2, 0.3 and 0.4) are performed in a triple combination. 27 different winglet models are analyzed and winglet which has the best L/D was selected. Cant angle 59.4°, sweep angle 30° and taper ratio 0.2 showed better performance by having highest L/D ratio about 7.93% higher than the clean wing configuration. This best is chosen to go further in the analysis to investigate the effect of toe and twist angles. Toe angle (-5°, -3°, -1°, 1°, 3°, 5°) and twist angle (-5°, -3°, -1°, 1°, 3°, 5°) were applied to the best winglet design selected in the first part. Analysis demonstrated that winglet with toe angle 3° (toe out angle) has highest L/D ratio and it increased the L/D ratio of the wing which was selected from the first part as best case by an amount of 0.43%. As a final design, winglet has cant angle of 59.4°, sweep angle of 30°, taper ratio of 0.2 and toe angle of 3°. The wing with best designed winglet is improved of 8.32% in L/D ratio compared to clean wing configuration.

Cant angle demonstrated more dominant effect on both C_L and C_D variation compared with other parameters. When three parameters (cant angle, sweep angle and taper ratio) are evaluated among each other, taper ratio has the major effect on L/D compared with others (C_L/C_D increases by about 2.15% when taper ratio changes to 0.4 to 0.2 at sweep angle 0° and cant angle 90°). It is concluded from the analysis and comparison of the winglet design parameters, taper ratio has a crucial effect on the aerodynamic efficiencies of winglet compared to other parameters in terms of L/D variation (aim of study).

Viscous and pressure components of drag and lift forces for the best case and clean wing were also studied. When clean wing and wing of best case were compared, viscous drag force remained same in both cases but pressure drag force is 8.23% lower in the best case. Again, viscous lift force effect remained same for both cases but pressure lift force is 4.95% higher in the best case configuration. This prove that, winglet implementation causes a drag reduction and a lift increase for a wing configuration.

TİHAS performance calculation were done and according to Lance's formula, TİHAS endurance and range were increased as 7.81% comparing to the clean wing.

As a result, according to identified design algorithm, a winglet which has the highest L/D value was designed and effects of parameters were examined on winglet's performance. As a consequence, TİHAS aerodynamic performance was increased.

REFERENCES

[1] D. McLean, "Wingtip Devices: What They Do and How They Do It" presented at the Boeing Performance and Flight Operations Engineering Conference, 2005

[2] John D. Anderson, JR., Fundamentals of Aerodynamics, 5th ed. Mc Graw Hill Companies.2011.

[3] M. D. Maughmer, The Design of Winglets for Low-Speed Aircraft,2006

[4] A. C. Kermode, Mechanics of Flight, 9th ed. Longman Scientific & Technical, England, 1972.

[5] D. P. Raymer, Aircraft Design: A Conceptual Approach, 5th ed. AIAA Education Series, July, 2012.

[6] R. T. Whitcomb, a Design Approach and Selected Wind-Tunnel Result at High Subsonic Speed for Wing-Tip Mounted Winglets, NASA TN D-8260, July, 1976.

[7] J. R. Chambers, Concept to Reality: Contributions of the NASA Langley Research Center to U.S: Civil Aircraft of the 1990s, NASA, SP-2003-4529

[8] I. Kroo, "Drag Due to Lift: Concepts for Prediction and Reduction," *Annual Review of Fluid Mechanics*, Vol.33, No. 1, 2001, pp. 587-617.

[9] R. Babigian and S. Hayashibara, Computational Study of the Vortex Wake Generated by a Three-Dimensional Wing with Dihedral, Taper, and Sweep, 27th AIAA Applied Aerodynamics Conference, 22-25 June, 2009.

[10] "No Title." [Online]. Available: http://www.aviastar.org/air/usa/rutan, 26 December, 2015

[11] "No Title." [Online]. Available: http://www.boeing.com/commercial/737ng/, 26 December, 2015

[12] "No Title." [Online]. Available: http://www.a350xwb.com/photo-gallery, 26 December, 2015

[13] "No Title." [Online]. Available: http://www.ga-asi.comaircraft-platforms, 26 December, 2015

[14] “No Title.” [Online]. Available: http://www.airliners.netphotoNetherlands---ArmyBoeing-X-200-ScanEagle2580441L, 10 June, 2015

[15] A. Noth, Design of Solar Powered Airplanes for Continuous Flight, September, 2008.

[16] J. Weierman, and J. D. Jacob, Winglet Design and Optimization for UAVs, 28th AIAA Applied Aerodynamics Conference, 28 June-1 July, 2010.

[17] F. W. Lanchester, Aerodynamics, Bradbury, Agnew, & Co. LD, London, UK, 1907.

[18] K. Miles, Winglet Design for the Pipistrel Taurus Electro G2 and Twin-Taurus G4 with Performance Comparison Made Using Flight-Path Optimization, December, 2012.

[19] W. E. Somerville, Coal City, IL, U.S. Patent for “A Flying-Machine,” Docket No. 1154214, patented 21 September, 1915.

[20] “No Title.” [Online]. Available: http://www.ilavhalloffame.org/members_10.htm

[21] V. J. Burnelli, New York, NY, U.S. Patent for “Airfoil Control Means,” Docket No. 1774474, patented 26 August, 1930.

[22] R. T. Whitcomb, “Methods for Reducing Aerodynamic Drag,” NASA Conference Publication 2211, Proceedings of Dryden Symposium, Edwards, California, 16 September 1981.

[23] P. D. Gall, and H. C. Smith, Aerodynamic Characteristics of Biplanes with Winglets, Journal of Aircraft, vol. 24, no 8., pp. 518-522., August, 1987.

[24] P. C., Masak, “Winglet Design for Sailplanes,” Free Flight, pp, 6-8, April/May 1992.

[25] L. B., Gratzer, “Blended Winglet,” ed: Google Patents, 1994.

[26] M. K. V. Sankrithi, and B. J., Frommer, “Controllable Winglets”, United State Patent Document, Patent No. US2008/0308683, 2008.

[27] N. R. El Haddad, and L. Gonzalez, Aerodynamic Design of a Winglet for the Dassault Falcon 10, AIAA Aerospace Science Meeting, San Diego, California, USA, January, 2016.

[28] T. Krebs, and G. Bramesfeld, An Optimization Approach to Split-Winglet Design for Sailplanes, AIAA Aerospace Science Meeting, San Diego, California, USA, January, 2016.

[29] J. E. Cooper, I. Chekkal, R. C. M. Cheung, N. J. Allen, S. Lawson, A. J. Peace, R. Cook, P. Standen, S. D. Hancock, and G. M. Carossa, Design of a Morphing Wingtip, Journal of Aircraft, vol. 52, no.5, September-October, 2015

[30] S. Khosravi, and D. W. Zingg, A Numerical Optimization Study On Winglets, 15th AIAA/ISSMO Multidisciplinary Analysis and Optimization Conference, AIAA Aviation, 2014.

[31] F. Kody, G. Bramesfeld, and S. Schmitz, Winglet Design for Sailplanes Using a Multi-Objective Evolutionary Algorithm, 51st AIAA Aerospace Science Meeting Including the New Horizons Forum and Aerospace Exposition, 7-10 January, 2013.

[32] L. Falcao, A. A. Gomes, and A. Suleman, Design and Analysis of an Adaptive Wingtip, 52th AIAA/ASME/ASCE/AHS/ASC Structures, Structural Dynamics, and Materials Conferences, 4-7 April, 2011.

[33] A. A. Gomes, L. Falcao, and A. Suleman, Study of an Articulated Winglet Mechanism, 4th AIAA/ASME/ASCE/AHS/ASC Structures, Structural Dynamics, and Materials Conferences, April 8-11, 2013.

[34] M. R. A Diaz. T. R. Yechout, and E. M. Bryant, 'The Raket'- A Wingtip Modification Approach to Improve Endurance, Range and Fuel Savings, 50th AIAA Aerospace Science Meeting Including the New Horizons Forum and Aerospace Exposition, 9-12 January, 2012.

[35] R. Babigian, and S. Hayashibara, Computational Study of the Vortex Wake Generated by a Three-Dimensional Wing with Dihedral, Taper and Sweep, 27th AIAA Applied Aerodynamics Conference, 22-25 June, 2009.

[36] J. G. Verstraeten, and R. Slingerland, Drag Characteristics for Optimally Span-Loaded Planar, Wingletted, and C Wings, Journal of Aircraft, vol.46, no.3, May-June, 2009.

[37] A. Shelton, A. Tomar, JVR Prasad, M. J. Smith, N. Komerath, Active Multiple Winglets for Improved UAV Performance, 22nd Applied Aerodynamics Conference and Exhibit, 16-19 August, 2004.

[38] D. J. Ogurek, and J. Ashworth, Experimental Investigation of Various Winglet Designs for a Wing in Ground Effect,22nd Applied Aerodynamics Conference and Exhibit, 16-19 August, 2004.

[39] N. Conley, Winglet Toe-Out Angle Optimization for the Gates Learjet Longhorn Wing, Journal of Aircraft, vol.17, no.12, Article no. 79-1831R, December, 1980.

[40] P. Panagiotou, P. Kaparos, and K. Yakinthos, Winglet Design and Optimization for MALE UAV Using CFD, Aerospace Science and Technology, 19 September, 2014.

[41] P. Bourdin, A. Gatto, and M. I. Friswell, The Application of Variable Cant Angle Winglets for Morphing Aircraft Control, 24th Applied Aerodynamics Conference, 5-8 June, 2006.

[42] A. Beechook, J. Wang, Aerodynamic Analysis of Variable Cant Angle Winglets for Improved Aircraft Performance, Proceedings of the 19th International Conference on Automation & Computating, Brunel University, London, UK, 13-14 September, 2013.

[43] M. J. Smith, N. Komerath, R. Ames, O. Wong, and J. Pearson, Performance Analysis of a Wing with Multiple Winglets, AIAA-2407, 2001.

[44] M. Dinesh, T. Yokesh, and P.S. Premkumar, Performance Investigation of an Aircraft Wing at Various Cant Angles of Winglets using CFD Simulation, Altair Technology Conference, 2015.

[45] A. Hossain, A. Rahman, J. Hossen, P. Iqbal, N. Shaari, and G. K. Sivaraj, Drag Reduction in a Wing Model Using a Bird Feather Like Winglet, JJMIE, vol. 5, no.3, June, 2011.

[46] P. R. Arora, A. Hossain, P. Edi, A. A. Jaafar, T. S. Younnis, and M. Saleem, Drag Reduction in Aircraft Model Using Elliptical Winglet, March, 2014.

[47] M. A. Azlin, C. F. Mat Taib, S. Kasolang, and F. H. Muhammad, CFD Analysis of Winglets at Low Subsonic Flow, Proceeding of the World Congress on Engineering, vol.1, 6-8 July, 2011.

[48] N. N. Gavrilovic, B. P. Rasuo, G. S. Dulikravich, and V. B. Parezanovic, Commercial Aircraft Performance Improvement Using Winglets, FME Transactions, vol.43, no.1, 2015.

[49] L. B. Gratzer, Blended Winglet, Google Patents, US 5348253 A, 1993.

[50] F. F. Felker, Aircraft with Elliptical Winglets, Google Patents, US 6484968 B2, 2000.

[51] M. D. Maughmer, T. S. Swan, and W. M. Willits, The design and Testing of a Winglet Airfoil for Low-Speed Aircraf, 19th AIAA Applied Aerodynmaics Conference, 11-14 June, 2001.

[52] "No Title." [Online]. Available: http://www.airfoiltools.com/airfoil/details?airfoil=mh114-il

[53] P. W. Jansen, R. E. Perez, and J. R. R. A.,Martins, Aerostructural Optimization of Nonplanar Lifting Surfaces, Journal of Aircraft, vol. 47, no. 5, 2010, pp. 1490-1504.

[54] K. Takenaka, K. Hatanaka, W. Yamazaki, and K. Nakahashi, Multidisciplinary, Design Exploration for a Winglet, Journal of Aircraft, vol. 45, no. 5, September-October 2008.

[55] "No Title." [Online]. Available: http:/www.cfd-online.com/Wiki/Y_plus_wall_distance_estimation

[56] A. Inc., "ANSYS FLUENT 16.0 Theory Guide."

[57] L. W. Traub, Range and Endurance Estimates for Battery-Powered Aircraft, Journal of Aircraft, vol. 48, no. 2, pp. 703-707, March-April 2011